HEAT TRANSFER STUDIES OF FLAME JET IMPINGING OVER WEDGE

Thesis

Submitted in partial fulfillment of the requirements for the degree of

DOCTOR OF PHILOSOPHY
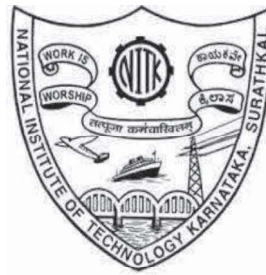
by

RITESH KUMAR PARIDA

(165008 ME16P02)

Under the guidance of

Dr. Vasudeva M

Assistant Professor

DEPARTMENT OF MECHANICAL ENGINEERING
NATIONAL INSTITUTE OF TECHNOLOGY KARNATAKA
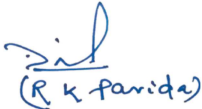**SURATHKAL, MANGALORE -575025**

May 2021

DECLARATION

I hereby declare that the Research Thesis entitled **"Heat transfer studies of flame jet impinging over wedge"** which is being submitted to the **National Institute of Technology Karnataka, Surathkal** in partial fulfillment of the requirements for the award of the Degree of **Doctor of Philosophy in Mechanical Engineering** is a *bonafide report of the research work carried out by me*. The material contained in this Research Thesis has not been submitted to any other Universities or Institutes for award of any degree.

Register Number: **165008 ME16P02**

Name of the Research Scholar: **Ritesh Kumar Parida**

Signature of the Research Scholar: (R k parida)

Department of Mechanical Engineering

Place: NITK Surathkal

Date: 27 May 2021

CERTIFICATE

This is to certify that the Research Thesis entitled **"Heat transfer studies of flame jet impinging over wedge"** submitted by **Ritesh Kumar Parida. (Register Number: 165008 ME16P02)** as the record of the research work carried out by him, *is accepted as the Thesis submission* in partial fulfillment of the requirements for the award of the Degree of **Doctor of Philosophy.**

Research Guide

Dr. Vasudeva M
Assistant Professor
Department of Mechanical Engineering
National Institute of Technology Karnataka, Surathkal

Chairman-DRPC

Department of Mechanical Engineering
National Institute of Technology Karnataka, Surathkal

Seal:

Date: 27|05|2021

ACKNOWLEDGMENTS

ABSTRACT

A transient inverse heat conduction problem concerning jet impingement heat transfer has been solved analytically in this work. Experimentally obtained transient temperature history at the non-impinging face, assumed to be the exposed surface in real practice, is the only input data. Towards developing and validate the experimental setup, a study on the effect of pressure on the volumetric flow rate of compressible gas flowing through a rotameter is undertaken. Both air rotameter (range $40 - 500$ milliliters/ minute at STP) and methane rotameter (range $400 - 5000$ milliliters/ minute at STP) are calibrated using a standard Soap Bubble Flow Meter (SBFM). The experimental observations towards change in the volumetric flow rate at STP with a change in gas pressure are in agreement with theoretical understanding. The predicted methane-air mixture flow rates are further verified using the blow-off flame stability concept, thus validating the experimental set up.

This study aims to estimate two unknown parameters - heat transfer coefficient and adiabatic wall temperature - at the impinging face simultaneously. The Green's Function Approach to accommodate both the transient convective boundary conditions and radiation heat loss is used to derive the forward model, which is purely an analytical method. Levenberg Marquardt Algorithm, a fundamental approach to optimisation is used as a solution procedure to the inverse problem. An in-house computer code using MATLAB (version R2014a) is used for analysis. The method is applied for a case of a methane-air flame impinging on one face of a flat 3mm thick stainless steel plate. It keeps Reynolds number of the flame 1000, and dimensionless burner tip to impinging plate distance equals to 4 while maintaining the equivalence ratio one. Inclusion of both radiation and convection losses in the Green's function solution for the forward problem, enhances the accuracy in the forward model, thereby increasing the possibility of estimating the parameters with better accuracy. The results are found to be in good agreement with the literature. This methodology is independent of external fluid flow and heating conditions; and can be applied even to high-temperature applications.

Heat transfer characteristics of impinging flame jet over a wedge-shaped structure similar to a deflector plate of a missile launch-pad are studied using the same analytical technique. The transient temperature of the non-impinging surface of the 4-mm-thick

test object made of stainless-steel is measured experimentally. Multiple experimental cases are considered in this work by varying methane-air gas mixture Reynolds number (800-1500), non-dimensional nozzle tip to test object distance (2-6), and wedge-angle (90º and 120º). The observations concerning heat transfer characteristics are discussed in detail. Uncertainty of estimation is evaluated using the Monte Carlo technique.

Keywords: Flame jet impingement, Inverse heat conduction problem (IHCP), Analytical transient heat transfer, Green's function, Flame deflector.

CONTENTS

Topic	Page

LIST OF FIGURES

LIST OF TABLES

NOMENCLATURE

a   Plate thickness (m)

d   Inner diameter of burner (m)

e   Error function

f, g   mathematical function

G   Green's function

h   Heat transfer coefficient (W m^{-2} K^{-1})

H   Ratio of heat transfer coefficient to thermal conductivity (m^{-1})

k   Thermal conductivity of plate material (W m^{-1} K^{-1})

Nu   Nusselt number

Pr   Prandtl number

Re   Reynolds number

r   Radius or radial distance from stagnation point (m)

q   Rate of heat transfer (W m^{-2})

t   Time (s)

T   Temperature (K)

x,y,z   Axial representation

W   Burner tip to impinging plate distance (m)

Greek Symbols

α Thermal diffusivity (m^2 s^{-1})

ε Emissivity

λ_n Eigen value

σ Stefan-Boltzmann Constant (W m^{-2} K^{-4})

θ Transformed temperature (K)

τ Variable time in Green's function (s)

Subscripts

amb   Ambient

aw   Adiabatic wall

conv   Convection

nat   Natural

rad   Radiation

Chapter 1

INTRODUCTION

1.1   Background

In the recent past, the impinging jet configuration has received considerable attention mainly due to high convective heat transfer, faster heating or cooling response, complex jet flow characteristics, and the possibility of local heating or cooling, non-uniform heat flux distribution, maximum heating rate near the stagnation point. Impinging jets have generated a wide range of interests amongst scholars, mainly due to typical fluid flow characteristics and influence on heat transfer. Flow characteristics of a jet are highly complex, and consequently, the heat transfer from or to the impinging surface is highly dynamic. When the impinging jet temperature is extremely high, the heat transfer characteristics of such jet over the impinging surface are complex due to the transient effect of convection and radiation. Numerous jet configurations have been studied and observed that fluid flow and the heat transfer in the case of impinging jets are affected by numerous physical and geometric parameters.

The high convective heat transfer rate and hence faster cooling or heating rate experienced by the targeted surface explain its widespread use in industrial applications where thermal efficiency is of primary interest. Such heat transfer applications are turbine blade cooling, aircraft leading edge heating for anti-icing purpose, cooling during re-entry of spacecraft, cooling during missile launching, and cooling of tissue in cryosurgery. Faster heating response time, the possibility to heat or cool locally, heating up and cooling down periods being much shorter, and improving product quality or process efficiency are the reason for extensive study on the topic. One of the critical factors to be noted in the case of jet impingement heat transfer is non-uniform heat flux near the stagnation point. Fundamental and application-oriented studies on these kinds of dynamic and transient heat transfer processes require simplified, accurate, and well documented experimental databases providing complete information about the flow field and heat transfer rates.

Aerospace vehicles such as rockets and missiles gain momentum and take off from the launch pad because of the reaction forces generated by the exhaust gases. Missile exhaust gas temperature is very high, an order of $2500 - 3500$ K, which depends on the capacity (thrust) of the engine required. The gas velocity is supersonic, generally an order of 5-8 Mach. The exhaust gas impinges on a deflector plate for faster spreading and exit of exhaust gases as well as the faster distribution of such high heat flux from the launch pad. The nature of heat transfer during the impingement of hot exhaust to the deflector plate are transient. Because of the very high velocity of exhaust, which impinges over the deflector plate, the stagnation point temperature goes up much higher than the exhaust gas temperature. The resulting temperature at the stagnation point is generally high enough to cause dissociation of atmospheric gases or melting of metals exposed. In the case of missile launching, the deflector plate is expected to withstand such high transient temperature. A very high heat flux arises at the stagnation point, which is transient.

Any heat transfer problem remains transient at the beginning of the process, and later the same process may turn steady depending upon its boundary conditions. In other words, in the case of a heating process, a steady-state comes only after a transient state. The temperature during the steady-state is bound to remain higher in comparison to the corresponding transient state. The transient mode of heat transfer, in such cases, associates minimum heat loss in comparison with the steady-state mode of heat transfer. In most engineering applications such as heat transfer within a furnace, heat transfer from the exhaust of a missile to the deflector plate in the launch-pad, or heat transfer due to air friction over the spacecraft entering earth atmosphere; transient mode of heat transfer involves lower heat loss rate. The boundary conditions involving both convection and radiation remain transient.

1.2   Modes of heat transfer due to flame jet impingement

Flame jet impingement studies available in literature bring out six types of heat transfer mechanisms, namely, convection (forced and natural), conduction (steady-state and transient), radiation (surface, luminous, and non-luminous), thermochemical heat release (TCHR) (equilibrium, catalytic, and mixed), and water vapor condensation and boiling (internal and external). Contribution by each during impingement depends upon

thermal and flow conditions. Detailed description of these modes are noted by Baukal (2000). Few of those are discussed in this report.

1.2.1 Convection

Convection is a predominant mode of heat transfer mechanism when target surface placed in open space is at ambient condition and flame temperature is less than 1800 K as the heat release by TCHR is negligible. Convective heat transfer is dependent on many factors, such as the aerodynamics of the jet, the turbulence intensity, burner tip to impingement surface spacing, geometry of the target plate, air-fuel mixture equivalence ratio, TCHR and whether the jet is a premixed or diffusion flame. Natural convection is reported to be significant, for flame jets with low Reynolds number.

1.2.2 Radiation

The influence of radiation is considered if target is placed in isolation or in an enclosure. In isolation, two components contribute to the thermal radiation heat transfer at the impingement plate: Nonluminous radiation and luminous radiation. Nonluminous radiation is generated due to carbon dioxide and water vapor produced by combustion of gaseous fuel. Magnitude of radiation produced by the burnt gases depends on the gas temperature, the optical path length through the gas, partial pressures and concentration of each emitting species. Luminous radiation is a significant component of the radiation heat transfer where the amount of soot formation is high as in case of solid and liquid fuels. In case of gaseous fuel, this mechanism is considered important for either fuel rich flame or diffusion flame, which has tendency to form soot. Soot particle radiations can be assumed approximately same as black body radiation.

1.2.3 Thermochemical heat release (TCHR)

Among all the alternative names, TCHR includes the aspects of thermodynamics, chemical reactions and exothermic energy release, suggested by Baukal and Gebhart (1996). Flame jets can be produced by using oxy rich fuel which leads into higher burning velocity that ultimately results in higher temperature. Moreover, absence of nitrogen which acts as heat sink in combustion products, results in higher flame temperature. At higher temperature, many combustion products contain free radicals

due to dissociation of species and degree of dissociation goes on increasing as temperature increases. When flame impinges on cooler surface, these products cool down by losing energy exothermically to form more stable products. During this radical recombination, additional heat releases known as thermochemical heat release (TCHR). It can have same magnitude as that of convection at high temperature. As TCHR is very difficult to separate out from convection, its effect is considered along with convection.

Two mechanisms are observed in TCHR, namely equilibrium TCHR and catalytic TCHR. In gaseous phase, chemical reaction takes place in the boundary layer. When free radical experiences less diffusion rate comparative to the chemical reaction rate, chemical reactions occur in the boundary layer. This reaction rate ensures equilibrium effect and consequently equilibrium TCHR. If dissociated species have insufficient time to react before reaching the surface, catalytic TCHR takes place at the surface. Since these reactions occur at the surface, material of surfaces may catalytically accelerate the reactions known as catalytic TCHR.

1.2.4 Boiling and condensation

In many studies, to estimate heat transfer from the impingement target, target surface is cooled from the non-impingement side. Boiling and condensation may occur on the surface during flame impingement unknowingly. Internal and External boiling can occur when flame impinges on wet surfaces. Internal boiling occurs on the opposite side of impinging surface where coolant gets heated above its boiling temperature. Due to impinging flame, the condensed water on cold surface gets heated above the boiling point, and the phenomenon is called external boiling. Condensation of water vapor in the products of combustion can also occur, if target surface temperature is less than dew point temperature of water vapor.

1.3 Outline of the thesis

The thesis is divided into six chapters. Introduction and literature review of jet impingement heat are discussed in chapter 1 and chapter 2, respectively. Chapter 3 details the theoretical background of the transient inverse heat conduction problem (IHCP) methodology using Green's function approach for parameter estimation. IHCP

is a well-established technique, which has gained popularity over decades due to its applicability to engineering problems. Engineering applications pertaining to high temperature requiring transient analysis of heat transfer, bring in greater scientific challenges to measure or estimate thermal parameters at the desired location. These challenges are mainly due to following reasons:-

(a)   The desired location may not be accessible view geometrical conditions. For example, measuring transient temperature at the outer surface of a spacecraft during re-entry to earth atmosphere is not advisable.

(b)   The desired location may not be accessible view environmental or physical conditions. For example, measuring temperature at the impinging face of missile deflector is not advisable view very high temperature and pressure at that location.

(c)   In case an instrument is fitted at the impinging face, it may affect the external flow condition, or the instrument itself malfunction due to existing extreme physical conditions.

Many a times the measurement of basic thermal parameters such as temperature is possible only at an undesired location (such as non-impinging face) view above discussed environmental or instrument related constraints. Two such random examples are listed below for better appreciation:-

(a)   In order to undertake thermal analysis of inner or intermediate surfaces of refractory material used in a furnace, only possible (which is easy and direct) approach to measure temperature is at the outer surface of the furnace.

(b)   Similarly, to undertake any kind of heat transfer related analysis at the impinging face of a deflector plate during which the missile exhaust is impinging over it, ideal location for temperature measurement is the non-impinging face.

Engineering problems having known thermal effects at an undesirable location (or time) measured using existing techniques and unknown cause (non-measurable) at the desirable location are categorized as inverse problems. These are otherwise called ill-posed problems, because the cause of the situation is unknown and the effect may be

known partially or fully. To be specific, the difficulty of estimating the true cause of a noticeable thermal effect is much higher in cases of high-temperature and transient applications. Present study analyses one such ill-posed problem in transient domain and recommends transient temperature analysis instead of steady-state analysis analytically. It is also observed that higher accuracy in predicting the cause is possible if the measured effect during the beginning of the experiment for a minimum possible duration is analysed. In order to include all kinds of thermal losses during experimentations, a superior mathematical approach called Green's function is used. Green's function can handle transient convection and radiation boundary conditions while formulating the analytical forward model to the IHCP. The Monte Carlo technique to estimate the uncertainty of the estimated parameters is used in this study. Design and development of experimental setup; experimental procedure and validation of transient analytical IHCP algorithm are discussed in the fourth chapter. The experimental setup includes a high resolution thermal imaging camera to measure (non-contact mode) transient temperature at the impinging face of the test object. Experiments on flame jet impingement over flat plate are undertaken to validate the analytical technique. The results and discussion of heat transfer characteristics of impinging flame jet over wedge-shaped test objects are presented in chapter 5. Results derived from the analytical analysis of multiple experimental cases by varying the flame Reynods number, nozzle tip to impinging surface distance and wedge angle are deliberated. Chapter 6 is dedicated for conclusions and future scope of work.

Chapter 2

LITERATURE REVIEW

2.1   Jet impingement

Jet impingement heat transfer has been the topic of interest for researchers working in material processing using flame jets, heat transfer in gas turbine combustor, cooking stove, and thermal effect deflector plate of a missile launcher. A study on flame jet heat transfer by Bee and Chigier (1968) proves that total heat transfer can be enhanced by a factor of three by direct impingement, because the convective heat transfer alone, amounts to about 70% of the total heat transfer in the region of impingement. A study on methane-air flame jet impingement onto a cold plate by Milson and Chigier (1973) submits that impinging jets have a high potential to increase the convective heat transfer rate. The flow characteristics of impinging jets have been proved complex to predict through numerical simulation (Zuckerman and Lior, 2006; Dewan et al., 2012) despite the geometric simplicity of the configuration. Hence, the impinging jet configuration is still a reference test case for research.

Hydrodynamics and convective heat transfer of impinging jets have been undertaken in the past. This flow can be divided into three regions (figure 2.1); the free jet region, the stagnation flow region, and the wall jet region.

In the free jet region due to shear interaction between gas and surrounding fluid, there is entrainment of the surrounding fluid, which increases mass flow rate, decrease in jet temperature, and non-uniform radial velocity. However, the impingement plate effect is not notable in this region (Van der Meer, 1987). In the stagnation flow region, the axial flow sharply decelerates, and the radial flow accelerates, giving rise to increased pressure in this region. Characteristics of the stagnation flow region depend strongly on the dimensionless nozzle to plate distance (W/d). It extends from 1.2d in axial distance from the plate to 1.1d in the radial direction for the small nozzle to plate distances (W/d < 12). As heat transfer is maximum and transient in this region, it requires more attention and hence studied extensively.

In the wall jet region, the fluid spreads out radially over the surface in a decelerating flow. The jet impingement region is usually referred to as the stagnation zone and characterized by high-pressure gradients caused by the rapid development in gas velocities. As the gas flow turns radially away from the jet centerline, a transition region develops. This development is followed by a boundary layer flow along the wall with an external gas flow outside the boundary layer and parallel to the wall.
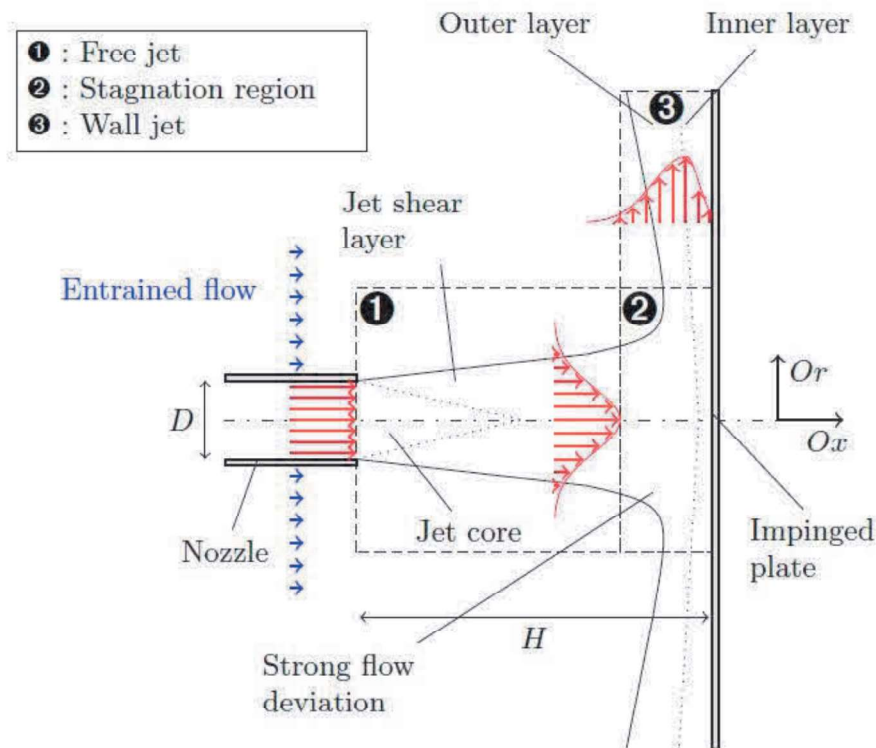
Figure 2.1 Characteristic regions of a round jet impinging over a flat plate (Grenson et al. 2016)

2.2. Experimental studies on jet impingement heat transfer

Experimental investigation (Jackson and Kilham, 1956) of forced convection heat transfer from combustion products when impinged perpendicularly over a cylinder revealed that the dominating mode of heat transfer in case of impinging jets is forced convection as compared to conduction and radiation. One of the first reviews on heat transfer characteristics of air and flame jet impingement (Viskanta, 1993) focusing on applications in the material processing brings out that fundamental knowledge on the

relative importance of radiative versus convective heat transfer from flame jet impingement is required for predicting total heat flux from industrial-scale flames and in high-temperature industrial applications. Comprehensive studies by (Baukal and Gebhart, 1996-a,b) on experimental flame impingement heating for aerospace applications, such as rocket re-entry into the earth's atmosphere, have discussed extensively on semi-analytical relations to estimate forced convection heat flux. A comparative study on heat transfer distribution of impinging flame and air jets is reported by Kadam et al. (2016). Effect of flame shapes and flame stabilization, different experimental configurations, operating conditions, burner geometry, and separation distance are reported by Chander and Ray (2005) towards estimating total heat flux in cases of flame jet heat transfer. The effect of various geometrical, as well as flow parameters - Reynolds number, Mach number, the non-dimensional radial distance from stagnation point (r/d), non-dimensional burner tip to impinging plate distance (W/d), turbulence, and the shape of the nozzle, are studied by Jambunathan et al. (1992); Zuckerman and Lior (2006) experimentally. In a recent study (Qiu et al. 2019), flow structure and heat transfer characteristics of jets impinging on a curved surface with different jet arrangements and Reynolds number (10,000–40,000) are numerically investigated. These papers bring out fundamentals on both flow characteristics and heat transfer characteristics of an impinging jet and varied modern-day applications, ranging from industrial to space technologies.

Early experimental studies on impinging jets (Fay and Riddell, 1958; Sibulkin, 1952) have focused on the study of flow characteristics to derive its heat transfer characteristics at stagnation points. Several fundamental studies have been carried out to gain adequate information and knowledge on the fundamental principle of jet impingement heat transfer. A review of the experimental work on heat transfer to impinging jets is reported by Carlomagno and Ianiro (2014); Dewan et al. (2012); Jambunathan et al. (1992); Viskanta (1993). From these reviews, it is clear that heat transfer rates and heat transfer characteristics of impinging jets are dependent on various parameters like Reynolds number, jet-to-plate spacing, the radial distance from stagnation point, Prandtl number, target plate inclination, confinement of the jet, nozzle geometry, curvature of target plate, roughness of the target plate and turbulence

intensity at the nozzle exit. Experimental studies on impinging jets over a solid surface reveal the exact influence of the parameters towards a higher rate of heat transfer in impinging jets. The experimental studies in the field of impinging jets during the 20th century have led to the development of empirical correlation between non-dimensional parameters towards expressing the rate of heat transfer. A review of the empirical studies on jet impingement heat transfer confirms that the most straightforward correlations for local Nusselt number should be of the form Nu = f (Re, W/d, x/d, Pr). Many such empirical correlations proposed are for average heat transfer coefficients, as reported by Zukerman and Lior et al. (2006). Few correlations for stagnation point Nusselt numbers available are based on regression analysis from experimental data.

Cooper et al. (1993); Craft et al. (1993); Gardon and Akfirat (1965) and Hoogendoorn (1977) have discussed the significance of jet turbulence on heat transfer. The jet turbulence mainly depends on the jet exit conditions such as velocity or velocity profile and pressure. As jet exit, most studies used either convergent nozzles, for which turbulence is only confined in thin boundary layers or fully developed pipe flow. The dependence of the heat transfer on the Reynolds number (Re) and the nozzle-to-plate spacing was thoroughly examined by Lytle and Webb (1994); Hofmann et al. (2007); Katti and Prabhu (2008); Lee (1999) that followed the novel work of Baughn and Shimizu (1989).

Numerical study on quenching jet impingement by Ghasemian et al. (2019) analyses the effects of conjugation and mass transfer comprehensively. Similar experimental studies by Mozumder et al. (2006) and Karwa et al. (2011) on heat transfer characteristics of quenching jet impingement have undertaken transient heat transfer analysis. A detailed analysis by Gan et al. (2019) on a combination of jet impingement and dimples to cool micro-electronic devices have proved to improve heat transfer characteristic due to the alleviation of drift phenomenon. Micro-pin characteristics on flow and heat transfer of a circular impinging jet are studied both experimentally and numerically by Hadipour et al. (2020), proving that micro-pins have a significant effect on improving heat transfer rate. Determination of the heat transfer coefficient distribution of a two-phase air-water bubbly jet impingement (Kowsary et al. 2020) is undertaken in the transient domain while investigating uncertainties due to indefinite

lateral boundary conditions, temperature dependency of thermal conductivity, and the non-uniformity of the initial temperature distribution.

2.2.1. Stagnation point heat transfer
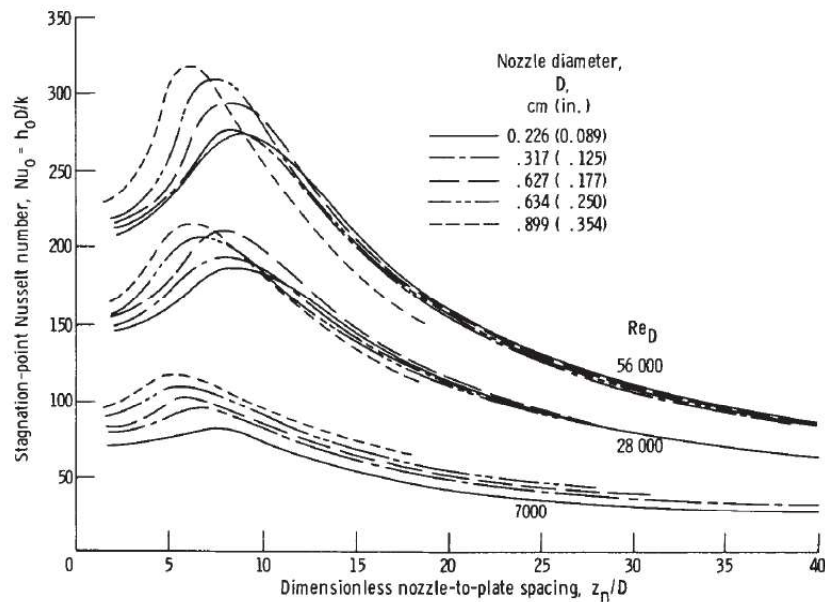
Figure 2.2   Stagnation point Nusselt number due to impinging flame jet (Gardon 1962).

The stagnation point is that physical location, where the impinging jet's axis meets the surface being impinged. The scientific study of the heat transfer at this point is of importance because the rate of heat transfer at and around this point is comparatively more than the normal modes of convective heat transfer for a given temperature condition. Gardon (1962), Chander and Ray (2008), and Buchlin (2011) have discussed the experimental results to explain a few fundamental parameters relating to jet impingement heat transfer. The variation of stagnation point Nusselt number with Reynolds's number, dimensionless nozzle to plate spacing, and nozzle diameter is shown in figure 2.2. Similarly, the variation of heat transfer coefficient with dimensionless distance from the stagnation point is illustrated in figure 2.3. A higher rate of heat transfer at the stagnation point is mainly due to increase heat transfer coefficient because of the thinner thermal boundary layer and higher turbulence.

11
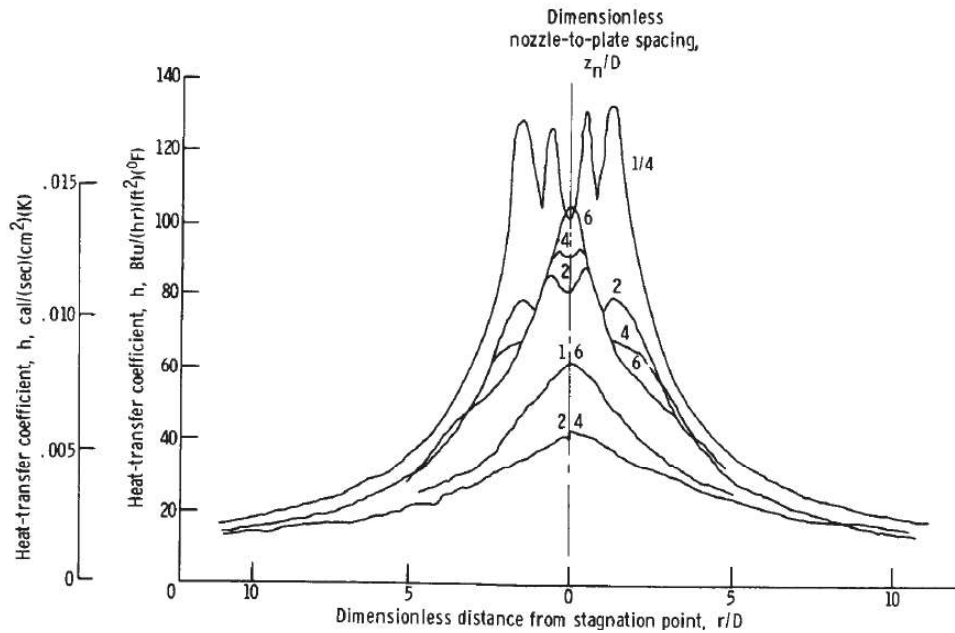
Figure 2.3   Radial variation of heat transfer between a plate and an impinging jet (Gardon, 1962).

2.2.2   Effect of nozzle-plate spacing

The experimental data of Lytle et al. (1994), Vinze et al. (2017) concluded that the local Nusselt numbers depend on the nozzle design and the nozzle-to-plate ratio, which is shown in figure 2.4. The nozzle diameter, nozzle-to-impingement surface distance, angle of incidence to impingement surface, and nozzle design also influence the heat transfer performance of a single impinging jet.

The influence of nozzle geometry and confinement concerning jet impingement heat transfer is studied. It appears that nozzle geometry affects the generation of turbulence in the shear layer. For nozzle-to-plate spacing of fewer than ten times the nozzle diameter, the use of an orifice will probably yield higher rates of heat transfer than a contoured nozzle.

In shorter distances, heat flux rate and the temperature are higher as the air entrainment is lesser, and flame widening is least. At $W/d = 3$, the inner reaction zone just touches the surface, resulting in maximum heat flux and surface temperature. If the separation distance is further reduced, the point of maximum heat flux and surface temperature is

12

shifted away from stagnation point in a radial direction as inner reaction cone spreads around the stagnation point and reaction zone touches the surface at some distance away from stagnation point. At shorter distances, as the turbulent mixture directly impinges on the stagnation region, it has been observed that heat flux at the stagnation point reduces zero or is even negative.
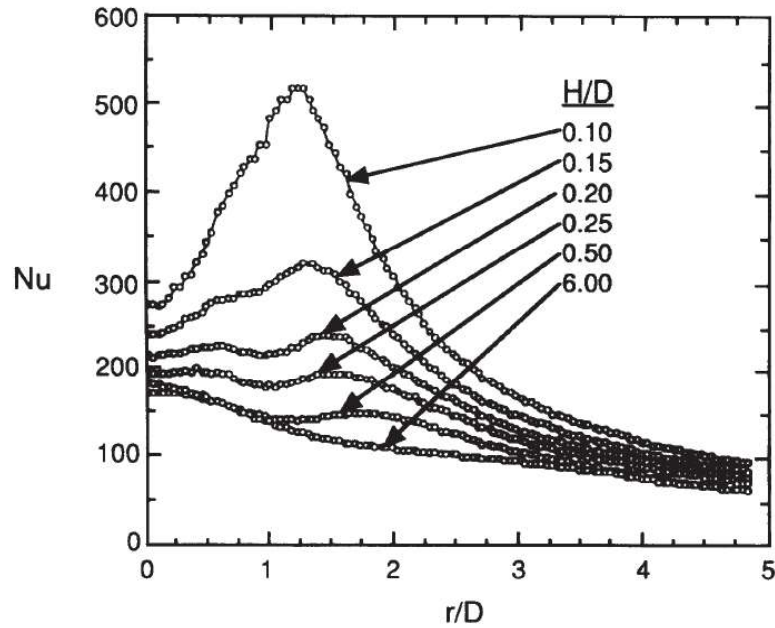
Figure 2.4   Variation of local Nusselt number with geometrical parameters (Lytle et al., 1994).

2.2.3   Effect of Reynolds number

Reynolds number influences the heat transfer rate to or from the impinging surfaces significantly. Reynolds number ranging from 300, for laminar flames to 35000 for turbulent flames, is experimented in the study of flame impingement. It has a significant influence on the heat transfer rate to the plate. It affects on flame length (both primary and reaction). High Reynolds numbers have been used mostly to study diffusion flames, while Reynolds numbers up to 2500 have been used to laminar premixed flames.

Figure 2.5 shows the effect of Reynolds number on heat flux and surface temperature distribution along radial direction for a methane-air flame for tube burner of 10 mm

diameter for non-dimensional nozzle-to-plate distance equals to 4, and equivalence number equals to 1.
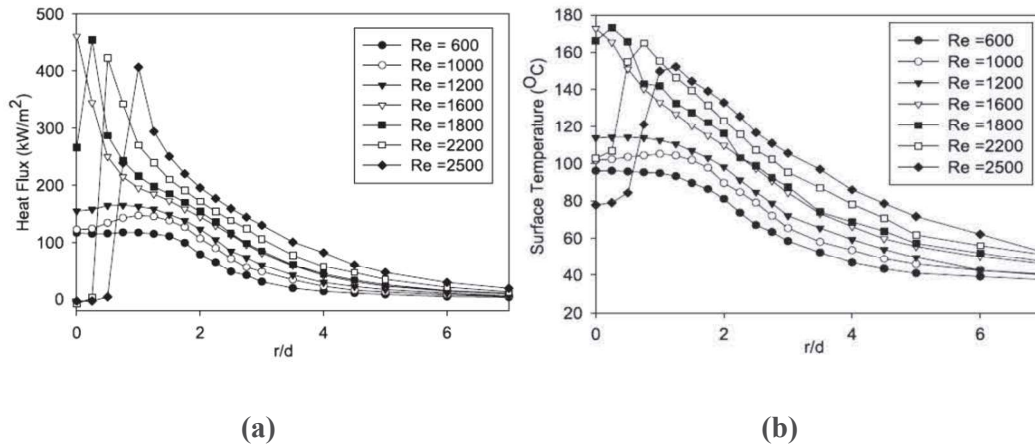
Figure 2.5 (a) Heat flux and (b) surface temperature, distribution for methane/air flame for a tube burner of diameter 10 mm, for various Reynolds numbers at W/d = 4 and ϕ = 1.0 (Chander and Ray, 2006).

The experimental study by Chander and Ray (2006) explores that the rate of heat transfer and surface temperature is lower at lower Reynolds numbers, as the high-temperature zone located far away from the plate. As Reynolds number increases, flame cone height also increases, resulting in an increase in heat flux and surface temperature values at the stagnation and wall jet regions. It results in more convective heat transfer. At Reynolds number 1600, flame cone just comes in contact with surface giving maximum heat flux value 461 kW/m^2. The maximum heat flux point shifts away from the stagnation point for Reynolds number higher than 1600. It happens because the inner cone intercepted by surface, and it spreads out towards the wall jet region. At a very high Reynolds number, it has been observed that heat flux at the stagnation point reduces to zero value or even negative, because of the impingement of unburnt cold mixture directly on the stagnation region.

2.3   Techniques to estimate jet impingement heat-transfer characteristics

Review on impinging jets by Viskanta (1993) consolidated the experimental studies concerning heat transfer to and from solid surfaces and impinging isothermal gas and flame jets. Computing local and average heat transfer rates to or from highly turbulent impinging jets at higher temperature applications with the available models accurately is a challenge. At higher temperature and corresponding pressure and the velocity of the imping fluid in engineering applications, the accurate and timely information about heating or cooling is of prime importance.

Remie et al. (2007 and 2008) have derived analytical expressions for the heat flux distribution of a laminar flame impinging on a flat plate having both two-dimensional and axisymmetric cases. Numerical studies of heat transfer characteristics of an impinging flame jet are presented by Conolly and Davies (1972) and many other researchers. Hindasageri et al. (2014 b) have proposed a numerical-analytical method for estimating adiabatic wall temperature to estimate the Nusselt number and effectiveness. This study has further presented a novel method of estimating the steady-state heat flux distribution of impinging flame jets in an enclosure using the Inverse Heat Conduction Problems (IHCP) technique. Experimental and numerical studies have been undertaken to estimate the wall heat flux and heat transfer coefficient. A unique and vital case - the measurement of heat transfer of jet impingement with high injection temperature – has been proposed by Fenot et al. (2005). Chander and Ray (2011) has conducted a numerical and experimental study on the occurrence of the off-stagnation peak in heat flux and explained that the shift in peak heat flux from stagnation point is due to a corresponding peak in the axial velocity profile.

A numerical study (Conolly and Davies, 1972) to predict the convective heat transfer coefficient at the stagnation point of a blunt body immersed in the flame focuses on the fundamentals of jet impingement heat transfer. Heat transfer measurements using a steady-state calorimeter have been reported by Hargrave and Kilham (1984) for premixed methane-air flames and hot air jets impinging normally on hemispherical nosed bodies. Estimation of heat transfer coefficient by measuring the flow structure and heat transfer of impinging flame jets and impinging isothermal jets was studied by Van der Meer (1991) experimentally.

Thin metal foil technique (Kuntikana and Prabhu, 2016-a) is used to analyse the steady-state surface temperature to perform local energy balance. It is established that heat transfer characteristics of a cold and hot jet are independent of jet temperature, provided appropriate reference temperature is chosen for a hot jet. Observation on higher heat transfer distribution from a flame jet at closed proximity compared with air-jet is reported. Higher flame jet Nusselt number than that of air-jet for all Reynolds number at locations away from stagnation region is confirmed in the literature.

Measurement of heat flux from the combustion products impinging on a colder surface is studied experimentally (Conolly and Davies, 1972) using a calorimeter. Zhen et al. (2012); Chander and Ray (2006); Huang et al. (2006) have used a heat flux sensor to record local heat flux, in respect of heat transfer from a flame jet near the stagnation point. The average size of a heat flux sensor is around 4-6 mm, limiting the number of locations at which readings can be obtained. These studies are steady-state in nature. Chander and Ray (2005) report about heat flux measurement using heat flux sensors. The size of heat flux sensors is around 4-6 mm in diameter. Heat flux has been measured directly by using heat flux gauges whose hot and cold ends are exposed to flame and water, respectively. These gauges are generally made up of high conductivity material like copper and flushed with the surfaces always. Phosphor thermometry technique (Remie et al. 2008) for validating the analytical convective heat-flux relation is reported in the literature.

The unaccounted energy loss in any heat transfer experiment, which is highly transient in nature, is the primary cause of concern, as it always keeps the observations away from reality. It is natural for any experiment requiring a finite duration to attain a steady-state. Therefore, energy loss in the case of steady-state analysis remains higher as compared to unsteady cases. In other words, the transient experimental data for a suitable duration, where the unaccounted energy losses are minimum, and computational efficiency is higher, shall be considered for analysis, thereby ensuring a very high probability of predicting the correct result.

Frankel et al. (2008 and 2010) derived a new integral relationship between heat flux and temperature for a transient two-dimensional heat-conducting cartesian half-space ($x>0$ and $-\infty<y<\infty$) having an orthotropic thermal conductivity. The proposed

observations offer new insight into experimental measurements for acquiring the heat flux based on embedded temperature sensors. This technique suggests direct measurement of heating or cooling rate may reduce or remove the ill-posed nature complex problems like jet impingement heat transfer. This relationship provides a secure window to estimate the local heat flux perpendicular to the front surface at any location within the half-space. Integral relationships of this type are highly useful for experimental investigations since the in-depth heat flux can be extracted from well-established temperature transducers. Kulish et al. (2003) developed integral relationships for temperature and heat flux for moving boundaries based on the Laplace transform. In this technique, the temperature profile was acquired from the given history of heat flux.

Recent studies on the field of spot cooling of electronic components, cooling of gas turbine blades, tempering of glass, etc. motivate scholars to estimate the heat transfer coefficient over the impinging plate in a very simplified manner. In such applications, the jet injection temperature differs from the ambient temperature and the surface temperature. Under these conditions, entrainment of ambient air/ gas into the jet changes its temperature, and hence the heat flux exchanged does not vary linearly with respect to temperature difference as per Newton's law of cooling. Fenot et al. (2005 and 2008) explain a method to calculate both the varying heat transfer coefficient and corresponding adiabatic wall temperature even for a large difference in jet injection temperature and ambient temperature.

Most of the researches in this field neglect radiation (Chander and Ray, 2005), as it contributes approximately 5% of total heat flux. However, radiation becomes significant when we talk about an engineering application, which deals with high-temperature jet. Few of the important applications of hot-jet impingement are aerospace vehicles re-entering the atmosphere (Cremers et al. 2010), launching of rocket or missile (Calle et al. 2010; Evans et al. 1963) apart from the important industrial applications like metal processing, cooling of gas turbine components, cooling of electronic components, etc. A few studies involving high velocity and high-temperature jet impingent, which tend to give a very high rate of heat transfer, are cited in the literature (Evans et al. 1963; Grenson et al. 2016). Apart from all these industrial

applications of jet impingent, one of the current studies relating to the field of jet impingement is the development of new aerospace material required in the thermal protection system in space crafts. The heat shields must be highly effective while remaining relatively lightweight. The development of such material requires a thorough understanding of the relationship between transient heat flux and temperature variation within the material. Therefore, it is necessary to undertake a study on hot jet impingement heat transfer.

It is understood that a fundamental knowledge base on the relative importance of radiative vs. convective heat transfer in flame jet impingement heat transfer is established. This is required, especially for predicting total heat flux from industrial-scale flames and in high-temperature industrial furnaces. For low-velocity, high-temperature flame jets, radiative heat transfer from the flame can be of the same order of magnitude or even lower than convective heat transfer, particularly if the angle of incidence is relatively large.

2.3.1   Inverse heat conduction problem

Inverse heat conduction problems are those problems where thermal effect due to heat transfer is known, and the cause of the same is to be predicted. Prediction of the transient temperature of the slab in a reheating furnace, or prediction of the impinging effect of atmospheric gases over the body of a re-entry vehicle, etc., fall in these categories of problems.

A heat conduction problem in a solid with the initial and boundary conditions completely specified is a well-posed one that can be solved by various analytical and numerical methods. In contrast, when the boundary condition such as the heat flux is to be determined from measurement data inside the solid, the problem is an ill-posed, which is known as the inverse heat conduction problem (IHCP). The inverse heat conduction problems (IHCPs) reported by Beck et al. (1985); Sparrow et al. (1964) and Hindasageri et al. (2014 a) have received considerable attention from researchers.

Transient studies in case of flame jet impingement are very few, mainly due to difficulty inaccurate measurement of temperature and complexity involved in the analysis of

transient data. Wall heat flux and temperature are estimated using numerical IHCP (Loubat et al. 2004).

Transient heat flux is determined indirectly using the recorded temperature. In this method, an uncooled surface is allowed to reach a certain temperature or else heated for a specific amount of time. Sensible heat gain by surface, in either case, gives flux. The temperature profiles are measured at or near impingement surface by using a number of thermocouples, and then inverse conduction heat transfer computational technique is used to estimate transient heat flux. Laubat et al. (2004) and Hindasageri et al. (2014 a) explain the method to estimate heat flux from impinging flame jets.

Subsequently, with an assumption that wall heat flux and temperature are linearly dependent with each other, Nusselt number and reference temperature at the impinging face are predicted. In a similar study by Hindasageri et al. (2014 c), numerical as well as an analytical approach, was applied to characterize heat transfer due to flame jet impingement. The transient semi-infinite conduction model with flux boundary condition was used with an assumption of constant heat flux (during the transient phase) at the impinging face to estimate the heat transfer characteristic of the impinging flame jet. The adiabatic wall temperature (reference temperature) was obtained experimentally, and the heat transfer coefficient was estimated analytically. In a recent study on transient flame jet impingement (Kadam et al. 2018), heat flux and wall temperature at the impinging face were estimated using the concept of modal analysis. Linear rate law between impingement side surface temperature and its corresponding heat flux was utilized to obtain heat transfer characteristics at the impinging face.

Feng et al. (2011) used Laplace transform as a basic mathematical tool and demonstrates a method of solving the three-dimensional inverse heat conduction problem with a thin plate or sheet. In measurements of high surface temperatures, there are situations when direct measurements of temperature and heat flux are not feasible. A surface heated by a high-intensity laser is an example. Conventional sensors can hardly withstand the intense heat flux and temperature. Temperature and flux measurements using non-contact sensors are affected by the out-going radiations from the heated surface. The objective of the work is to infer the front surface temperature and heat flux from the back surface measurements by solving an inverse heat

conduction problem based on the transient temperature or/and heat flux measured at the back surface. This technique helps in predicting the inaccessible surface temperature or flux from the knowledge of similar information on the opposite face. This technique is valid for thin sheets.

In the mathematical formulation of the inverse problem, either temperature or heat flux can be measured at the back surface. Most previous researchers prefer temperature measurements because the temperature can be measured with fewer uncertainties compared to heat flux measurements.

2.4   Jet impingement over the inclined face

The impingement of jets on an inclined plane surface to the jet axis is one of the important problems in the study of flame jet heat transfer and fluid flow in the vicinity of stagnation point. Limited studies on the rate of heat transfer related to the inclined jets are available in the open literature. For inclined jets, the free jet flow is turned and spread laterally onto the flat surface. This rate of turning and spreading of the jet is influenced by the impingement angle, as reported by Kowsary et al. (2020).

The shift of points of maximum heat transfer was first observed and measure by Sparrow and Lovell (1980). The considered parameters varied were: the jet Reynolds numbers varying from 2500 - 10000 and jet-to-plate distances in the range of 7–15. Non-uniform distribution of local heat transfer coefficients over the test plate, which is diminishing more quickly on the uphill side than that on the downhill side, was reported—empirical data as a function of inclination and separation. Stevens and Webb (1991) performed the experimental study to investigate the local heat transfer coefficients from a constant heat flux surface due to the impingement of a circular liquid jet. The angle of inclinations and Reynolds numbers are varied in the range of 40°–90° and 6,600–52,000, respectively. The shift of the maximum heat transfer points was observed to be extending in the range of 0.5 nozzle diameters. Goldstein and Franchett (1988) measured the local heat transfer characteristics of inclined jet impinging through an opening like square-edged orifice keeping jet Reynolds numbers and jet-to-plate distances in the range of 10,000–30,000 and 4–10 respectively; and developed the Nusselt number correlations from empirical data as a function of inclination and

separation. Ma et al. (1997) carried out an extensive experimental analysis to find out the effect of jet angles in the range of 40°–90° and Reynolds numbers in the range of 235–1,745. Yan and Saniei (1997) undertook a transient experimental study using liquid crystal technique to estimate the rate of heat transfer for an impinging obliquely circular air jet to the flat surface. Jet angles of 45°–90°, Reynolds numbers of 10,000–23,000, and the jet-to-surface spacing of 2–10 are studied.

Oblique impingement of a circular air jet to the flat plate by varying Reynolds number, angles of impingement, and dimensionless distance at 8,200, 30°–90°, and eight respectively in cases of both jet impingement cooling and heating technique for the same geometry were studied by Vipat et al. (2009). For cooling jet, the rise in inclination reduces the local effective temperature values, and in the case of a heating jet, conversely increases the local surface temperature. Despite, the displacement of stagnation points toward the uphill side from the origin of the test plate is observed. The effect of angle of incidence of a flame jet has been studied by Dong et al. (2002) and found that the location of maximum local heat flux shifts away from the geometrical imping point when the angle of incidence reduces. A decrease in the angle of incidence enhances the maximum local heat flux. A numerical study by Agrawal et al. (2010) on heat transfer characteristics of premixed fame impinging upwards to plane surfaces inclined with the flame jet axis shows that the heat flux in the uphill part is higher as compared to that at corresponding locations in downhill part. The local heat flux in the downhill part of the plate increases with a reduction in the plate inclination angle, while in the uphill part, the local heat flux at locations away from the plate center is almost independent of the plate inclination angle. The local heat flux decreases with an increase in heating height, and a fuel-rich mixture upsurges the plate heat flux. Oblique flame jet impingement study by Kuntikana & Prabhu (2016-b) finds that normal impingement is better that oblique impingements for better thermal effectiveness.

2.5   Flame deflectors and heat transfer challenges in missile launching

In the preceding paragraphs, a generalized literature study of jet impingement heat transfer and its heat transfer characteristics have been presented. The ultimate objective of the current research is to study the thermal interaction of the impinging flame jet

over a wedge, in laboratory condition. The same experiment can be extended to a case where the missile exhaust impinges over the flame deflector.

The high thrust rocket engines used in present-day missiles release large quantities of energy in the form of exhaust gases. In other words, the temperature, pressure, the velocity of the exhaust are extremely high. These high-temperature exhaust jets at supersonic velocity, create serious hazards to personnel, ground support structures, and equipment, at the launch platform. The continuing trend toward larger and higher thrust engines makes it essential to understand the thermal behavior of launchpad structures, which are directly impinged by hot exhaust jet. This will certainly help to develop accurate methods in predicting and controlling the exhaust jets. The hot exhaust released from a missile, during launching, impinges directly over flame deflector plate. A schematic diagram of the missile launching system and side view of the flame deflector is shown in figure 2.6.
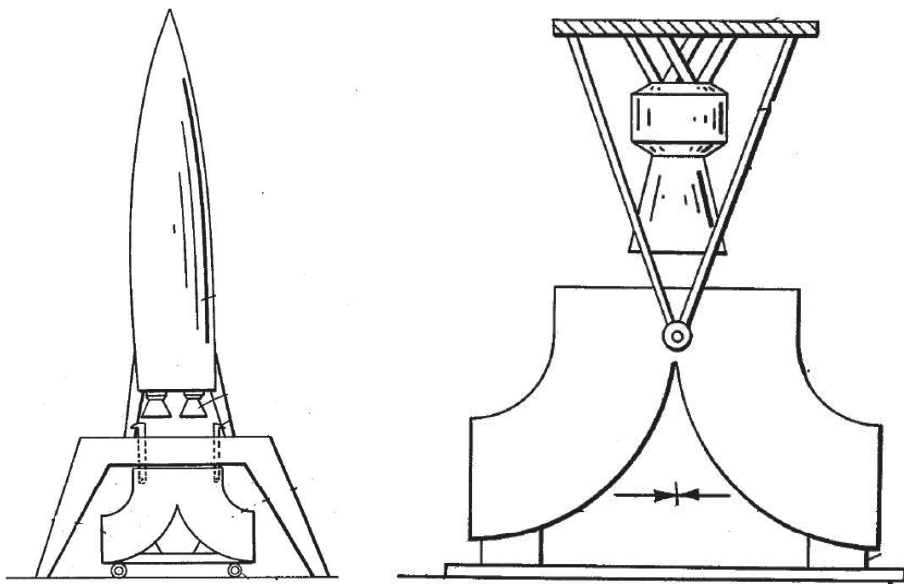
Figure 2.6   **Schematic diagram of the missile launching system and Side view of the flame deflector (Santora et al. 1960).**
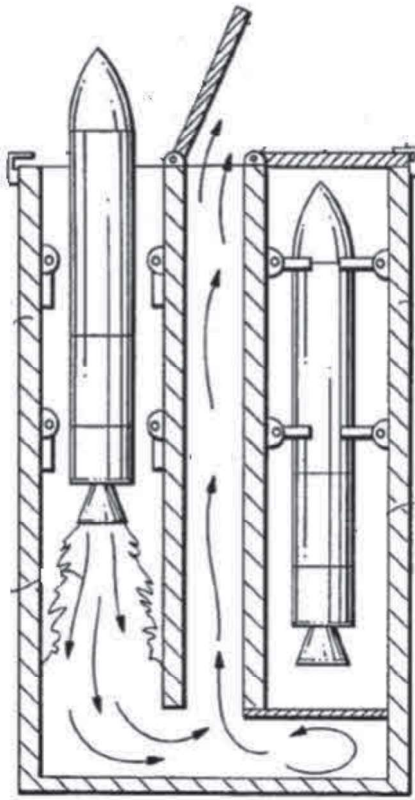
Figure 2.7   Schematic of a Vertical Launching System (VLS) for storing and firing missiles on board a warship (Piesik 1990).

In military applications, missiles ready for launching are safely positioned adjacent to the magazine chamber or the canister. In the contemporary vertical launching system shown in figure 2.7, a missile gathers momentum in exchange for the momentum of its exhaust gases produced during the process of launching. The exhaust deflector gets subjected to the missile exhaust, and then the exhaust flows onto a plenum and moves out through an uptake channel in the vertically upward direction, reported by Piesik (1990). Missile exhaust deflector is used for mechanical deflection of exhaust blast emanating from a solid or liquid-fuelled jet type propulsion unit. A report by Anderson (1961) suggests that it helps to eliminate ground erosion and alleviate dust during missile launching, which in turn reduces the possibility of detection by the enemy. In the case of small size and weight structures like warships, it helps withstand force and

pressure load. Blast deflectors are also designed to balance external forces acting upon it, thereby eliminating time-consuming anchorage of ships.

At the moment of a missile leaving the launcher, the momentum of the missile is about 16% higher than the impulse of rocket thrust and gravity, as reported by Fu & Hao (2015), neglecting the influence of friction force. The missile exhaust stream speeds are typically in the range 1200-1500 m/s (4000-5000 feet per second), and temperature exceeds 3000 K (Yagla 1997), where the recovery temperature and thermal conductivity near the entrance region of the missile exhaust could not be measured view intense heating at the same location. The exhaust gas impinges on a deflector plate for faster spreading and exit of exhaust gases as well as the faster distribution of such high heat flux from the launch pad. The phenomena of heat transfer during the impingement of hot exhaust to the deflector plate are transient in nature. Because of the very high velocity of exhaust, which impinges over the deflector plate, the stagnation point temperature goes up much higher than the exhaust gas temperature.

2.5.1 Vertical Launching System

A **vertical launching system (VLS)** is an advanced system for holding and firing missiles on mobile naval platforms, such as surface ships and submarines. A typical missile launch system of a surface vessel is comprised of a module of eight cells arranged in two rows of four cells each. A schematic diagram of a VLS is shown in figure 2.7. The exhaust gas is allowed to escape through a narrow channel between the rows of cells. Plenum provided at lower end couples all the cells together.

A vertical launch system can be either *hot launch*, where the missile ignites in the cell, or *cold launch*, where the missile is expelled by gas produced by a gas generator, which is not part of the missile itself, and then the missile ignites. In the cold launch, the gases produced are relatively cold compared with rocket engine exhaust temperature. A hot launch system does not require an ejection mechanism but does require some way of disposing of the hot exhaust and heat as it leaves the cell. In the hot launch, the cell must withstand the tremendous heat generated without igniting the missiles in the adjacent cells.

The existing VLS ensures that hot exhaust gases are directed away from the vessel when a missile is launched. The plenum is lined with a relatively thick coating of refractory material to withstand the exhaust temperature and ablation. The flame deflectors are exposed to a very high heat flux of order of tens of megawatts per unit area. This makes rapid heating of key structures, posing a serious concern towards the thermal design of launcher (Yagla, 1997; Kennedy et al. 1998; Briggs et al. 2003). In addition, it also poses a serious concern to the safety and security of weapons and mobile launchers.

2.5.2 Missile flame deflectors

Direct impingement and uncontrolled flow of missile exhaust gases during a launching would create serious hazards to the launch vehicle and ground equipment due to spilling, melting of metallic objects, and dislodgment in the direct impingement area. A flame deflector is a mechanical device placed in the exhaust stream to prevent the blast impinging directly on the launch pad and to channel the exhaust away from the launcher area to reduce or eliminate these hazards. Distribution of the exhaust is controlled by the type and design of the deflector, as reported by Martin et al. (2012); Evans et al. (1963).

In a cooled deflector, the coolant absorbs a large amount of heat from the exhaust, thus reducing the energy in the exhaust stream. An uncooled deflector absorbs only a small amount of the heat and reduces the energy level of the exhaust jet very little when an exhaust jet impinges on the deflector, its velocity decreases while the temperature and pressure increase.

Studies related to 'Refractory materials for flame deflector protection reported by Calle et al. (2010) reveals about the constant deterioration of launchpad flame deflectors. The refractory materials used in the launchpad flame deflectors have become very susceptible to failure, resulting in large pieces of refractory material breaking away from steel based structure, during launches. One of the major reasons for the failure of these refractory materials is high temperature and large temperature variations over short intervals. Convective and radiative heat transfer during liftoff leads too large thermal stresses in refractory material. The repair of these failures is a costly and time-consuming process. Improvised cooling of existing refractory material based flame deflectors will improve the supportability of the launch facility. The required

compressive strength of refractory material used in flame deflector shall be approximately 310 bar (4500 PSI), and maximum heat flux that a refractory material can withstand is approximately around 37000 kW/ m^2.

Cooled deflectors

Water is used to cool the deflector to maintain the temperature of the deflector surface below the melting point of the material used. Several deflector designs of this type have been developed based on different methods of employing the water coolant. One method used is to introduce water into the exhaust stream through spray nozzles located upstream from the deflector to reduce the exhaust temperature and maintain the surface material below the melting point. Another method frequently used is to circulate water through a manifold beneath the deflector plate through which many small holes have been drilled. All, or a portion of, the water may be forced through these holes into the impingement area to provide evaporation and film cooling of the deflector surface.

These methods are effective but require a large water supply, a high capacity pumping and plumbing system, and extensive maintenance, which results in high initial and operating costs. Therefore, this type of cooled deflector is impractical for use with tactical missiles and operational space vehicles. However, when long-duration static firings are required, a water-cooled deflector is usually provided. A static test site, the cooled deflector, provides an additional advantage by reducing the sound pressure level through the reduction of the energy level in the exhaust stream.

Uncooled deflectors

Uncooled flame deflectors must rely on their physical properties to withstand the erosive action and high temperatures of the engine exhaust. They may be generally classified as "heat-sink" or "ablation" type based on the characteristics method of heat transfer employed to control surface temperatures. In a heat-sink type deflector, a material with high thermal conductivity is used to conduct the heat away from the surface rapidly enough to prevent melting. Theoretically, this type of deflector will not lose surface material and should, therefore, have a long life.

An ablation type deflector is designed to take advantage of the erosive effect of the exhaust. The deflector base material is coated with an erodible material with low

thermal conductivity. As the surface material erodes under the action of the exhaust stream, heat is removed with the eroded particles, which reduces the surface temperature and the amount of heat transferred to the base material. Periodic replacement of the erodible surface material is required, depending upon the thickness of the material used, the duration of each exposure, and the rate of erosion. In conclusion, it should be noted that many deflectors depend on the heat-sink principle and ablation material for their operation.

2.5.3   Propellants used in missile

As military missiles or Inter-continental Ballistic Missiles (ICBMs) need to be stored in various conditions for large periods of time and launch at a moment's notice, inert fuels such as hydrazine and other hypergolic fuels are used. Missile propellants are mainly of two types – solid propellants and liquid propellants. In the case of liquid propellants, for example, liquid oxygen (LOX), which must be maintained at a temperature of about 88 K (-300ºF) to prevent excessive boil-off losses, are made storable through the use of storable oxidizer (Sutton 2006). Most of the fuels used in missile propellant combinations are storable at ambient temperatures. Therefore the use of an oxidizer with similar storable characteristics makes a mixture referred to as 'storable propellant.' Few liquid fuels used for rocket propulsion along with corresponding oxidizers are listed below:-

Liquid Fuel	Oxidizer
'92% percent Ethyl achohol.'	LOX
Methyl alcohol/Hydrazine hydrate mixture	LOX
Unsymmetrical dimethylhydrazine (UDMH)	Nitrogen tetroxide or RFNA (Red Fuming Nitric Acid)
50% UDMH / 50% hydrazine	Nitrogen tetroxide or RFNA
Amine mixture	LOX

However, some missiles, because of the difficulties handling and storing liquid fuels, usually military missiles use solid fuel.

2.5.4 Challenges pertaining to heat transfer

Evans et al. (1963) report the temperature distribution in the exhaust (nozzle area ratio 25:1) of an 355 kN (80000 pound) thrust engine having a temperature of 3588 K (6000 °F) within a range radial distance 0.762 m (2.5 feet) and axial distance 15.24 m (50 feet), that is equivalent to nozzle exit stagnation temperature whereas nozzle exit static temperature reported for the same case is 1700 K (2600 °F). The propellant used is a mixture of LOX and RP-I at chamber pressure 45 bar (659 PSI) and nozzle exit pressure 0.2 bar (2.8 PSI). The extract of the report is shown in figure 2.8.

The major problems associated with the design of uncooled flame deflectors evolve from the high rate of heat transfer from the exhaust jet to the deflector surface and the limited heat transfer capabilities of the deflector materials, which must remove this heat rapidly enough to prevent melting. Although the exhaust gases flow over the deflector surface at high velocities, a film of stagnant gas forms next to the surface and acts as an insulator, which reduces the rate of heat transfer to the surface material.
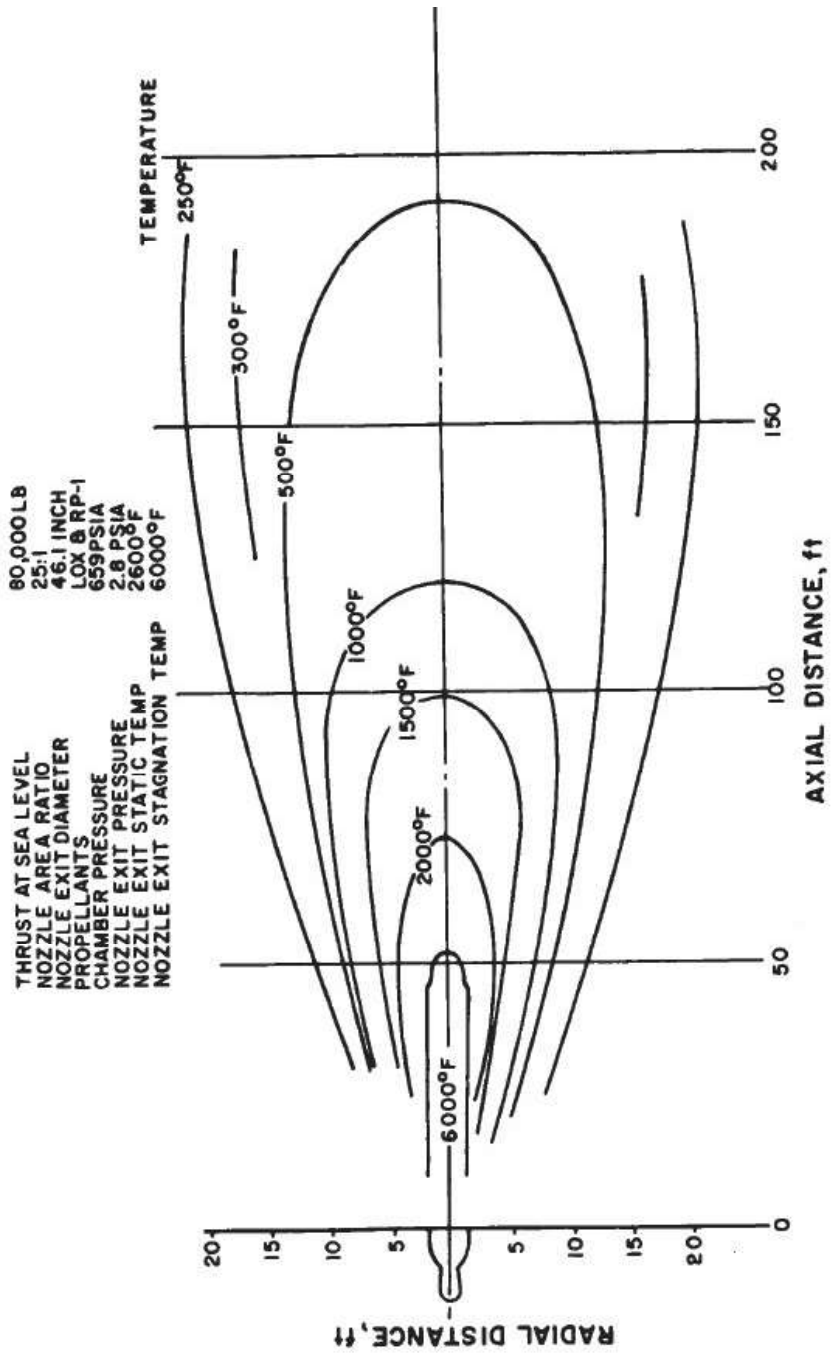
Figure 2.8 Temperature distribution in the exhaust of a 355 kN (80000 pounds) rocket engine (Evans et al. 1963).

2.6   Transient heat conduction techniques

In most such applications such as heat transfer within a furnace, heat transfer from the exhaust of a missile to the deflector plate in the launchpad, or heat transfer due to air friction over the spacecraft entering earth atmosphere; transient mode of heat transfer involves lower heat transfer rate. The boundary conditions involving both convection and radiation remain transient. These kinds of transient heat conduction problems having transient boundary conditions are easy to solve analytically by using Green's Function approach (Fernandes et al. 2015; Ozısık 1993) being the most general and powerful mathematical technique for solving transient and nonhomogeneous conduction problems. The most fundamental principle behind Green's function is that solution of any such problem having any kind of boundary conditions can be expressed analytically only in terms of Green's function. It has been mathematically established (Morse and Feshbach 1953; Ozisik 2002; Carslaw and Jaeger 1959) that once the Green's function of a given problem is established, in case of conduction problems, the temperature distribution can be easily expressed.

The need to have a transient study to predict thermo-physical changes at an inaccessible location leaves no choice but to choose inverse heat conduction technique (Colaço et al. 2006; Orlande 2012; Naphon et al. 2019; Beck et al. 1985). In an inverse problem, the unknown cause(s) are estimated from the knowledge of effect. One such experimental scenario of methane-air flame jet impingement, heating a flat stainless steel plate, is considered to demonstrate the analytical inverse methodology for simultaneous estimation of two parameters, namely heat transfer coefficient and adiabatic wall temperature at impinging face from the knowledge of transient temperature at the non-impinging face. It may be noted that the heat transfer coefficient and adiabatic temperature are fundamentally dependent on each other, and cannot be estimated separately. Knowledge of both these parameters with a higher degree of accuracy is critical from two perspectives. One such thermal properties cannot be measured, but estimated and second, accurate estimation of these thermal properties holds a great deal of importance for practical applications towards understanding the thermal behavior.

This technique does not require any information about the flow dynamics, which is a very complex phenomenon. Measurement of transient temperature at non-impinging face using IR camera is relatively convenient as compared to the measurement of any thermodynamic parameter at the impinging face. Higher accuracy for the desired duration of time and a higher spatial resolution in measuring the transient temperature at the accessible face (non-impinging face) are the reasons to use the IR camera. The rear face is painted black to have a higher possible value of emissivity, as is a requirement of a thermal imaging camera. The scope of the research work is to develop a transient inverse heat conduction technique while accounting transient convective boundary conditions and radiation heat loss using Green's function within a Stainless Steel flat plate and predict the convective heat transfer characteristics at the impinging surface (wedge-shaped object).

2.7   Summary of Literature Review

A detailed literature study to summaries the concept of jet impingement heat transfer is carried out along with various techniques to predict the jet impingement rate of heat transfer. Additionally, a comprehensive review of heating effects on a missile deflector plate is undertaken. Following conclusions are drawn from the reported literature:-

(a)   The phenomenon of heat transfer from an impinging jet is complex because of its complex flow structure, transient nature, and dependence on multiple physical as well as geometrical parameters. Convective mode of heat transfer plays a major role in jet impingement heat transfer, and most of the studies are limited to it. Most studies pertaining to the estimation of heat transfer characteristics of impinging jets ignore the effect of radiation.

(b)   Though convection is the primary mode of heat transfer from an impinging flame jet, a fundamental understanding of the relative importance of radiative versus convective heat transfer in flame jet impingement heat transfer requires improvement for predicting heat transfer characteristics with higher accuracy in high-temperature applications. Additionally, the number of transient studies pertaining to jet impingement heat transfer are limited.

(c)   There exists no analytical technique, which can estimate both convection heat transfer coefficient and adiabatic wall temperature at the impinging face by considering both convection and radiation heat transfer at the exposed surfaces. These convective paramters such as heat transfer coefficient and adiabatic wall temperature, which are inter-related with each other, remain a key area of study.

(d)   No scientific studies have been undertaken to analyse heat transfer characteristics of a flame jet impinging onto a wedge-shaped structure, where the edge of the wedge is being impinged by a flame jet so that the flame gets split into two halves. This kind of study resembles with missile exhaust impingement over the deflector plate, where the missile exhaust is forced to get deflected immediately after exiting from the exhaust plume. The thermal impact of the exhaust on a deflector plate is similar to that of a flame jet impinging on the edge of a wedge.

2.8   Research gaps

An extensive literature review is undertaken in this study. The complexity, criticality, and transient nature of impinging jet heat transfer bring in the difficulty to capture the thermal variations experimentally within the jet impingement region to understand the true heat transfer characteristics in various applications. Based on the conclusions drawn, two major research gaps have been identified. The proposed plan of work is to establish an analytical technique to study heat transfer characteristics of an impinging jet having radiation corrections and study the heat transfer characteristics of a methane-air flame jet impinging over a wedge-shaped object equivalent to high-temperature missile exhaust being impinged over a flame deflector.

2.8.1 **Technique to estimate convective heat transfer coefficient and adiabatic wall temperature simultaneously.** Various studies explain that the phenomenon of jet impingement heat transfer is complex because of its inherent transient nature. Further, the complexity increases as the temperature of the jet become extremely high or low. Prediction of local heat transfer characteristics is also equally difficult to explain the heat transfer characteristics or other natural phenomena taking place during impingement. In addition to these, the prediction of internal temperature distribution within the jet or the impinging body remains another challenge.

Research gap 1: There have been active studies going on to develop analytical models and modern devices to estimate the exact heat transfer coefficient and adiabatic wall temperature for various advanced engineering applications. For a case of flame jet heat transfer, which is transient in nature, it's important to develop a mathematical model as well as a standard technique to estimate the convective heat transfer coefficient and adiabatic wall temperature simultaneously. In the case of high-temperature impinging jet applications, radiation effects need to be considered part of the analysis. It may be noted that problems of this nature will have transient convective as well as radiation boundary conditions. Suitable mathematical techniques such as Green's function need to be adopted as part of the solution procedure.

2.8.2 **Heat transfer characteristics of a wedge at high temperature.** Supersonic jet impingement occurs extensively in the applications of rocket and aerospace, such as vertical/short aircraft take-off, multistage rocket separation, and missile launching. The concentric canister launcher (CCL) is an important concept of vertical launching system (VLS) for launching missiles from surface ships and submarines. When the jet plume with high speed and high-temperature exhausts from the missile impinges on the hemispherical end cup of CCL, then the design challenge of the CCL is to contain the impact of high-speed hot jet flows on the deflector and safe discharge of same, away from the launch pad. The exhaust gas impinges on the deflector plate as a jet. The resulting temperature at the stagnation point is generally very high up to 3500K, which develops a very high transient heat flux at the deflector plate. Heat transfer from high-temperature gases to axis-symmetric and blunt-nosed bodies has been studied, and several semi-analytic solutions have been proposed for calculating such fluxes.

Research gap 2: Missile launching technology has developed very fast in the last few decades. A lot of effort is still on to improve the same to match the advanced and strategic military requirements, mainly the higher thrust of the missile system. As the thrust power of the missile or rocket improves, it's natural to encounter higher temperature of the working fluid. A detailed study of thermo-physical behavior of heat transfer distribution over the deflector plate being impinged by hot exhaust lacks in literature.

2.9 Aims and objectives

Based on the literature review and existing research gaps, the aim of this study is as below:-

(a)   To develop an analytical technique to estimate convective heat transfer coefficient and the adiabatic wall temperature over a flat plate, due to flame jet impingement, from a known temperature history; and validate the same experimentally.

(b)   To study the heat transfer characteristics over a wedge-shaped object for varying wedge-angle of test object, Reynolds number of methane-air flame jet and burner to deflector plate distance, experimentally.

The objectives of the present study are,

(a)   To undertake studies on experimental as well as analytical techniques on flame jet impingement to study heat transfer characteristics at the impinging face.

(b)   To develop an analytical inverse heat conduction technique using Green's function to estimate the heat transfer coefficient and reference temperature at the impinging face.

(c)   To undertake a parametric study on flame jet impingement over flat and wedge-shaped Stainless Steel surface at varying experimental conditions such as Reynolds number 800, 1000, and 1200; non-dimensional nozzle tip to impinging surface distance 2, 4 and 6; wedge-angle 90° and 120°.

Chapter 3

IHCP MODELLING USING GREEN'S FUNCTION

3.1   Heat transfer

Because of the nature of the impinging jet's flow structure, the convection mode of heat transfer remains the main contributor to heat transfer during jet impingement. Mostly the heat transfer remains transient. The rate of heat transfer based on Newton's law of cooling is stated as,

$$q = h \ (T - T_{aw}) \tag{3.1}$$

Here, knowledge of convection heat transfer coefficient (h) and adiabatic wall temperature (T_{aw}) is critical from a scientific point of view. Knowledge of these two parameters remains the focus area of research. When fluids encounter solid boundaries, the fluid in contact with the wall is at rest and viscous effects, thus retard a layer in the vicinity of the wall. For large Reynolds Numbers, these viscous layers are thin compared to it's length. When the wall is at a different temperature than the fluid temperature, there is similarly a small region where the temperature varies across the layer. These regions are the velocity and thermal boundary layers. It is imperative, concerning equation 3.1, to mention that none of the physical parameters at the impinging face are known in any real-life situation. It is practically impossible to directly measure these parameters to view the transient nature of heat transfer and space constraints in actual or experimental situations. Additionally, measuring instruments do obstruct the impinging jet. In the case of high-temperature heating or cooling impinging jet applications, most of the measuring instruments get damaged, and hence, measurements remain unreliable. Therefore, direct measurement of any of the physical parameters at the impinging face is not recommended in any impinging jet study.

The Blasius solution to express the heat transfer in terms of flow conditions shows that Nusselt number can be expressed as

$$Nu_x = 0.332 \, Pr^{1/3} \, Re_x^{1/2} \quad (0.5 < Pr < 15) \tag{3.2}$$

Equation 3.2 simply shows that with a rise in Reynolds number; the Nusselt number and hence the heat transfer coefficient improves. When the Reynolds number increases a relatively smaller thermal boundary layer thickness exists. This reduction in boundary layer thickness lowers the thermal resistance, thereby increasing the heat flux within the boundary layer. A transient study (for Re = 14000 to 34000 for W/d = 4 to 8) on effects of surface roughness on the average heat transfer of an impinging air jet by Beitelmal et al. (2000) has concluded that surface roughness disrupts the boundary layer and promotes turbulence of the wall jet, which increases heat transfer. The average Nusselt number was increased by up to 6% over the whole surface area. A 0.5-mm-high circular array of protrusions were used to create roughness over the surface. In a similar study on heat transfer distribution of premixed methane-air laminar flame jets (Re = 600 to 1800 for W/d = 2 to 4) impinging on ribbed surfaces (0.5-mm-high circular, triangular, square ribs) by Kadam et al. (2019) reports no significant improvement in heat transfer distribution in case of laminar flame jet impingement on ribbed surfaces.

It may be noted that direct measurement of any parameter at non-impinging face may be convenient and accurate, because the temperature and the rate of temperature change are relatively lower than those at impinging face. In most of the cases, the non-impinging face is accessible. In the present study of estimating convection heat transfer characteristics of impinging jets requires estimation of both heat transfer coefficient and adiabatic wall temperature, simultaneously. Both these parameters are closely associated with each other, and are related based on Newton's law of cooling as well as the boundary layer concept. Therefore, the simultaneous estimation of these parameters is appropriate. These kinds of problems fall under the category of multivariate problems to be solved using the IHCP concept.

Any IHCP solution procedure requires a forward model. A forward model is nothing but an analytical or a numerical conduction heat transfer equation for estimating the theoretical value of the measurable parameter based on assumed values of the parameters to be estimated. In the present case, the measured parameter is transient temperature at the non-impinging face, and parameters to be estimated are both heat transfer coefficient and adiabatic wall temperature at impinging face. The forward

model is chosen to be one-dimensional heat conduction across a flat plate and solved analytically, considering convection as well as radiation heat transfer at both impinging and non-impinging faces. It may be noted that both the boundary conditions are transient during impingement, which helps to avoid any kind of fluid flow situation within or outside the boundary. Solution procedure to solve the forward model with transient-convection boundary conditions with radiation correction is made simple by using Green's function. The same may be followed by our previous work on an analytical solution to the transient IHCP technique using Green's function.

3.2   Transient heat conduction using Green's function

Let a flat stainless steel plate be impinged by a methane-air flame jet at the stagnation point, 'O' as shown in figure 3.1. The plate thickness is 'a.' The plate is impinged at one face (say front face) for 5 seconds, and the temperature variation at the opposite face (say rear face) is measured using a thermal imaging camera for the same duration. Methane-air flame jet at Reynolds number equals to 1000 and equivalence ratio equal to one with a non-dimensional burner tip to impingement plate distance equal to four is discussed in this study to demonstrate the proposed methodology. Due to the radial distribution of flame, the surface area being impinged is circular.
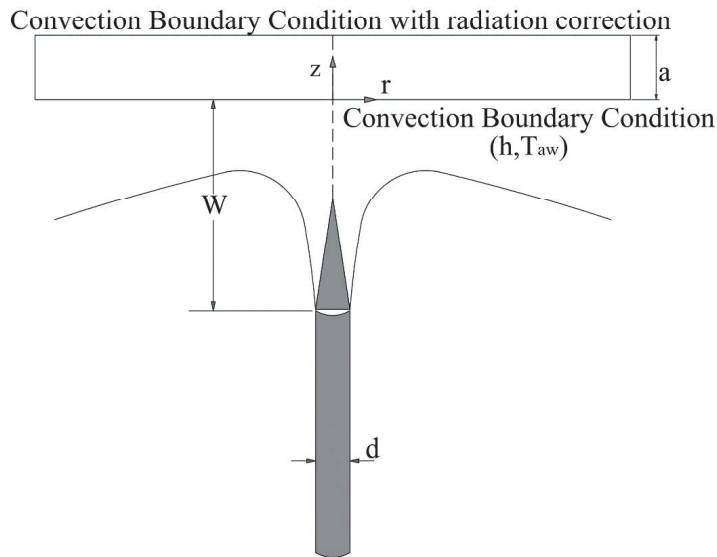
Figure 3.1   Schematic representation of a flame jet impinging a flat plate.

The current case is axisymmetric. The primary mode of heat transfer from the flame to plate at the impinging surface is forced convection, and the same within the plate material is pure conduction. The lateral conduction within the plate is assumed to be negligible compared to the conduction across the plate because of a relatively lesser temperature gradient in the lateral direction. In this experiment, the plate thickness is kept much lesser than the length (approx. 1:8). Therefore, one-dimensional conduction across the plate is considered suitable for analysis. The boundary conditions at both faces are transient. The heat absorbed at the impinging face is due to both radiation and convection, and the same is considered as heat transfer in the form of convective boundary conditions. The effect of temperature on the thermal properties of the impinging plate is assumed to be negligible.

The mathematical formulation of the problem under consideration is given by,

$$\frac{\partial^2 T}{\partial z^2} = \frac{1}{\alpha} \frac{\partial T}{\partial t} \quad \text{in } 0 < z < a, \quad t > 0 \tag{3.3}$$

The boundary conditions are,

$$-k \frac{\partial T}{\partial z} = h\left(T_{aw} - T\right) \quad \text{at } z = 0, \quad t > 0 \tag{3.3.1}$$

$$-k \frac{\partial T}{\partial z} = h_{nat}\left(T - T_{amb}\right) + \in \sigma\left(T^4 - T_{amb}^4\right) \quad \text{at } z = a, \quad t > 0 \tag{3.3.2}$$

And the initial condition is,

$$T(z,0) = g(z) \quad \text{in } 0 < z < a \tag{3.3.3}$$

The heat loss accounted at the rear face (i.e., $z = a$), a function of time is expressed at equation (3.4) below, and the same can be evaluated as the temperature at the non-impinging face can be measured experimentally. The heat transfer coefficient for natural convection and the emissivity of the surface can be noted from the standard data table. For simplifying the problem at equation (3.3), let us assume $\theta = T - T_{amb}$, where T_{amb} is the ambient temperature and

$$h_{nat}\left(T(a,t) - T_{amb}\right) + \in \sigma\left(T(a,t)^4 - T_{amb}^4\right) = q(t) \tag{3.4}$$

Accordingly, equation (3.3) gets transformed as below,

$$\frac{\partial^2 \theta}{\partial z^2} = \frac{1}{\alpha} \frac{\partial \theta}{\partial t} \quad \text{in } 0 < z < a, \quad t > 0 \tag{3.5}$$

$$-\frac{\partial \theta}{\partial z} + H\theta = H\left(T_{aw} - T_{amb}\right) \quad \text{at } z = 0, \quad t > 0 \tag{3.5.1}$$

$$\frac{\partial \theta}{\partial z} = -\frac{q(t)}{k} \quad \text{at } z = a, \quad t > 0 \tag{3.5.2}$$

$$\theta(z, 0) = g(z) - T_{amb} \quad \text{in } 0 < z < a \tag{3.5.3}$$

where

$$H = \frac{h}{k} \tag{3.5.4}$$

The boundary condition at z = 0 (inaccessible front face) is unknown, as both the heat transfer coefficient and adiabatic wall temperature at that face are unknown. Equation 3.5 and its boundary conditions are non-homogenous. The exact analytical expression for transient temperature distribution across the plate thickness is obtained using Green's function. The detailed derivation for the Green's function is explained at appendix A.

The expression of the Green's function for the problem under consideration is

$$G\left(z, t \middle| z', \tau\right) = \sum_{n=1}^{\infty} \frac{2\left(\lambda_n^2 + H^2\right)}{a\left(\lambda_n^2 + H^2\right) + H} * \cos\left(\lambda_n\left(a - z\right)\right) * \cos\left(\lambda_n\left(a - x'\right)\right) * e^{-\lambda_n^2 \alpha(t - \tau)} \tag{3.6}$$

where, $\lambda_n \tan(\lambda_n a) = H$, n = 1,2,3, ... $\tag{3.6.1}$

The eigenvalues (λ_n) are the roots of the transcendental equation (3.6.1).

The solution of the set of differential equations mentioned at equation (3.5) in terms of Green's function (Ozısık, 1993) is,

$$\theta(z,t) = \int_0^a G\left(z, t \middle| z', 0\right)\left(g(x') - T_{amb}\right)dz' + \alpha \int_{\tau=0}^t G\left(z, t \middle| 0, \tau\right) * H\left(T_{aw} - T_{amb}\right)d\tau$$

$$+ \alpha \int_{\tau=0}^t G\left(z, t \middle| a, \tau\right) * \frac{\left(-q(\tau)\right)}{k} d\tau \tag{3.7}$$

The initial temperature at equation (3.3.3) can be taken equals to the ambient temperature (T_{amb}), because the impingement plate before flame impingement was at atmospheric condition. Therefore, the term "$\left(g(z') - T_{amb}\right)$" in equation (3.7) is

approximately equal to zero, and the first term of equation (3.7) can be neglected. Equation (3.7) gets simplified as

$$\theta(z,t) = \alpha \int_{\tau=0}^{t} G(z,t|0,\tau) * H(T_{aw} - T_{amb}) d\tau + \alpha \int_{\tau=0}^{t} G(z,t|a,\tau) * \frac{(-q(\tau))}{k} d\tau \qquad (3.8)$$

Introducing the Green's function expressed at equation (3.6) to equation (3.8) above, and upon simplifying, the exact analytical expression for transient temperature distribution across the plate, which is the forward model for the problem under consideration, is given by

$$T(z,t) = T_{amb} + \alpha \sum_{n=1}^{\infty} \frac{2(\lambda_n^2 + H^2)}{a(\lambda_n^2 + H^2) + H} * \cos(\lambda_n(a-z))$$

$$* \left[\cos(\lambda_n a) * H(T_{aw} - T_{amb}) * \int_{\tau=0}^{t} e^{-\lambda_n^2 \alpha(t-\tau)} d\tau + \int_{\tau=0}^{t} \frac{(-q(\tau))}{k} e^{-\lambda_n^2 \alpha(t-\tau)} d\tau \right] \qquad (3.9)$$

3.3 Transient inverse heat conduction procedure

If an unknown cause is predicted from the knowledge of its effect, the problem is categorised as inverse problem. In a direct problem, the cause is known, and the effect is determined. In the current case of impinging flame jet, the heat flux and hence the heat transfer characteristics at the impinging face is the unknown cause; and the effect of the same is the transient temperature variation within the impinging body. In other words, the measured transient temperature at the rear face is the known effect of jet impingement heating at the impinging face. Two unknown parameters are to be evaluated; first, heat transfer coefficient and second, adiabatic wall temperature at the impinging face. The only measurable data is the temporal variation of temperature over the plate surface but opposite to the impinging face. Concerning equation (3.9), measurable transient temperature (at LHS) is the effect, whereas 'H' and 'T$_{aw}$' are the unknown physical quantities, which are to be estimated.

Experimentally measured temporal variation of temperature at a predefined location over the surface of the impingement plate opposite to the impinging face is termed as Measured Variable (MV). Estimated Variable (EV) corresponding to the same location

and time with respect to MV can be evaluated using the forward model expressed at equation (3.9). The difference between MVs and EVs is the error component associated with the analytical estimation. The objective function of the inverse heat conduction problems under consideration is nothing but a Least Square Error (LSE) function. The sum of the square of the difference between MVs and EVs at each time step constitutes the Least Square Error (LSE) function. Such problems fall within the ambit of single-objective optimisation, where an objective function is to be minimised, and the corresponding values of the unknown variables (unknown causes) are the solution to the problem. Mathematically, the objective function is given by

$$F\left(h, T_{aw}\right) = \sum_{m=1}^{N} \left(MV_m - EV_m\right)^2 = \sum_{m=1}^{N} \left(T_{measured} - T_{estimated}\right)^2_m \tag{3.10}$$

Where, m = 1,2,3…N, the time steps

In the matrix form, equation (3.10) can be written as

$$F\left(h, T_{aw}\right) = \left(MV - EV\right)\left(MV - EV\right)^T \tag{3.11}$$

Where MV = [MV$_1$ MV$_2$ MV$_3$ … MV$_N$] (3.11.1)

and EV = [EV$_1$ EV$_2$ EV$_3$ … EV$_N$] (3.11.2)

The minimisation of the objective function expressed in equation (3.10) can be undertaken in two ways - the conventional methods and non-conventional methods of optimisation. Levenberg-Marquardt Algorithm (LMA) for Parameter Estimation, Conjugate Gradient Method for Parameter Estimation, and Conjugate Gradient Method with Adjoint Problem for both parameter estimation and function estimation fall under the category of conventional methods. Most of the real-life engineering optimisation problems are mathematically nonlinear, having multiple local extremes (maximum or minimum) while having a single global maximum or minimum and requirement of having more than one unknown parameter to estimate. The existing conventional methods of optimisation are problem-specific and faster as well as accurate for a given problem. Similarly, the non-conventional methods such as Genetic Algorithm and Particle Swarm Optimisation are more robust while having much lower mathematical complexities. The non-conventional methods of optimisation are more likely to search

the global maxima or minima of a wide variety of problems as desired while being slow in approaching the optimum solution. When a problem is proposed to be solved using an inverse technique, the nonlinearity of the forward problem and the higher possibility of having more than one unknown are the significant challenges.

In the current study, the optimisation technique used is the Levenberg-Marquardt Algorithm (LMA) reported by (Marquardt, 1963), which is an iterative method, suitable for handling highly nonlinear problems pertaining to parameter estimation. The solution procedure requires the computation of the Jacobian matrix. A Jacobian is defined as the rate of change of Estimated Variable with respect to the unknown parameter. Mathematically, Jacobian is expressed as

$$J_{m,n} = \frac{\partial \left(m^{th} Estimated\_Variable \right)}{\partial \left(n^{th} Unknown\_Parameter \right)}$$

(3.12)

Where 'm' is the time step, and 'n' is the iteration number.

Data Reduction

Levenberg-Marquardt Algorithm (LMA), a modified version of the Gauss-Newton Algorithm (GNA), minimises the difference between MVs and the forward model that approximates MVs by following an iterative procedure. The iterative process of searching the optimum value of unknown parameters by analysing the experimental data is discussed in this section. The general mathematical form of the forward model expressed in equation (3.9) is

$$T(z,t) = f\left(z,t,h,T_{aw},T_{amb},k,\alpha,\in,\sigma \right)$$

(3.13)

The experimental measurements (MV) are taken only on the impinging plate surface at z = a. Therefore, EVs are also required to be evaluated at the same location and hence, equation (3.13) can be modified as

$$T(t) = f\left(a,t,h,T_{aw},T_{amb},k,\alpha,\in,\sigma \right)$$

(3.14)

Where, h and T_{aw} are unknown constants, and $a,T_{amb},k,\alpha,\in,\sigma$ are known constants. Equation (3.14) is the general form of the forward model considered for the

implementation of the inverse heat conduction problem. The actual error associated with the estimated value of temperature compared with the measured value of temperature, corresponding to the mth time step is defined as

$$e_m = T_{measured}(t_m) - T_{estimated}(t_m)$$

(3.15)

The error function at equation (3.15) can be rewritten as,

$$e_m = T_{measured}(t_m) - f(a, t_m, h, T_{aw}, T_{amb}, k, \alpha, \in, \sigma)$$

(3.16)

In the present case, this objective function is nonlinear. The mathematical function at equation (3.16) is expanded using Taylor's series h T_{aw} to obtain a linear form. Such a linearisation procedure is a standard procedure for LMA. The initiation of the iteration is done with a suitably assumed initial guess value of the parameters to be estimated. These initial values are decided based on experience. For example, the adiabatic wall temperature will certainly be below flame temperature and can never be negative. The localised linear form of the function at equation (3.14), when expanded using Taylor's series, at any iteration 'n' is expressed as

$$f(t_m)_n = f(t_m)_{n-1} + \frac{\partial f(t_m)_{n-1}}{\partial h} \Delta h_{n-1} + \frac{\partial f(t_m)_{n-1}}{\partial T_{aw}} \Delta T_{aw,n-1} + HigherOrderTerms$$

(3.17)

Re-writing equation (3.16), by substituting equation (3.17), the estimated error at m^{th} time step of nth iteration and can be expressed as,

$$e_{mn} = T_{MV}(t_m) - f(t_m)_{n-1} - \frac{\partial f(t_m)_{n-1}}{\partial h} \Delta h_{n-1} - \frac{\partial f(t_m)_{n-1}}{\partial T_{aw}} \Delta T_{aw,n-1} - HigherOrderTerms$$

(3.18)

Further, by associating the higher-order terms of equation (3.18) into its error component, the equation can be simplified as,

$$T_{MV}(t_m) - f(t_m)_{n-1} = \frac{\partial f(t_m)_{n-1}}{\partial h} \Delta h_{n-1} + \frac{\partial f(t_m)_{n-1}}{\partial T_{aw}} \Delta T_{aw,n-1} + E_{mn}$$

(3.19)

Where E_{mn} is the modified error component at m^{th} time step of the nth iteration, which is the sum of both higher-order terms and e_{mn}. And,

$$\Delta h_{n-1} = h_n - h_{n-1} \tag{3.20}$$

$$\Delta T_{aw,n-1} = T_{aw,n} - T_{aw,n-1} \tag{3.21}$$

Equation (3.17) is now expressed in the form of a linear (locally) mathematical equation and the set of equations at all the time step (in matrix form) are expressed as

$$[D_{n-1}] = [Z_{n-1}][\Delta P_{n-1}] + [E_n] \tag{3.22}$$

Where,

The forcing function at n^{th} iteration, $D_{n-1} = \begin{bmatrix} T_{MV}(t_1) - f(t_1)_{n-1} \\ T_{MV}(t_2) - f(t_2)_{n-1} \\ T_{MV}(t_3) - f(t_3)_{n-1} \\ \dots \\ \dots \\ T_{MV}(t_N) - f(t_N)_{n-1} \end{bmatrix} \tag{3.23}$

The Jacobean matrix at n^{th} iteration, $Z_{n-1} = \begin{bmatrix} \dfrac{\partial f(t_1)_{n-1}}{\partial h} & \dfrac{\partial f(t_1)_{n-1}}{\partial T_{aw}} \\ \dfrac{\partial f(t_2)_{n-1}}{\partial h} & \dfrac{\partial f(t_2)_{n-1}}{\partial T_{aw}} \\ \dfrac{\partial f(t_3)_{n-1}}{\partial h} & \dfrac{\partial f(t_3)_{n-1}}{\partial T_{aw}} \\ \dots & \dots \\ \dots & \dots \\ \dfrac{\partial f(t_N)_{n-1}}{\partial h} & \dfrac{\partial f(t_N)_{n-1}}{\partial T_{aw}} \end{bmatrix} \tag{3.24}$

The unknown matrix $\Delta P_{n-1} = \begin{bmatrix} \Delta h_{n-1} \\ \Delta T_{aw,n-1} \end{bmatrix} \tag{3.25}$

The error matrix, which is to be minimised, $E_n = \begin{bmatrix} (Error)_{t_1} \\ (Error)_{t_2} \\ (Error)_{t_3} \\ \dots \\ \dots \\ (Error)_{t_N} \end{bmatrix}$ (3.26)

Using the approach of least square minimisation of error (Colaço, 2006; Marquardt, 1963), the optimised form of equation (3.22) is given by

$$\Delta P_{n-1} = \left[Z_{n-1}{}^T Z_{n-1} + \lambda_{n-1} \Omega_{n-1} \right]^{-1} Z_{n-1}{}^T D_{n-1} \tag{3.27}$$

Where, 'λ' is the damping coefficient, the numerical value of which is to be chosen suitably depending on the input data and 'Ω' is the diagonal matrix of $[Z_{n-1}{}^T Z_{n-1}]$. The value of the damping coefficient may be reduced or increased suitably over iterations if the objective function value reduces or increases.

With the knowledge of ΔP_{n-1} from equation (3.27), and by using equations (3.20 and 3.21), the value of both the parameters for n^{th} iteration can be estimated. When the estimated values of Δh and ΔT_{aw} attain a predefined limiting value, the iteration can be terminated. The corresponding values of h and T_{aw} are the desired solution.

3.4   **Uncertainty analysis**

The solution procedure of the transient IHCP is an iterative process, which undertakes a nonlinear regression. Uncertainty estimation procedure followed in this work is in accordance with the guidelines of 'Guide to the Expression of Uncertainty in Measurement' by ISO and 'Technical Note 1297' of National Institute of Standards and Technology (NIST). The uncertainty in the simultaneous estimation of two unknown parameters using IHCP is predicted using the Monte Carlo technique. The Monte Carlo technique for uncertainty estimation proposed by Cox and Siebert (2006); Kuczera and Parent (1998) and Hu et al. (2015) is based on a theoretical probability distribution of a variable.

We know, the uncertainty of a measurement can be determined by repeating the measurement to arrive at an estimate of the standard deviation of the measurand. It depends on the accuracy and precision of the measuring instrument. Similarly, the uncertainty of the solution procedure of IHCP is determined by repeating the same procedure for multiple numbers of sample input data generated using the normal distribution, a probabilistic approach. The samples are generated using a normal cumulative distribution technique. The fundamental inputs while generating the population are the exact mean, the standard deviation of the experimentally measured set of transient temperature, and randomly generated probability value. The sample size is kept equal to the size of the exact sample, measured experimentally. A higher number of populations will result in a better estimate of uncertainty.

In this study, the number of samples in each case is restricted to 500. Each randomly generated population of transient temperature is then treated as an input for IHCP analysis, and the corresponding values of h and T_{ref} are estimated. This way, for a given location on the impinging surface, 500 sets of h and T_{ref} are estimated. The estimated values of both the unknown parameters in all 500 samples do not follow a normal distribution. The only reason for the non-conformance of a normal distribution is the nonlinear forward problem considered in IHCP. Therefore, 95% confidence interval for both the unknown parameters, h and T_{ref} is considered while rejecting those samples which are within 2.5% of either extreme. Subsequently, the standard deviation of each parameter, which in turn is nothing but uncertainty is estimated. An in-house computer code is developed for uncertainty estimation using Monte Carlo technique. The same is included in Appendix E of the thesis.

Chapter 4

EXPERIMENTAL PROCEDURE AND ADOPTED ANALYTICAL METHOD

4.1 Design of experimental setup – Flame jet impingement over a flat plate

An experimental setup is designed to record the transient temperature of a metallic plate being impinged by a methane-air flame jet at a predefined Reynolds number and nozzle tip to plate distance. The experimental setup schematic is shown in figure 4.1, and a photograph of the laboratory set up is given in figure 4.2. The impingement plate material, in this case, is Stainless Steel. The plate thickness is 3 mm. The design of the setup is such, the impinging face is inaccessible and supposed to be very hot. The transient temperature of the accessible face (or the non-impinging face) is measurable using a thermal imaging camera. Key components of the experimental setup are thermal imaging camera (Model – FLIR A325Sc), compressor, methane rotameter, and air rotameter, cylindrical tube type stainless steel burner of internal diameter 10 mm and thickness 1 mm. The IR camera is having a resolution of 320 x 240 pixels, measurable temperature range up to 2000°C, and a recording speed of 60 frames per second (fps). The accuracy of temperature measurement varies within 2% of the actual temperature. Very high resolution in temperature measurement (both spatial and temporal) is possible, and effective when transient data analysis is necessary. Additionally, the thermal imaging camera is not required to be in physical contact with the target surface for temperature measurement.

The thermal imaging camera captures the Infrared (IR) radiations from the hot surface and senses the corresponding thermal intensity to measure temperature. The target surface is painted black, as it is a requirement of the thermal camera to maintain higher emissivity for better accuracy in measuring temperature. The numerical value of the emissivity of the rear surface is taken as 0.95 for all calculation purposes (Brandt et al. 2008). Rear face experiences natural convection, as the experiment is conducted in a closed room at room temperature and pressure with no external airflow over the plate. Current experimental data shows that the average change (from start to end of the

experiment) in surface temperature at non impinging face is 10 Kelvin. Corresponding Rayleigh number is an order of 10^6.
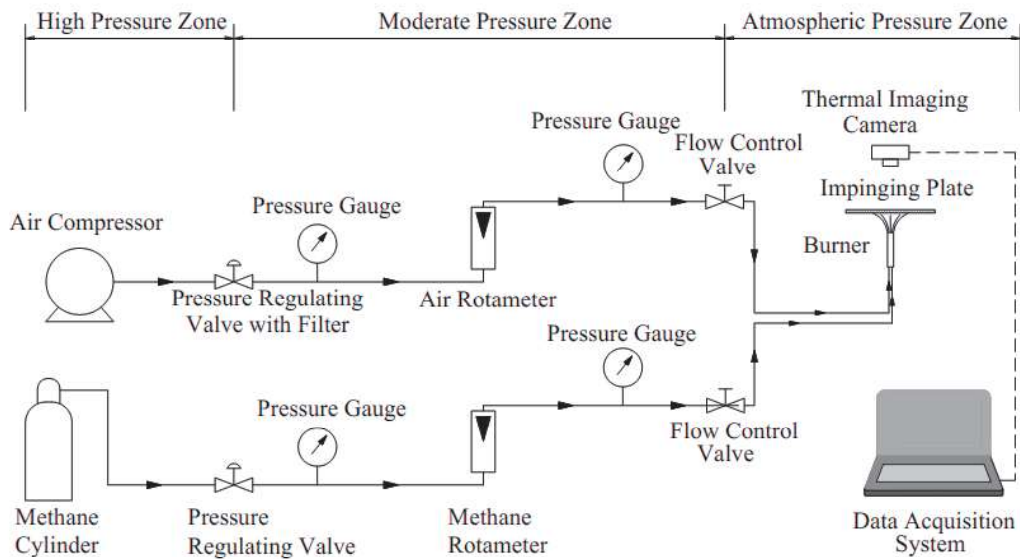
Figure 4.1   Schematic of the experimental setup for flame jet impingement.

Based on the fundamental studies (Bejan, 2013) on Natural convection over a flat plate, the average heat transfer coefficient (h_{nat}) at the rear face, is found to be 5 Wm^{-2}K^{-1}. The flow rate of air rotameter operated at 3 bar ranges from $1500 - 15000$ ml per min, whereas the same for methane rotameter is $150 - 1500$ ml per min. Rotameters are calibrated up to 3 bar using standard soap bubble meter at atmospheric conditions. A detailed calibration procedure is discussed in succeeding paragraphs.
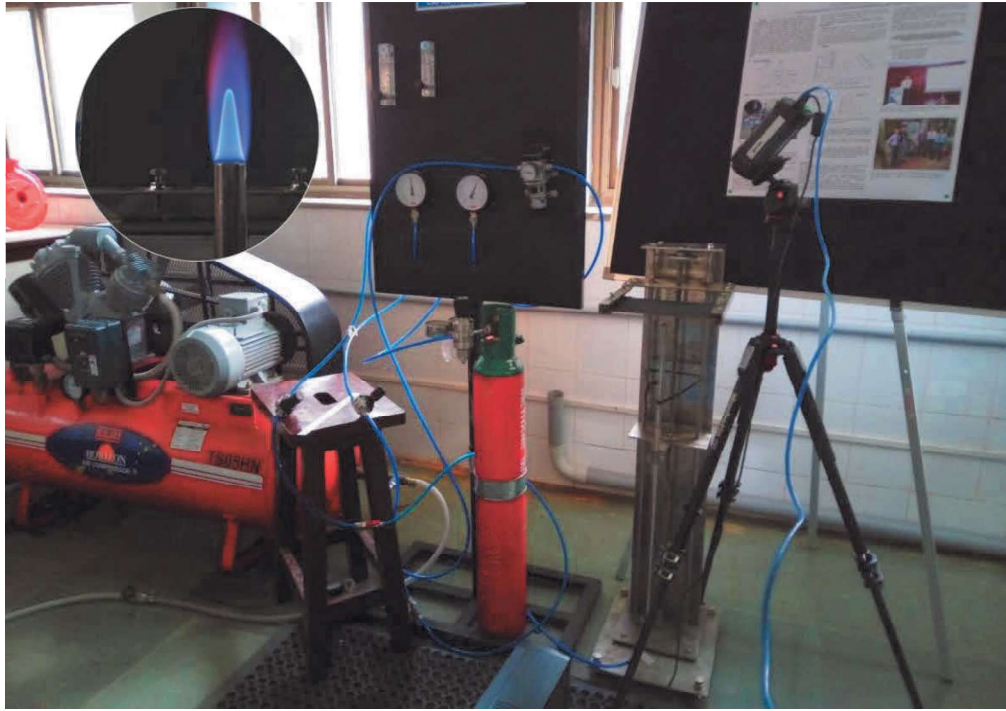
Figure 4.2   Laboratory experimental setup for the study of flame jet impingement.

4.2   Calibration of rotameters

Rotameters or Variable Area Flow Meters (VAFM) gas flow meters are generally used in flame emission, atomic absorption, and atomic fluorescence spectrometry to observe the flow rates of the various gases used in combustion and any other chemical process. These flow meters are generally a form of a variable orifice meter and usually consisting of a vertical, transparent tube having a tapered inside diameter containing a float of a predetermined shape, size, and material (density). It is a known fact that these kinds of flow meters are purely mechanical and, therefore, can never be exact in measuring the volumetric flow rate. However, these devices are reliable at all conditions subject to due calibration. Therefore, variable area flow meter, a reliable device, is widely used by ab-initio research work.

Mansfield and Winefordner (1968) addressed the issues concerning the monitoring of gas pressure change and its effect on the rotameter flow rate in the application of flame spectrometric methods. It was mentioned that two rotameter charts should be

used: one for converting the usual readings into flow rates and the other for further applying pressure corrections. Veillon and Park (1970) bring out the practical issues on the configuration of a rotameter and calibration procedure. The rotameters experience variable pressure either due to alteration done in flow range through a needle valve at upstream or partially clogging (which develops back pressure) in downstream burners. If the rotameter is to be used at a pressure for which it has been calibrated, the gas flow rate can be controlled by the downstream needle valve without affecting the calibration. Regardless of what occurs downstream, the pressure of the gas in the rotameter always remains constant, and the gas flow rate (atmospheric pressure) can be obtained directly from the calibration curve.

Urone and Ross (1979) and Webster (1977) have studied the effect of pressure change on flow rate. The experiment was carried out for measuring the airflow rate for decreasing pressure increments by maintaining a constant pressure at the rotameter. A notable variation found in theoretical and measured airflow rates concerning pressure change. The difficulty arises in ensuring desired Reynolds number of Methane-air gas mixture while studying its blow-off limit led to the development of this calibration procedure. The unit equivalence ratio of the gas mixture is maintained. The theoretical background (derivation) of relating Reynolds number with corresponding methane and airflow rate through rotameter is placed at **Appendix B**. The blow-off test is undertaken for validation of experimental setup, and the same is discussed later in this chapter. Two rotameters with range $500 - 5000$ ml per min and $50 - 500$ ml per min for air and methane are used to regulate the flow rate of gas mixture. Maximum possible Reynolds number of the mixture is 800 when rotameters are operated at atmospheric pressure. It was understood that the increase in gas pressure inside the rotameter would increase the actual volumetric flow rate at STP, and hence Reynolds number can easily be increased using the same rotameter. The theoretical correction factor for rotameters is discussed at **Appendix C**.

4.2.1 Experimental setup used to calibrate rotameters

A schematic of an experimental set up used for calibration of a rotameter-type variable area flow-meter using a Soap Bubble Meter is shown in figure 4.3. A Soap Bubble Meter is designed to read the volumetric gas flow rate at atmospheric conditions.

Design principle is very simple, which reads the time taken by a soap bubble to pass through a specified length in the gas (air) flow path and displays the volumetric flow rate. The flow meter (Rotametre) is maintained at constant pressure by carefully regulating the pressure regulating valve and the flow control valve. Two similar pressure gauges are installed before and after the rotameter to ensure a constant pressure within the flow meter. A minor pressure drop observed at pressure indicator for high flow rates can be recovered manually by readjusting the pressure regulating valve. This ensures a consistent gas flow rate even at higher pressure as the pressure is increased at the flow meter, the volumetric flow rate increases even at the same float height. The permissible ranger of the gas flow rate in SBM is 200-2000 ml per min at STP.
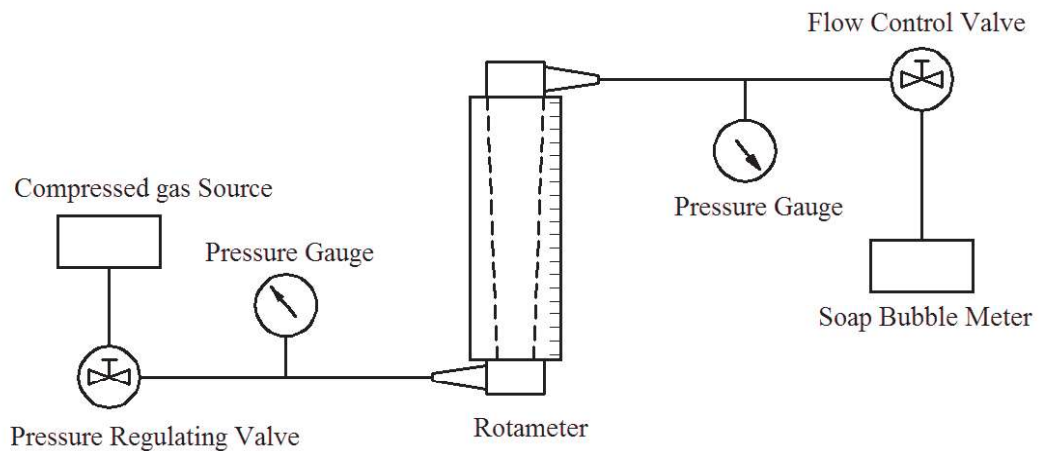
Figure 4.3 Schematic of the experimental setup, used for calibration of the rotameter.

4.2.2   **Results (air and methane rotameter).**

Initially, both the rotameters were calibrated at atmospheric pressure. The maximum achievable Reynolds number of the gas mixture was 800. Calibration of rotameters was undertaken at higher rotameter pressures to achieve required higher Reynolds numbers using the same set of rotameters. The calibration curves for both air and methane rotameter at various pressure are presented in figures 4.4 and 4.5. Linear variation of actual gas flow rate with respect to the indicated flow rate at all pressure (range $0 - 2$ bar) is convincing. Experimental results also prove that the range of volumetric gas flow rate increases with increase in gas pressure inside the rotameter.
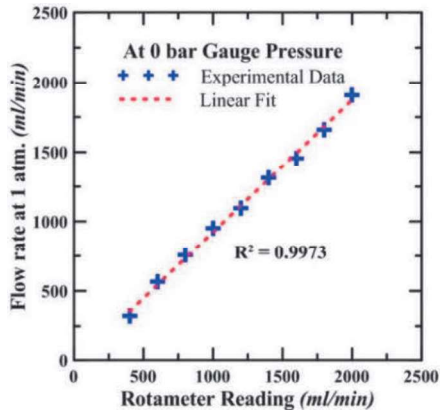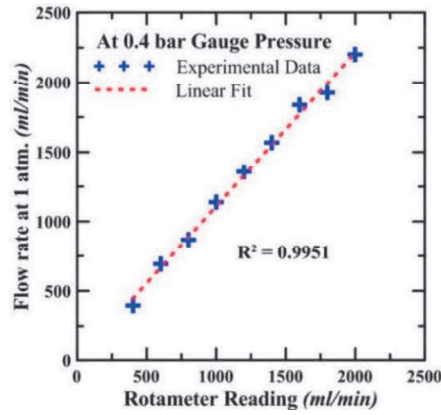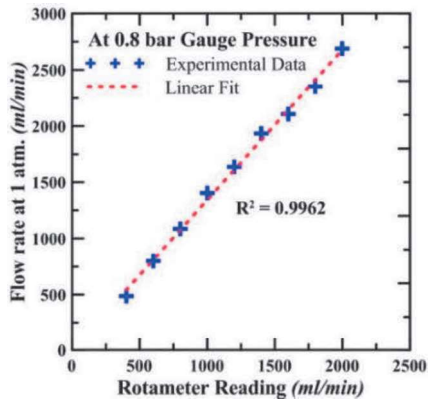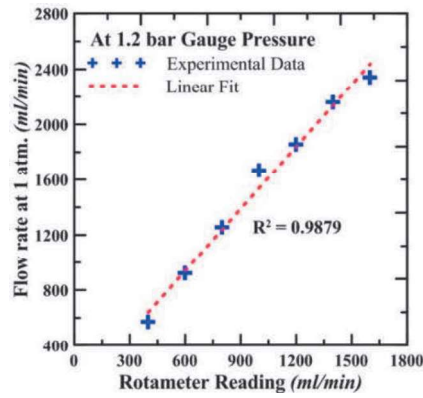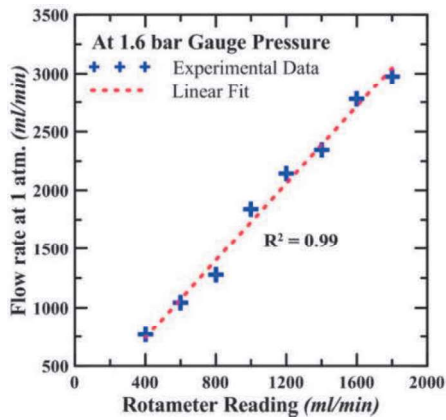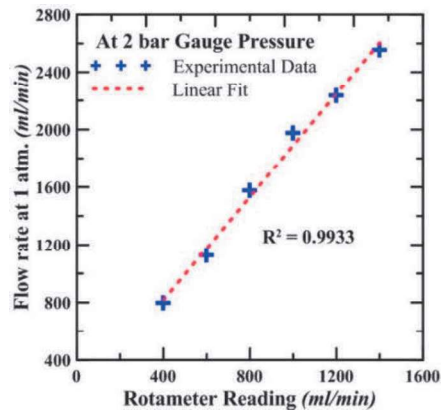
Figure 4.4 Calibration charts for air rotameter at (a) 0 bar, (b) 0.4 bar, (c) 0.8 bar, (d) 1.2 bar, (e) 1.6 bar and (f) 2.0 bar.
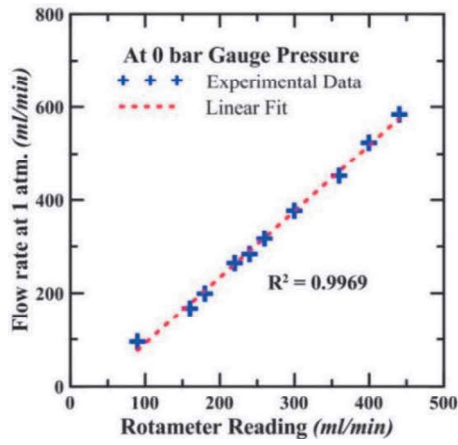
(a)
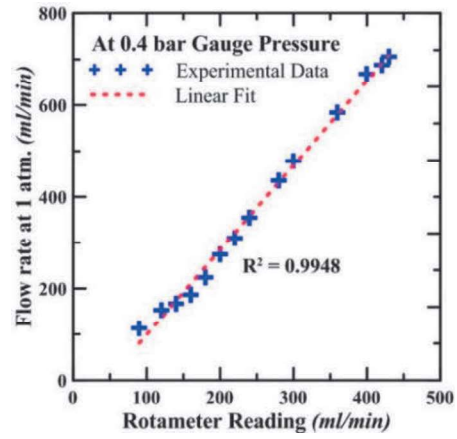
(b)
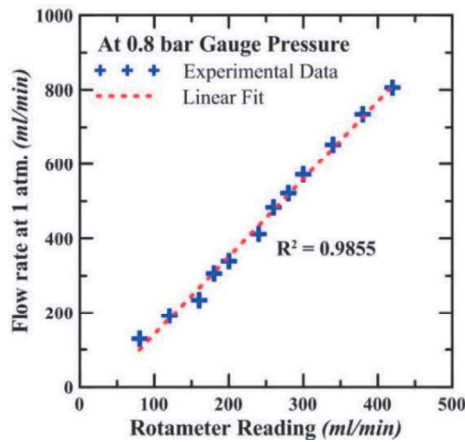
(c)
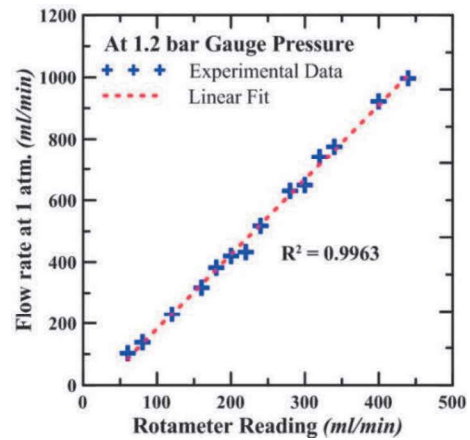
(d)
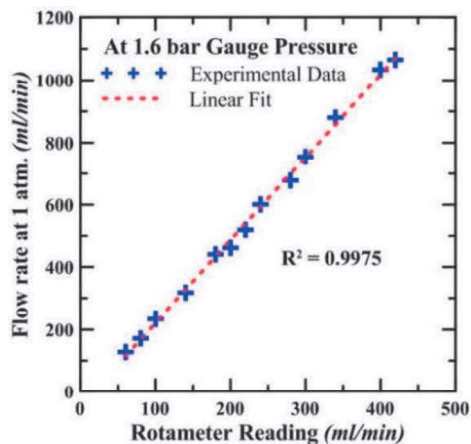
(e)
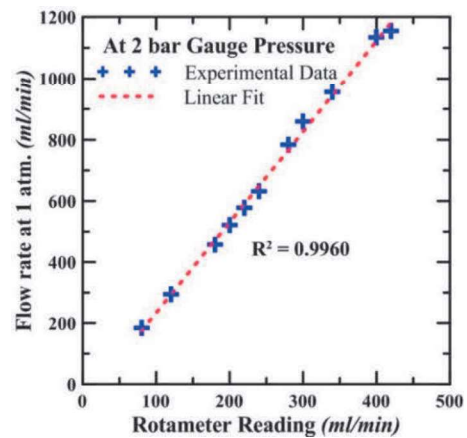
(f)

Figure 4.5 Calibration charts for Methane rotameter at (a) 0 bar, (b) 0.4 bar, (c) 0.8 bar, (d) 1.2 bar, (e) 1.6 bar and (f) 2.0 bar.
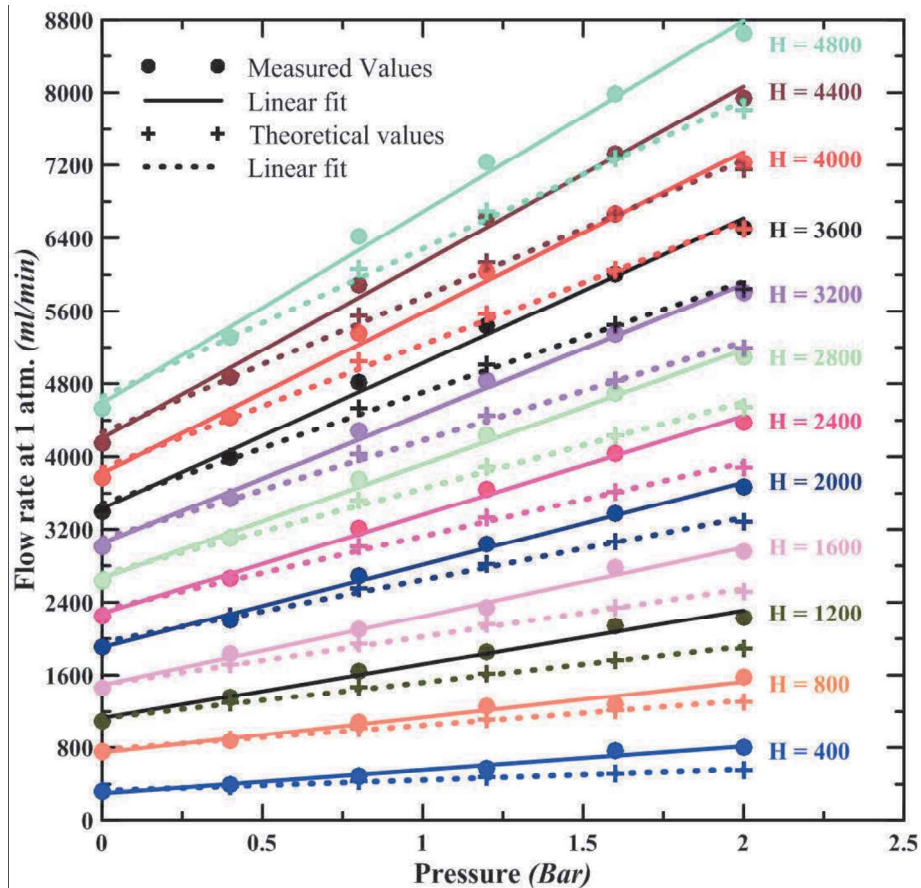
Figure 4.6   Effect of Pressure change on the actual flow rate of air for certain float height.

The results are further analysed to characterise a rotameter for the actual gas flow rate concerning varying pressure of the flowing gas inside the rotameter for a certain float height. A set of calibration curves showing the effect of pressure on the actual flow rate for air and methane is presented in figures 4.6 and 4.7. These calibration curves are mapped with the corresponding theoretically corrected values. As the pressure increases, the deviation of experimental results from the theoretical results increases. Equation C-1 (at appendix C) holds good only if the medium's density is minimal compared to the density of the float in rotameter. As pressure increases, the density of medium increases, and subsequently difference in density results in more deviation at higher pressure. Hence, it is clear that theoretically corrected data is in good agreement in a range near to calibration pressure.

In the case of methane rotameter (figure 4.7), considerable variation amongst theoretical and experimental results is observed. Rotameter for methane gas is designed for a minimal range (i.e. 50-500 ml/min), and thus there might not be a substantial difference in densities of float and methane gas. This might be the cause of significant variations. Therefore, at higher pressure, experimental results can be trusted for further calculations.
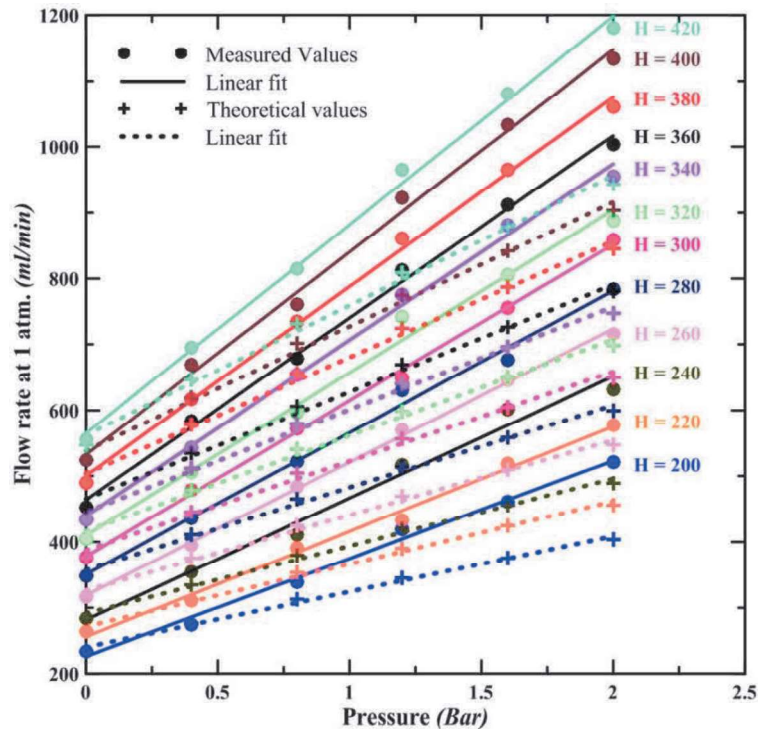
Figure 4.7   Effect of Pressure change on the actual flow rate of methane for certain float height.

The experiments were conducted to calibrate the rotameters for higher operating pressures. The predicted volumetric flow rates at higher fluid pressure in the same flow meter were validated using the concept of blow-off limit of methane-air premixed flame. Two separate variable area flow-meters for air and methane gas are used to regulate the flow. Rotameters are calibrated experimentally for pressure up to 2 bar in the interval of 0.4 bar, and further data is extrapolated (for higher pressure) to get desired Reynolds number. Data estimated through extrapolation for higher pressures are validated using the existing blow-off characteristics of methane-air premixed flame.
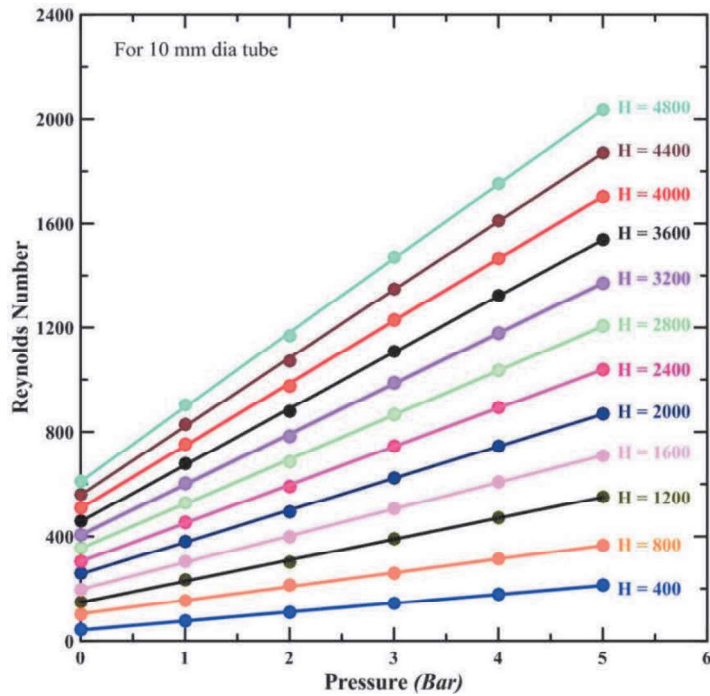
Figure 4.8 Change in Reynolds number with pressure for certain float height in air rotameter.

It would be appropriate to represent the data in the form of Reynolds number for a better understanding of the effect of pressure on flow rate. Figure 4.8 shows the effect of pressure in the air rotameter on corresponding Reynolds number for a 10 mm burner tube diameter. The data required at higher pressure (3, 4, and 5 bar) are extrapolated from the calibration chart shown in figure 4.6. The float height of 4800 ml per min in air rotameter at atmospheric pressure gives Reynolds number of 610, whereas, at 5 bar gauge pressure at the same float-height, Reynolds number would increase to 2030. Commonly used sets of rotameter readings required for experimentation purposes are tabulated in **Appendix D**.

4.3 Calibration of the experimental setup

The experimental setup shown in figure 4.1 is validated using the blow-off technique (Hindasageri et al. 2012). This validation procedure, in-turn, validates the rotameter calibration technique. In this setup, both the lines for air and methane are maintained at the same but higher pressure to ensure proper mixing of gases (methane and air) and a

higher range of mixture flow rate using the same rotameter to maintain desired Reynolds number in the burner tube. Stainless steel tube of 10 mm ID is used as a burner. For better appreciation, the basic structure of the experimental setup is shown in figure 4.9.
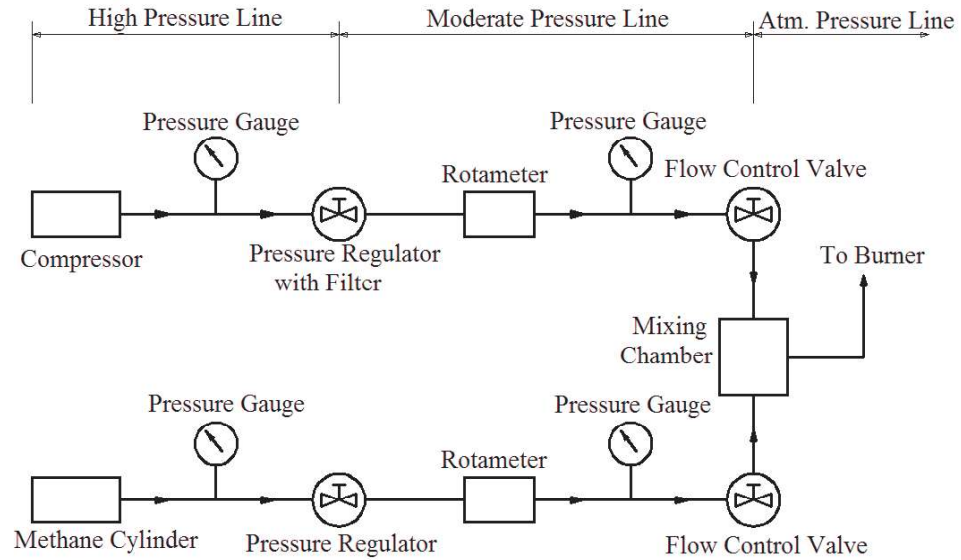
Figure 4.9 Schematic of Experimental set up for Blow-off study of methane-air flame.

The blow-off technique is based on the critical velocity gradient theory of flame stability. Lewis and Von Elbe (1943) developed the critical velocity gradient theory and concluded that the velocity gradient at the burner wall impacts the limit of flame stability of a burner. A schematic illustration of the blow-off limits is shown in figure 4.10. The blow-off limit governed by the critical velocity gradient (g_b) is defined by equation 4.1.

$$g_b = \lim_{r \to R} \left(\frac{-du}{dr} \right)$$ (4.1)

$$u(r) = 2\bar{u} \left(1 - \left(\frac{r}{R} \right)^2 \right)$$ (4.2)

where 'u' is the velocity of the unburnt gas mixture coming out of burner exit, and 'r' is the radial direction. For laminar flow through circular tubes, the velocity profile is given by equation 4.2, and accordingly, the critical velocity gradient parameter is given by equation 4.3.

$$g_b = \frac{8\bar{u}}{d}$$
(4.3)
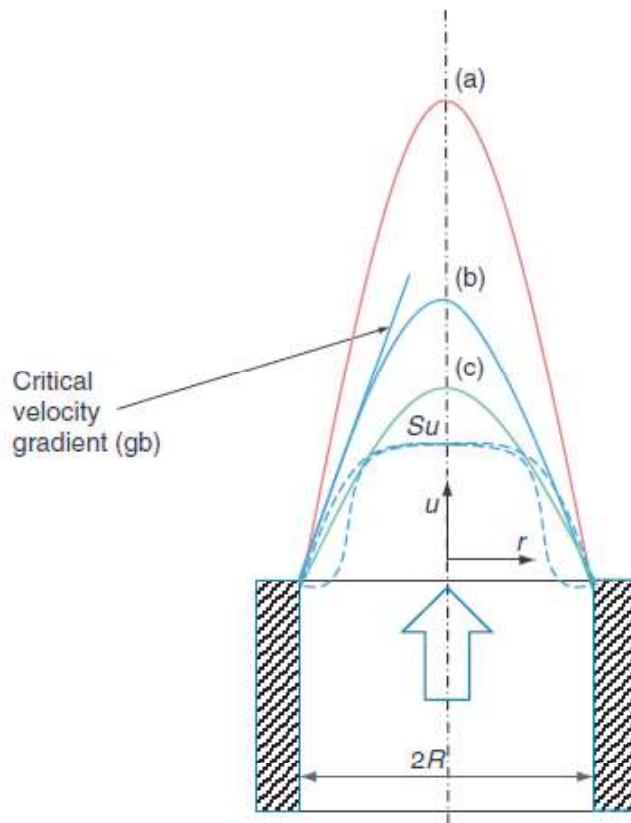
Figure 4.10   Illustration of flame stability criteria (Blow-off limit) showing the critical velocity gradient and mixture velocity profiles; (a) Unstable, (b) Stability limit, and (c) Stable (Hindasageri et al. 2012).

The flow of methane and air mixture to the burner is regulated using both the rotameters (as per the calibrated data at Appendix D) at a known pressure to achieve required Reynolds number of the gas mixture at the burner exit while maintaining the equivalence ratio of the mixture approximately one. Proper mixing of both the gases takes place before it reaches the burner exit. The length to the diameter ratio of the

burner is maintained 76. This ratio is far higher than the standard theoretical ratio (length to diameter ratio = 30) reported by Hindasageri et al. (2014), required for proper mixing of gases and fully developed flow inside the tube. The flow of the methane-air gas mixture is maintained laminar.
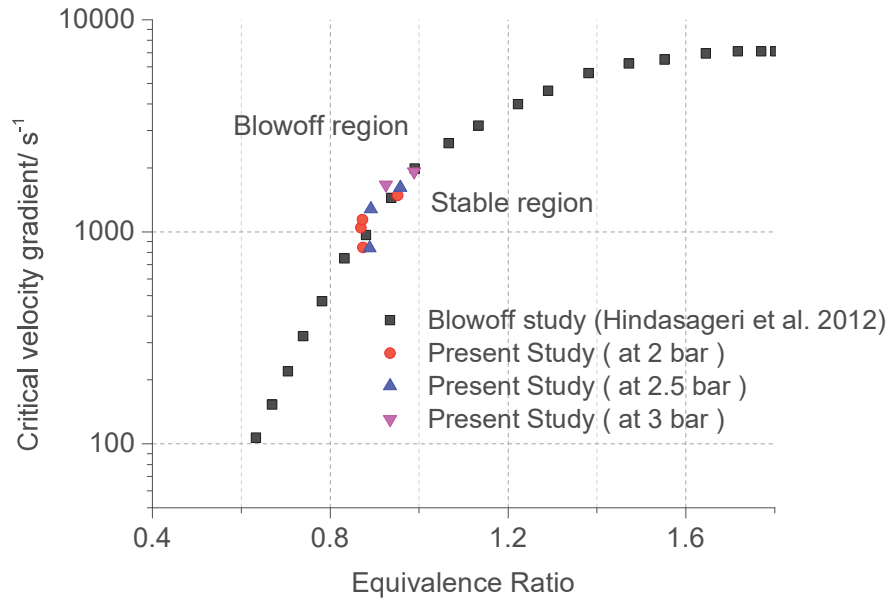
Fig. 4.11   A Methane-Air blow-off study - Comparison of critical velocity gradient parameter [2020].

Concerning the literature, the critical velocity gradient of the flame for equivalence ratio approximately equals to one is observed for validation. The validation curve is shown in figure 4.11. Since the estimated critical velocity of flame generated using the present experimental setup agrees with literature, it can be concluded that both the rotameters and the complete experimental setup are reliable.

4.3.1   Uncertainty analysis

The uncertainties related to the experimental settings and other derived quantities are considered in the calculations. The method suggested by Moffat (1986) is used to perform all the calculations. Deviation of 35 ml per min and 10 ml per min are found in the volume flow rate estimation at higher pressures. Uncertainties related to various parameters reported in the present study on rotameters are given in Table 4.1.

Table 4.1   Uncertainty of parameters.

Ser	Parameter	Maximum Uncertainty (%)	Minimum Uncertainty (%)
1.	Mixture mass flow rate	4.88	4.39
2.	Equivalence ratio	6.91	6.24
3.	Reynolds number	7.87	7.66
4.	Critical velocity gradient	6.75	6.37

A set of experiments, to calibrate two rotameters - one for air and the other for methane gas, are conducted at varying gas pressures. The calibration was conducted in two phases. In the first phase, a duly calibrated Soap Bobble Meter was used, and in the second phase, a methane-air premixed flame blow-off test was conducted. The concept of blow-off characteristics was extended for the indirect calibration of both the rotameters. In addition to this, the performance of both the rotameters for measurement of higher gas flow rates by maintaining relatively higher gas pressure within the rotameters was verified. Therefore it is concluded that exact gas flow rate (at atmospheric condition) can be predicted by operating the rotameters at higher pressure and by using the calibration charts.

4.4   Experimental setup – Impingement over a wedge-shaped object

Existing experimental setup for flame jet impingement over a flat plate is modified to undertake the experiments suitable to study the heat transfer characteristics of a flame jet impinging over a wedge-shaped structure with varying Reynolds number and non-dimensional nozzle tip to impinging surface distance. In this phase of experimentation, the aim is to undertake a parametric study on flame jet impingement over wedge-shaped stainless steel structure at varying experimental conditions such as Reynolds number 800, 1000, 1200 and 1500; non-dimensional nozzle tip to impinging surface distance 2, 4 and 6; wedge angle 90°. The wedge-shaped test object shown in figure 4.12 is used in this study, which resembles with missile exhaust flow and heating conditions over a deflector plate. The wedge-shaped test object is made of a 4-mm-thick stainless steel flat.
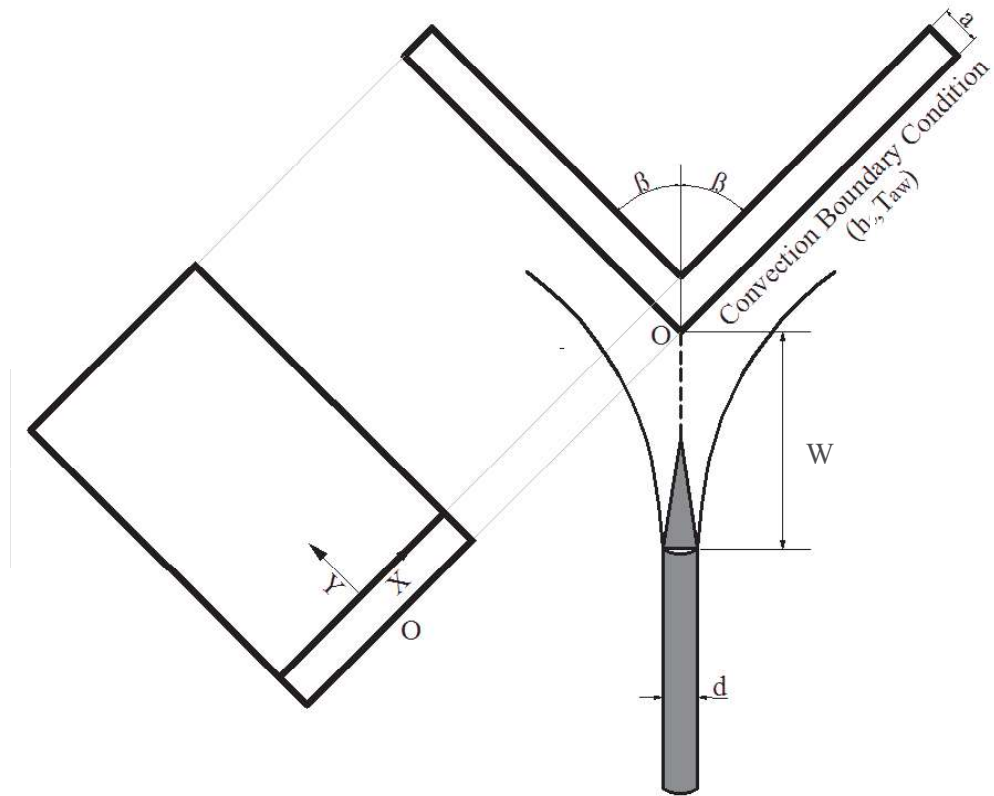
Figure 4.12   Schematic of a wedge-shaped object being impinged.

This experimental setup is designed to record transient temperature over a hot surface impinged by a methane-air flame jet. The flame can be regulated to achieve predefined Reynolds number. A wedge-shaped object made by joining two 4-mm-thick stainless-steel flat plates at a specified angle (i.e., 2β) is shown in figure 4.12. This angle (2β), is named wedge-angle of the test object. The design of the setup is such, the flame impinges at the wedge outer face and gets divided equally by virtue of symmetry of the test object. The impinging edge is positioned just above the burner exit at a predefined gap, which is the closest edge of the test object from the burner exit. The point at which the burner axis joins the test object is denoted as 'O', which is shown in both views of the test object. The impinging edge of the test object is represented along the x-direction, whereas y-direction is along the centerline of one of the wings of the test object through 'O'. The outer face of the test object, which is impinged by high-temperature flame jet is considered inaccessible, whereas the transient temperature of the accessible face (or the inner face) of the test object is measured using thermal

imaging camera. Since the test object is symmetric, the thermal effect at both the wings of the test object is expected to be the same. Therefore, temperature variation at one wing is required to be measured.
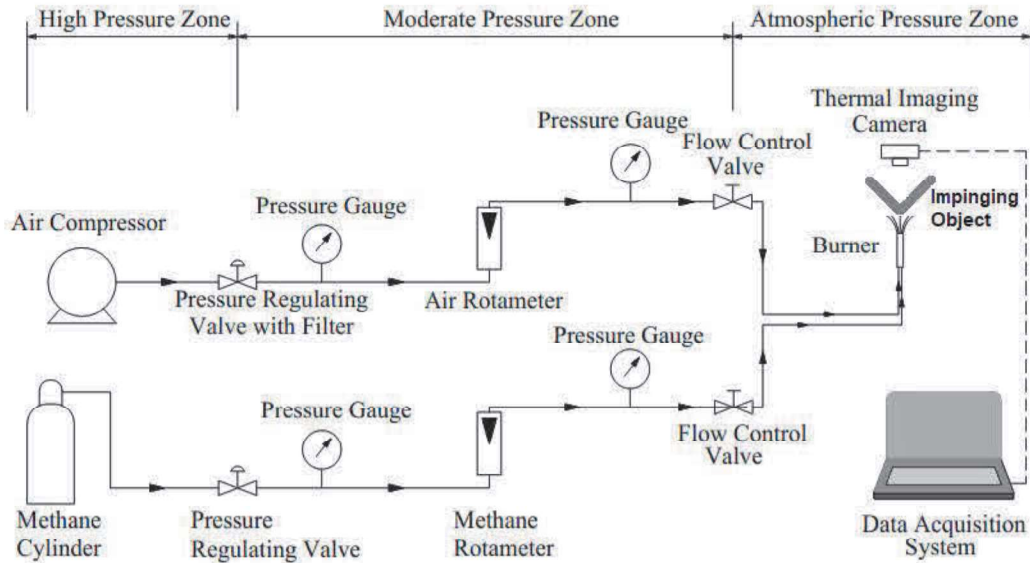
Figure 4.13   Schematic of the experimental setup for flame jet impingement over the wedge-shaped test object.

The schematic of the complete experimental setup is shown in figure 4.13, and a photograph of the laboratory setup is given in figure 4.14. Key components of the experimental set up are thermal imaging camera (Model – FLIR A325Sc), compressor, methane rotameter, and air rotameter, cylindrical tube type stainless steel burner of internal diameter 10 mm and thickness 1 mm. The IR camera is having a resolution of 320 x 240 pixels, measurable temperature range up to $2000^{\circ}C$, and a recording speed of 60 frames per second (fps). The accuracy of temperature measurement varies within 2% of the actual temperature. Very high resolution in temperature measurement (both spatial as well as temporal) is possible, and effective when transient data analysis is necessary. Additionally, the thermal imaging camera is not required to be in physical contact with the target surface for temperature measurement which is an additional advantage in this experiment.

Figure 4.14   Laboratory experimental setup for the study of flame jet impingement over the wedge-shaped test object.

A thermal imaging camera captures the Infrared (IR) radiations from the hot surface and senses the corresponding thermal intensity to measure temperature. The target surface is painted black, as it is a requirement of the thermal camera to maintain higher emissivity for better accuracy in measuring temperature. The numerical value of the emissivity of the rear surface is taken as 0.95 for all calculation purposes (Brandt et al. 2008). Rear face (the inclined surface) experiences natural convection, as the experiment is conducted in a closed room at room temperature and pressure with no external airflow over the plate. Current experimental data shows, the average change in temperature over the surface is 10 K. Corresponding Rayleigh number is an order of 10^6. Based on the fundamental studies (Bejan, 2013) on natural convection over the inclined plate, the average heat transfer coefficient at the rear face is 5 $Wm^{-2}K^{-1}$. The flow rate of air rotameter operated at 3 bar, ranges from $1500 - 15000$ ml per minute,

whereas the same for methane rotameter is 150 – 1500 ml per minute. Rotameters are calibrated up to 2 bar using standard soap bubble meter at atmospheric conditions.

The flow of methane and air mixture to the burner is regulated using both the rotameters at 2 bar and 3 bar to for Reynolds number of the gas mixture at the burner exit 800-1200 and 1500, respectively. The equivalence ratio of the mixtures is maintained at approximately one. The proper mixing of both the gases takes place in the long burner tube. The length to the diameter of the burner ratio is maintained 76, which is far higher than the standard theoretical ratio (length to diameter ratio = 30) reported in Hindasageri et al. (2014), required for proper mixing and fully developed flow inside the tube. The flow of the methane-air gas mixture is maintained laminar.

The temperature at the non-imping face of the test object was recorded at 30 frames per second (fps). Experimentally recorded transient temperature (up to 5 seconds) over the non-imping face of the test object is analysed to obtain the heat transfer characteristics. It is also noted that temperature gradient (refer figure 4.16) and hence lateral heat conduction along the lateral direction is significantly lesser during the first few seconds of impingement. Therefore, transient analysis using one-dimensional heat conduction for data up to 5 seconds is justified.

4.4.1   Sample measured temperature distribution

The contour plots of experimentally measured temperature at the non-imping face of the test object (wedge-shaped object) for Re = 1000, W/d = 4, wedge angle = 90º during first 5 seconds of methane-air flame jet impingement are shown at figure 4.15. These measured temperature for one-half of any one wing of the test object (view symmetry) is plotted to present sample experimental data. It may be noted that the rise in temperature from 1s to 2s is slightly higher than during 4s to 5s. This slow heating at later time is due to additional radiation loss at higher surface temperature and possible lateral conduction due to existing temperature gradient at that moment. This transient temperature data is analysed to predict both the heat transfer coefficient and adiabatic wall temperature at the impinging face of the wedge-shared object. Varying Reynolds number, nozzle-to-imping face distance, and wedge-angle are the parameters considered for analysis. All the cases are discussed in chapter 5.
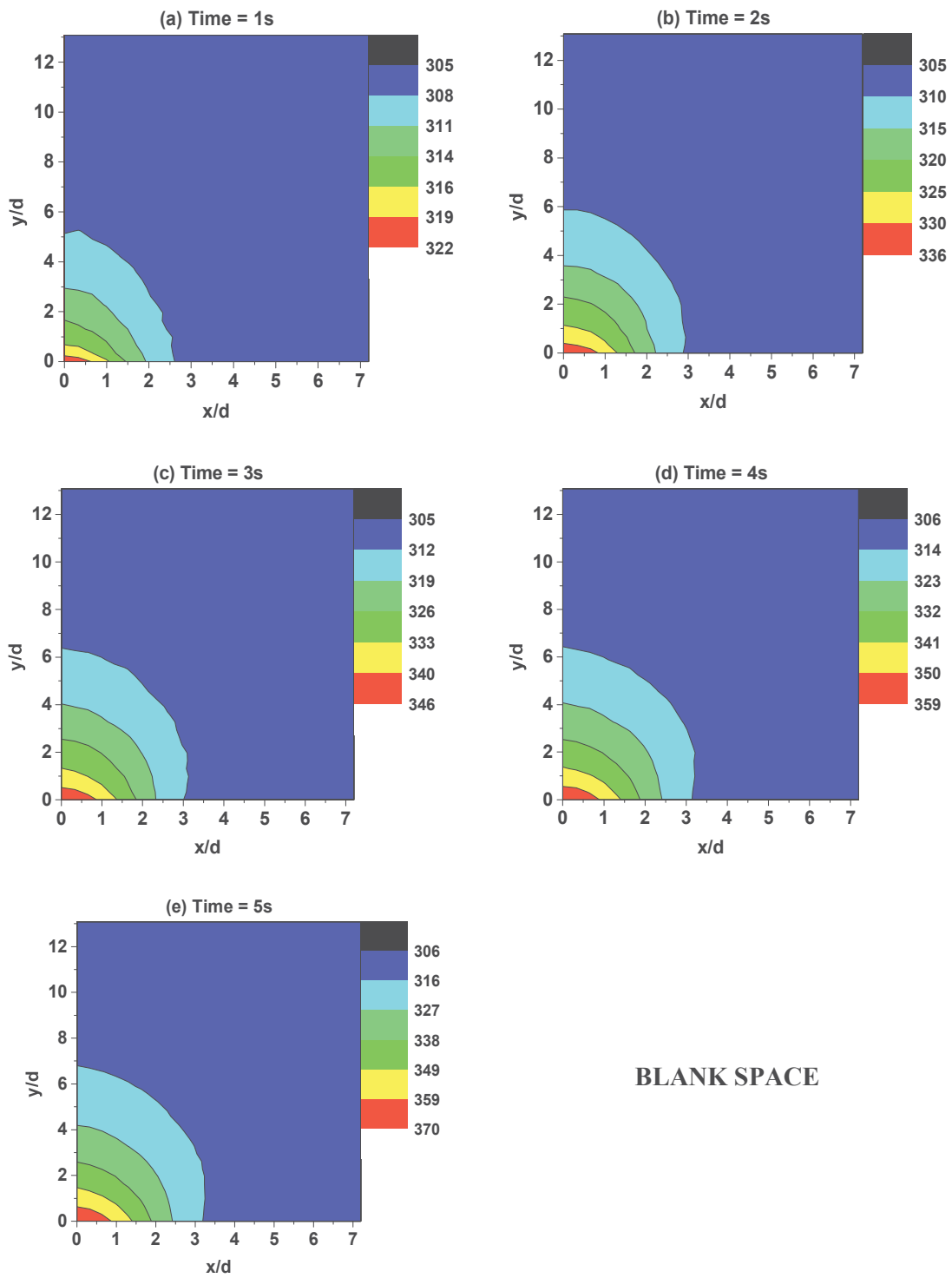
Figure 4.15 Temperature (in Kelvin) distribution over the non-impinging face of the test object with wedge angle = 90° impinged at Re = 1000, W/d = 4.

4.5　Transient inverse heat conduction algorithm

```mermaid
Start
```

Start

Read, (a) Thermal properties and thickness of the impinging plate, (b) Raw experimental transient temperature along a radial line over the impingement plate and refer the data as Measured Variable (MV), (c) Radial location (r/d) and time array.

Generate the initial value of unknown parameters (h, T_{aw}) and damping coefficient (λ) randomly, or assume suitably.

Estimate the transient temperature profile at a given radial location (r/d) using the forward model and refer it as Estimated Variable (EV).

Estimate the forcing function 'D', objective function 'F', and Jacobian matrix 'Z'.

Set the first and second elements of the matrix '$[Z^T Z + \lambda \Omega]^{-1} Z^T D$' as Δh and ΔT_{aw} respectively.

Set, $h = h + \Delta h$
and $T_{aw} = T_{aw} + \Delta T_{aw}$

if Δh, ΔT_{aw} and F fall below a limit.

No

Yes

Save h and T_{aw} for the current 'r/d'.

Change to the next radial location.

Are all the radial locations analysed?

No

Yes

End

The mathematical background for both the inverse as well as forward model of the algorithm presented (in previous page) is discussed in the last chapter. A MATLAB computer code is developed as per the algorithm and the same is placed at **Appendix E**. The key features of the algorithm are listed below:-

(a)   It requires the transient temperature (beginning of the experiment) at the non-impinging face for as low as two to three seconds as input data. It may be noted that temperature measurement in the present experiment is at 30 fps. This transient temperature at non-impinging face is the only experimental data required.

(b)   Green's Function Approach being capable of analysing conduction heat transfer with transient convection and radiation boundary conditions (discussed in last chapter) accommodates the transient heat losses, which in-turn minimises the possible errors while estimating the unknown parameters.

(c)   Inverse analysis of heat conduction within the impinging plate is undertaken to estimate both convective heat transfer coefficient and adiabatic wall temperature at the impinging face simultaneously. No external fluid flow analysis at the impinging face is required.

4.6   Validation of the algorithm

Post calibration of the experimental setup, validation of the proposed transient IHCP algorithm was undertaken using standard methane-air flame jet impingement over the flat plate to estimate heat transfer characteristics. The estimated parameters at the impinging face are compared with the literature to confirm the suitability of the algorithm. The temperature at the non-impinging face of the Stainless Steel plate when impinged by a methane-air flame at Reynolds number equals to 1000 and W/d = 4, was recorded at 30 frames per second (fps). The experiment is conducted multiple times and averaged to avoid possible bias and error in experimentation. Experimentally recorded transient temperature (up to 5 seconds) at various radial locations over the plate's non-impinging face is plotted and shown in figure 4.16.
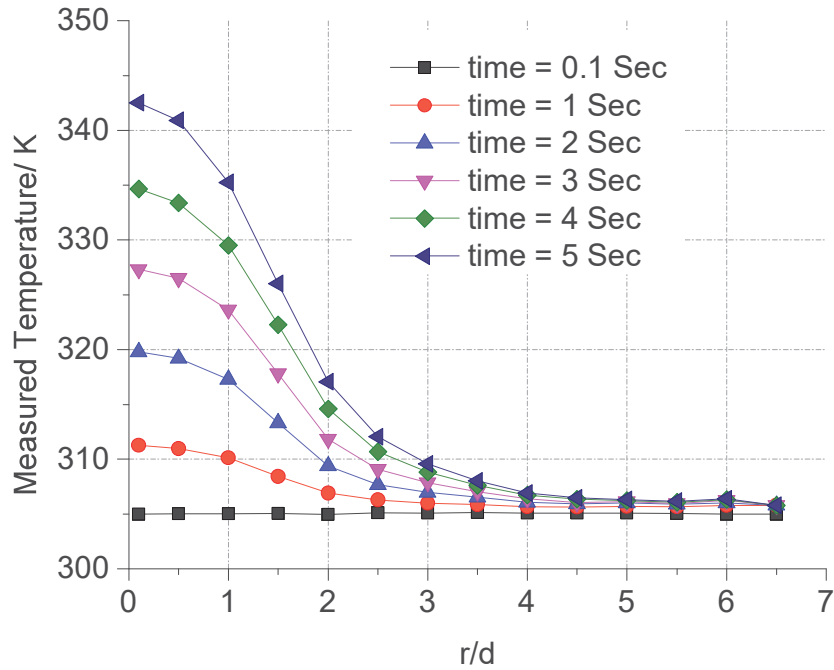
Figure 4.16   Radial distribution of transient temperature at the non-impinging face of a 3 mm Stainless Steel plate impinged by a methane-air flame jet at Re = 1000 and W/d = 4 [2020]

Transient data up to 3 seconds from the start of impinging the flame jet is considered for analysis to ensure minimum lateral conduction during the experiment. It is also noted from figure 4.16 that the temperature gradient along the radial direction is significantly lesser during the first few seconds of impingement as compared to later times. Therefore, it can be concluded that during the initial time of the flame impingement, the lateral heat conduction can be neglected.

The proposed methodology is an iterative process. The proposed methodology is analysed by observing the 'ratio of change in the cause to a unit change in its effect'. In the present case, the cause is the heating effect (heat transfer coefficient and adiabatic wall temperature) at the impinging face. The effect is the temperature variation at the non-impinging face, which further is transformed as an objective function (refer equation 3.10). The cause-effect ratio in respect of the heat transfer coefficient is represented as $\dfrac{Dh}{DF}$ and the same in respect of adiabatic wall temperature is $\dfrac{DT_{aw}}{DF}$. The

estimated values of these two parameters at various radial locations are shown in figures 4.17 and 4.18.
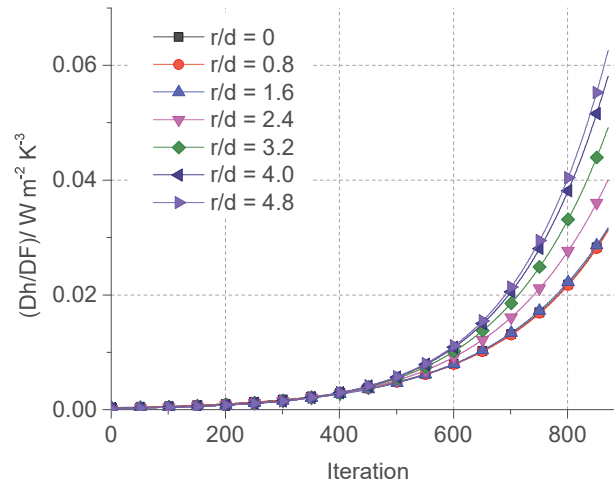
Figure 4.17   Change in heat transfer coefficient with respect to change in the least square error at different locations [2020].
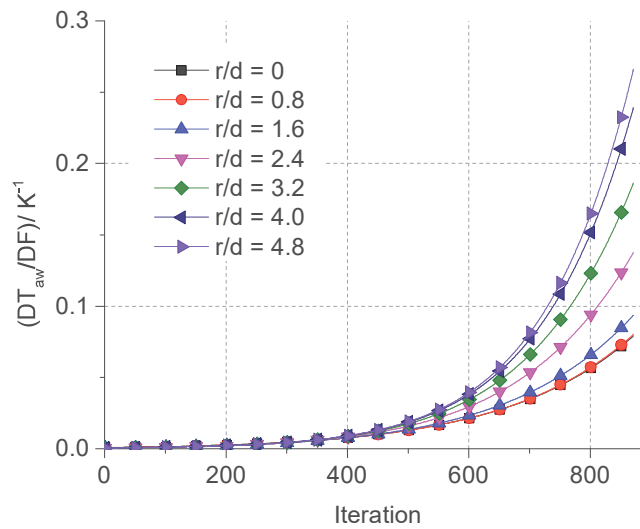
Figure 4.18   Change in adiabatic wall temperature with respect to change in the least square error at different locations [2020].

The ratio of change in the cause to a unit change in effect remains unchanged and closed to zero during the initial phase of iterations, which further increases asymptotically as

the iterations progresses. Initial slow change is because of a considerable change in the objective function compared to the change in the unknown parameter, whereas in the later phase of iterations, the objective function or the effect varies slowly as compared to the change in the cause. This confirms both convergences of the solution and smooth transition at each iteration. The trend also justifies a smooth reduction in objective function value. Therefore, it can be stated that solution is optimized when the graphs are steeper.

4.7   Discussions

The main aim of this study is to undertake a transient analysis of impinging flame jet experimental data measured using thermal imaging camera for simultaneous estimation of both heat transfer coefficient and adiabatic wall temperature at all the locations (r/d) on the impinging face. One experimental condition - flame jet Reynolds number equals 1000; equivalence ratio equals one and non-dimensional burner tip to impinging plate distance equals four - is considered for experimentation, analysis, and validation of proposed methodology. Transient temperature measured at the non-impinging face of the flat plate is considered for inverse heat conduction analysis using an in-house developed MATLAB code. Forward model of the solution procedure, one-dimensional transient heat conduction accounts for transient radiation losses at the exposed surface in addition to convection loss. Analysis of jet impingement heat transfer for very high-temperature applications in a transient stage can be performed, as the transient (instantaneous) radiation heat loss is considered for analysis. The use of Green's function technique makes it easier to handle all the transient boundary conditions, including transient radiation heat loss. It is pertinent to mention that the solution procedure demonstrates the analysis of the initial few seconds' transient data during which the lateral heat conduction within the plate material is negligible. Accuracy in predicting heat transfer coefficient and adiabatic wall temperature improves view minimum lateral conduction and accounting of radiation heat loss. The detailed discussion of the results obtained is presented in subsequent paragraphs.
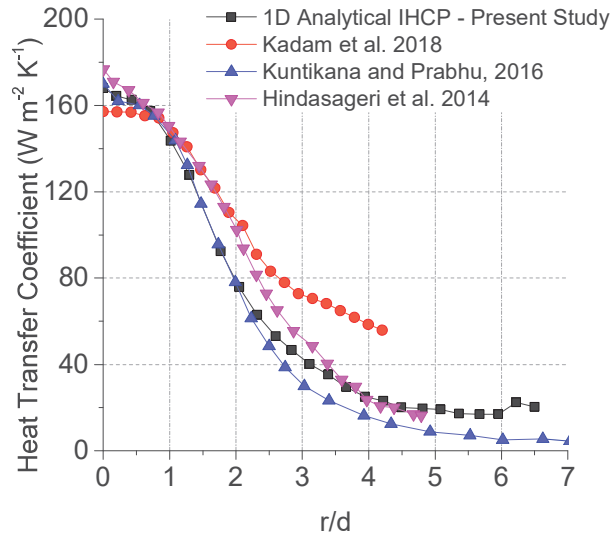
Figure 4.19   Variation of heat transfer coefficient at impinging face for Re = 1000, and W/d = 4 [2020].
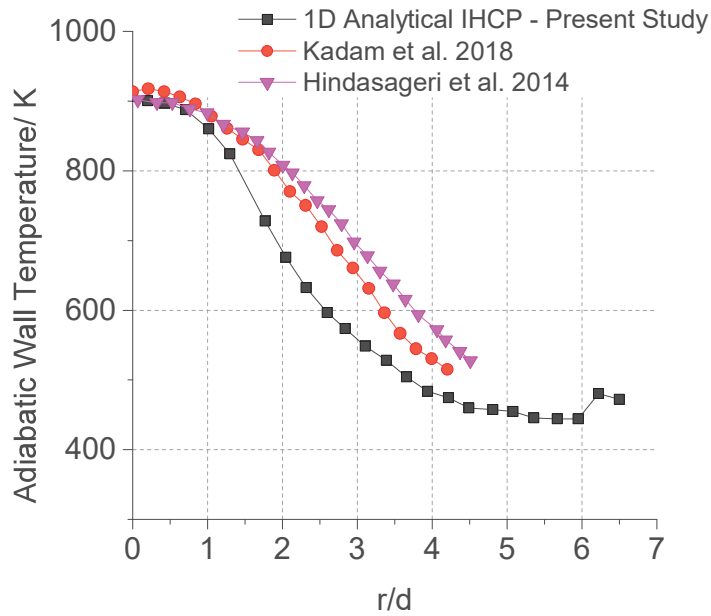
Figure 4.20   Variation of adiabatic wall temperature at impinging face for Re = 1000 and W/d = 4 [2020].

When impinged by a methane-air flame jet, the heat transfer coefficient and the adiabatic wall temperature at the impinging face of a flat stainless steel plate are estimated

71

simultaneously using analytical IHCP. The comparison of the predicted heat transfer coefficient and adiabatic wall temperature at the impinging face is undertaken with three recent studies, one of these studies is based on steady-state analysis (Kuntikana and Prabhu, 2016) and other two studies (Hindasageri et al. 2014; Kadam et al. 2018) are based on transient data analysis. The comparative graphs for the same are presented in figures 4.19 and 4.20. The flow and the geometric conditions of the present case are the same as those studies chosen for comparison purposes. The heating condition in all three cases is the same. The percentage error of estimated parameters with respect to the stagnation point data of the present study at selected radial locations is presented at table 4.2. Actual values of heat transfer coefficient and adiabatic wall temperature along with their deviations with respect to the present study are presented at Appendix F.

Table 4.2   Percentage error (rounded off to nearest integer) of estimated parameters (h_o and T_{aw}) with respect to the corresponding value of the same parameter (of the present study) at the stagnation point [2020].

r/d	3D Modal analysis (Kadam et al. 2018)		1D Semi-analytical technique (Hindasageri et al. 2014)		Thin foil technique (Kuntikana and Prabhu, 2016)
	The percentage error in respect of				
	h	T_{aw}	h	T_{aw}	h
0	7	1	5	1	1
1	3	2	4	1	2
2	17	11	14	12	1
3	17	10	5	14	8
4	20	5	1	12	5

The heat transfer coefficient matches reasonably well with the data in the literature, thin foil technique (Kuntikana and Prabhu, 2016), and 1D semi-analytical technique (Hindasageri et al. 2014). Deviation in results at radial locations away from the

stagnation zone observed in the 3D modal analysis (Kadam et al. 2018) may be due to its procedural limitations that it is valid only for thin impinging plate and requires evaluation of wall heat flux as well as temperature as intermediate parameters before estimating both heat transfer coefficient and the reference temperature. The estimated adiabatic wall temperature is observed to be varying between 1-15% when compared with literature (Hindasageri et al. 2014; Kadam et al. 2018). No data in respect of adiabatic wall temperature for the case under discussion is presented in the literature using thin foil technique (Kuntikana and Prabhu, 2016). The pattern of the adiabatic wall temperature (refer figure 4.20) shows that lateral heat conduction in the present study has been relatively lesser as compared to the other two experiments (Hindasageri et al. 2014; Kadam et al. 2018). The same is due to the consideration of early time data (up to 3 seconds) for analysis. The predictions in the stagnation zone agree with the literature. The variation of both the parameters beyond the stagnation point remains within the agreeable percentage. Additionally, the present analytical technique can analyse the transient temperature beyond r/d = 5, where the temperature variation is negligible. This implies that the present technique can also be used for applications having a little change in temperature over a given time interval.

One more set of experimental data for a different Reynolds number (i.e., Re = 1200) and a different dimensionless burner tip to impinging plate distance (i.e., W/d = 6) is considered for analysis to justify the reliability of the proposed methodology. The result is observed to be following a similar pattern as compared with the case presented in the manuscript. The new set of results is in good agreement with the literature (Hindasageri et al. 2014), and the corresponding plots are shown in figures 4.21 and 4.22.
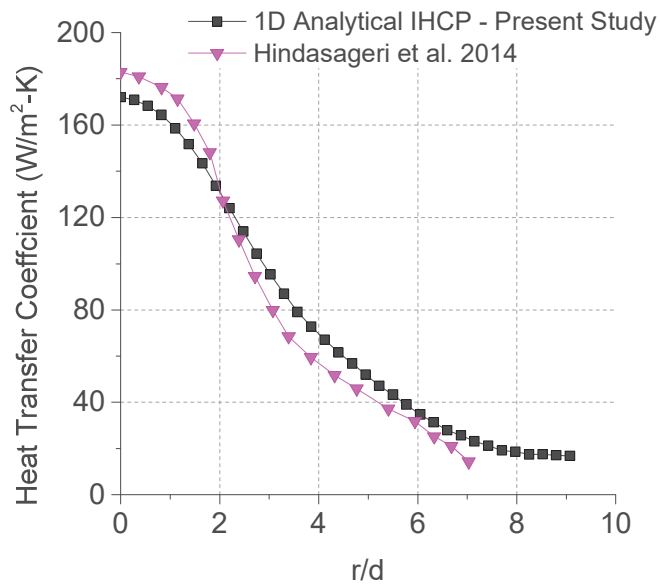
Figure 4.21   Heat transfer coefficient at impinging face for Re=1200 and W/d=6.
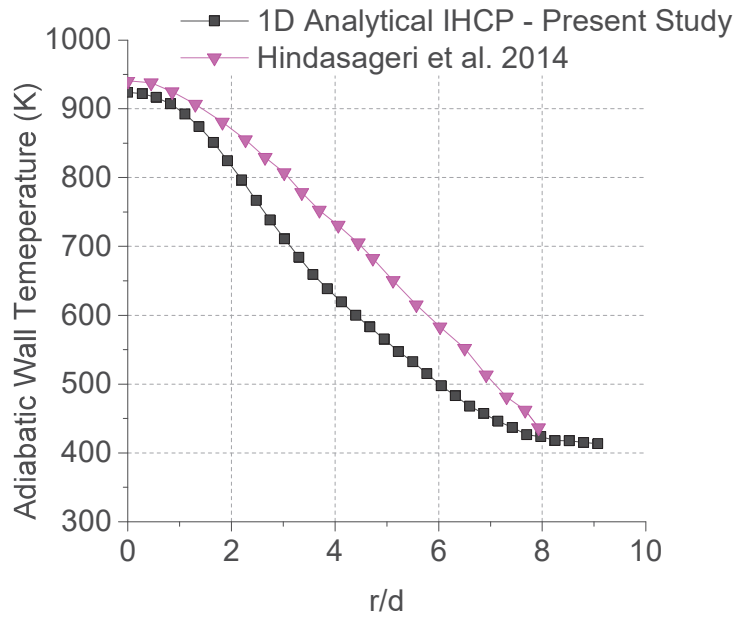
Figure 4.22   Adiabatic wall temperature at impinging face for Re=1200 and W/d=6.

Chapter 5

RESULTS AND DISCUSSION

5.1 Heat transfer characteristics of impinging flame jet over the wedge-shaped object

 The main aim of this study is to undertake heat transfer characterisation of the impinging flame jet onto a wedge-shaped object resembling a deflector plate of a missile launcher. The proposed experimental set up (figure 4.13) is designed to measure transient temperature at the non-impinging side of the wedge using a thermal imaging camera. The proposed analytical IHCP technique is used to undertake the analysis of measured raw experimental temperature. Following experimental conditions by varying input methane-air flame and geometrical conditions are studied:-

(a) Reynolds number 800, 1000, 1200 and 1500;

(b) Non-dimensional nozzle tip to impinging surface distance 2, 4 and 6;

(c) Wedge angle 90° and 120°

Transient temperature measured at one wing of the non-impinging (inner) face of the test object is considered for inverse heat conduction analysis using an in-house developed MATLAB code. The code is developed based on the algorithm placed in **Appendix E**. The forward model solution procedure based on Green's function technique accounts for transient radiation losses at the exposed surface in addition to the transient convection losses. The use of Green's function technique makes it easier to handle all the transient boundary conditions, including transient radiation heat loss. Heat transfer analysis for very high-temperature applications in the transient state is possible using this technique, as the transient (instantaneous) radiation heat loss is considered for analysis. The analysis is undertaken using transient data up to the first 5 seconds of impingement. Accuracy in predicting heat transfer coefficient and adiabatic wall temperature improves view minimum lateral conduction during the initial few seconds of the experiment and accounting of radiation heat loss. The detailed discussion of the result obtained is presented in subsequent paragraphs.

5.1.1 Wedge-angle 90º
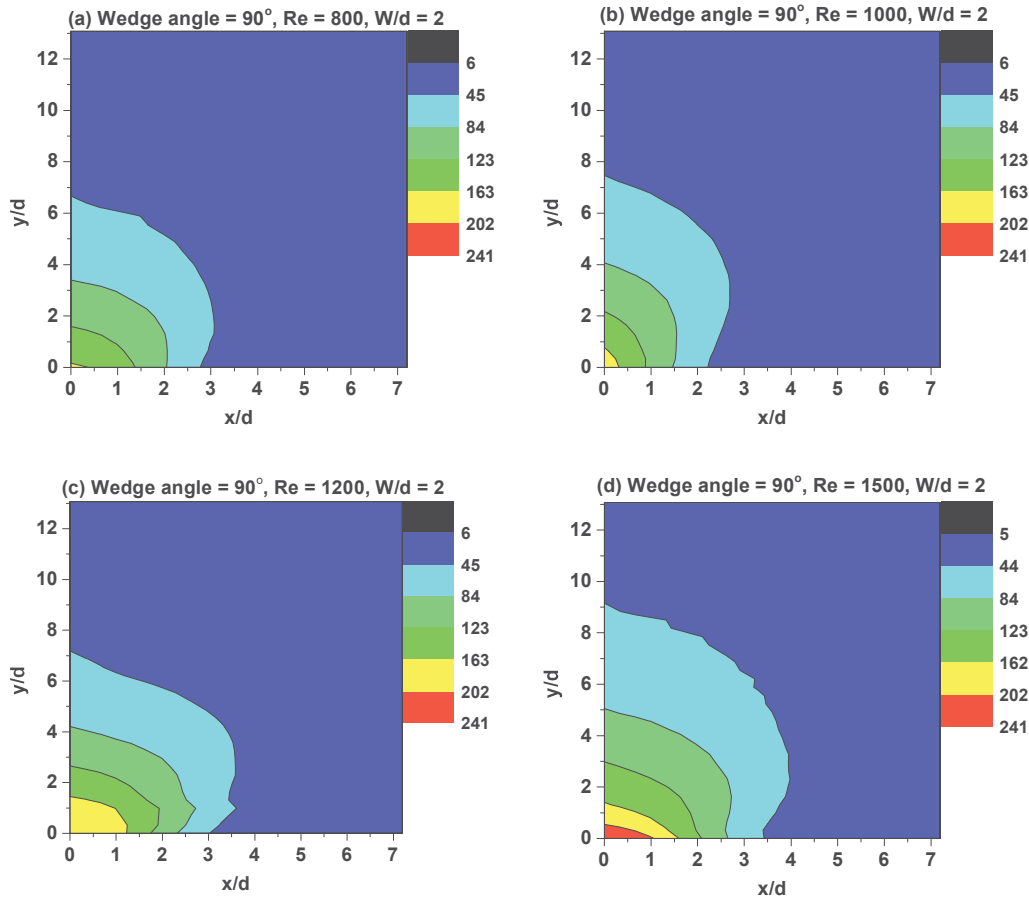
Figure 5.1   Effect of Reynolds number on heat transfer coefficient (Wm^{-2}K^{-1}) of methane-air flame jet impinging on a wedge-shaped test object (wedge-angle = 90º) at W/d = 2.

A wedge-shaped test object made of a 4-mm flat stainless steel plate is impinged by a methane-air flame jet. Nozzle axis is aligned such that the flame while impinging spreads equally onto both wings of the wedge. Experiments for wedge angle 90º and 120º are conducted to study the effect of wedge-angle on heat transfer characteristics. View symmetric nature of the test object, heat transfer characteristics at one-quarter of the test object surface is required to be plotted in contour plots, and the same is presented in this section. Dimensionless axis system – 'x/d' and 'y/d' – is used to

represent the estimated values of heat transfer coefficient and adiabatic wall temperature.

Variation of heat transfer coefficient at the impinging face of one of the wings of the test object for Reynolds number varying from 800 – 1500 at W/d = 2 is presented in figure 5.1. It is observed that the influence of impinging jet along y-direction (outward direction) is more as compared to x-direction (along the impinging edge of the wedge). The heating effect spreads maximum up to y/d = 10 in the y-direction, whereas the same spreads up to x/d = 3.5 in the x-direction. This additional heating effect along y-direction may be because of the natural convection along the lower face of the wings (an inclined surface) of the test object. The gas mixture (flame jet) post impingement would be gaining additional momentum due to natural convection and spreads more along the inclined surface of the test object than horizontal direction along the impinging edge. With a rise in Reynolds number of the flame, the heating effect improves. Heat transfer coefficient at the impinging zone increases from 170 $Wm^{-2}K^{-1}$ (Re = 800) to 241 $Wm^{-2}K^{-1}$ (Re = 1500).

Near the impinging zone, the heating effect along the y-direction is higher as compared to the x-direction. For example {refer figure 5.1(b)}, in case of Re = 1000 and W/d = 2, heat transfer coefficient at y/d = 1 is nearly 153 $Wm^{-2}K^{-1}$ whereas heat transfer coefficient at x/d = 1 is approximately 123 $Wm^{-2}K^{-1}$ and similarly, heat transfer coefficient at y/d = 2 is nearly 120 $Wm^{-2}K^{-1}$ whereas heat transfer coefficient at x/d = 2 is approximately 60 $Wm^{-2}K^{-1}$. This may be attributed to natural convection along y-direction as additional convection force leading to a higher heating effect.

Similarly, variation of adiabatic wall temperature at the impinging face of one of the wings of the test object for Reynolds number varying from 800 – 1500 at W/d = 2 is studied and presented at figure 5.2. It confirms the additional heating effect along y-direction. For example {refer figure 5.2(d)}, adiabatic wall temperature at x/d = 4 is approximately 540K, whereas the same at y/d = 12 is approximately 540K. This simply signifies improved convention heat transfer along y-direction compared to the x-direction. The maximum adiabatic wall temperature observed at impinging zone depends on Reynolds number of the flame. Adiabatic wall temperature rises when Reynolds number is increase. From figures 5.1 and 5.2, it may be concluded that heating

effect due to impinging flame jet over a wedge is always wider along the wedge direction (i.e. y-direction) as compared with x-direction.

Figure 5.2   Effect of Reynolds number on adiabatic wall temperature (K) of methane-air flame jet impinging on the wedge-shaped test object (wedge-angle = 90º) with W/d = 2.

Figure 5.3 represents the effect of Reynolds number on heat transfer coefficient of methane-air flame jet impinging on wedge-shaped test objects with non-dimensional nozzle-to-test object distance equals to 4. The rise in Reynolds number has affected the heat transfer coefficient all over the impinging face. The heat transfer coefficient observed at the impinging zone increases from 145 $Wm^{-2}K^{-1}$ (Re = 800) to 204 $Wm^{-2}K^{-1}$ (Re = 1500). Heating effect along y-direction in comparison with that along the x-direction is observed to be notable.
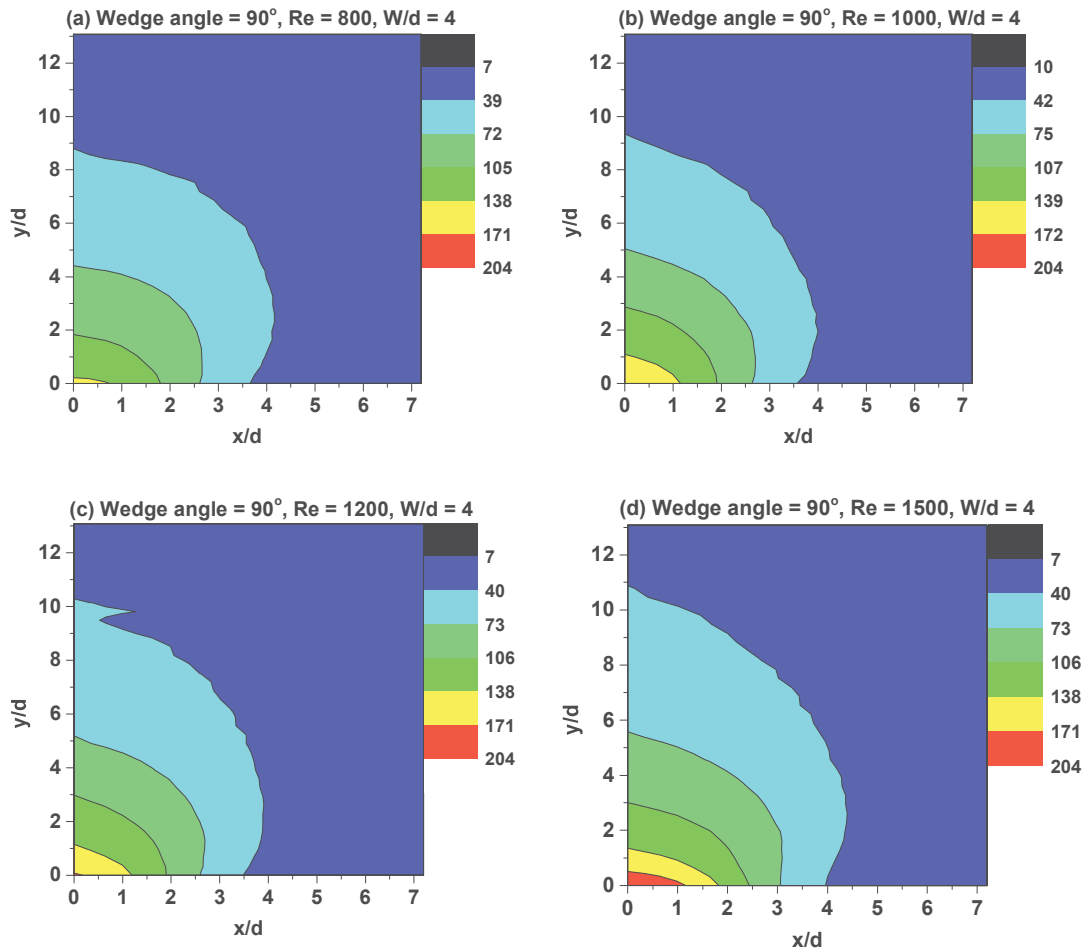
Figure 5.3 **Effect of Reynolds number on heat transfer coefficient (Wm⁻²K⁻¹)** **of methane-air flame jet impinging on the wedge-shaped test object (wedge-angle = 90º) with W/d = 4.**

With an increase of 'W/d' from 2 to 4 (refer figures 5.1 and 5.3), the stagnation point heat transfer coefficient for Re = 800, 1000, 1200, and 1500; reduces from 170 to 145, 182 to 172, 192 to 175, and 241 to 204 respectively. Approximately 15% drop in heat transfer coefficient at the impinging zone is observed when non-dimensional nozzle tip to test object distance increases from 2 to 4.
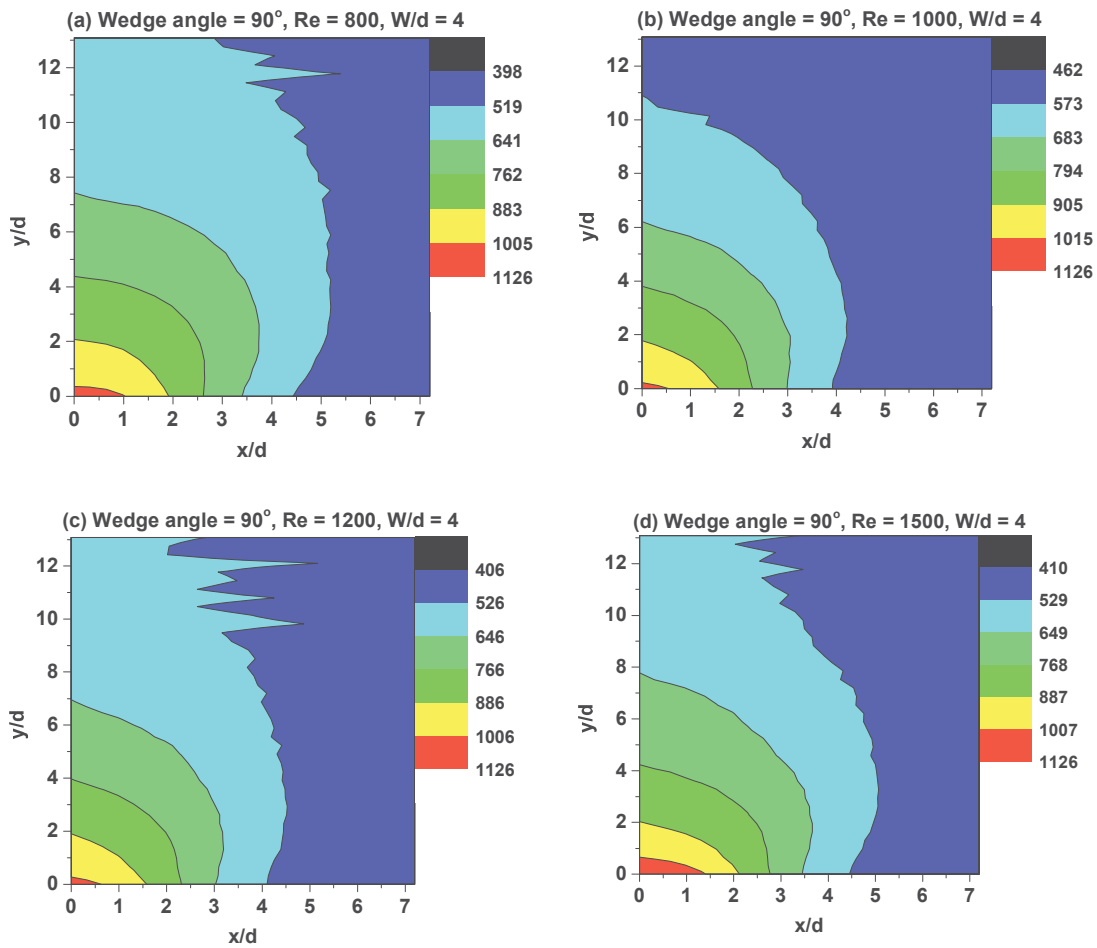
Figure 5.4   Effect of Reynolds number on adiabatic wall temperature (K) of methane-air flame jet impinging on wedge-shaped test objects (wedge-angle = 90°) with W/d = 4.

The effect of Reynolds number on adiabatic wall temperature of methane-air flame jet impinging on the wedge-shaped test object with W/d = 4 is shown in figure 5.4. The plots depict the apparent effect of natural convection along y-direction as an added factor to have a significantly higher heating effect compared to the x-direction. Effect of increasing the non-dimensional nozzle tip to test object distance from 2 to 4 (refer figures 5.2 and 5.4) on adiabatic wall temperature at the impinging zone is observed to be in the range of 5 - 10 % for Reynolds number 800 – 1500 respectively.
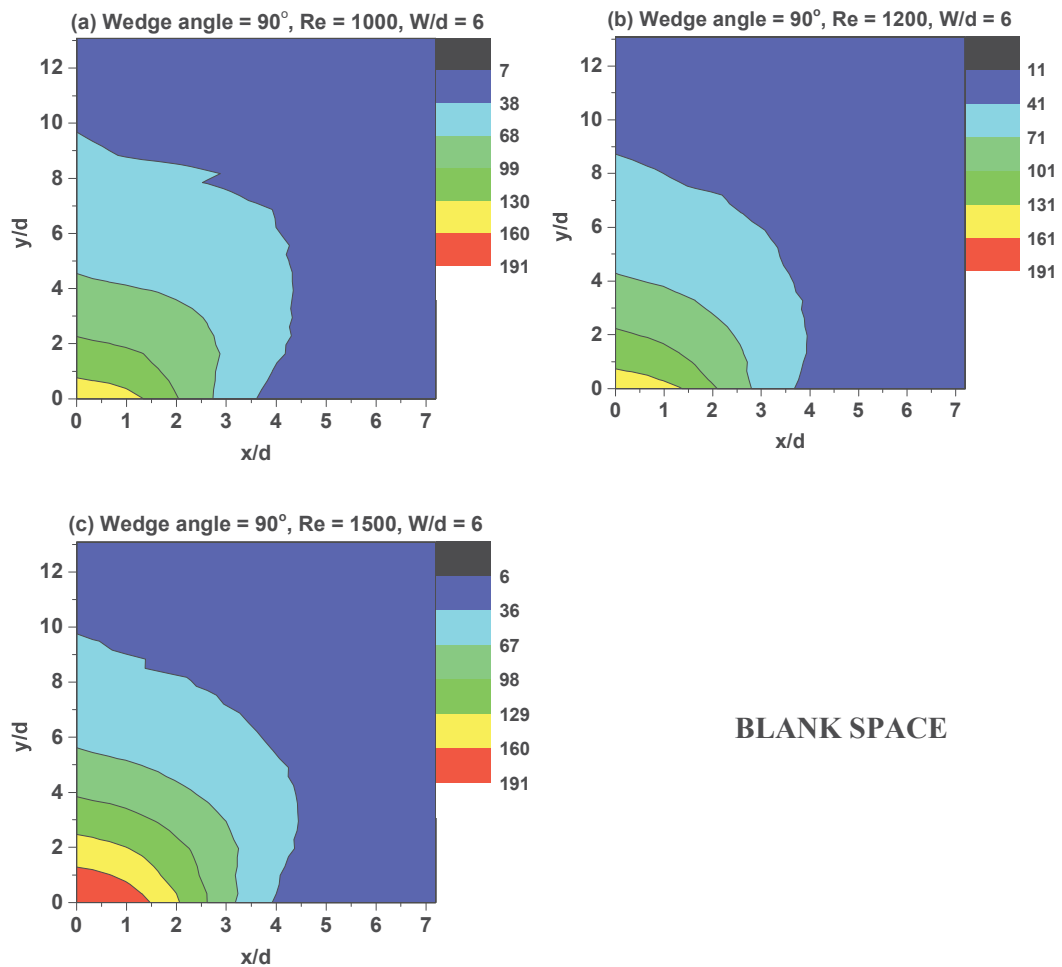
Figure 5.5   Effect of Reynolds number on heat transfer coefficient (Wm^{-2}K^{-1}) of methane-air flame jet impinging on the wedge-shaped test object (wedge-angle = 90º) with W/d = 6.

For W/d = 6, the effect of Reynolds number on heat transfer characteristics is graphically represented in figures 5.5 and 5.6. Reynolds number is varied from 1000 – 1500. A similar observation of having improved convective heat transfer rate along y-direction as compared to x-direction is significant. Hence, effect along y-direction spreads up to y/d = 12, whereas the same along x/d = 4. Approximately 5% drop in both heat transfer coefficient and adiabatic wall temperature is observed when the 'W/d' ratio is increased from 4 to 6. Heat transfer rate in case of W/d = 6 is comparatively lesser compared to W/d = 4 and 2. Therefore, it can be generalised that a significant rise in

estimated values of heat transfer coefficient and adiabatic wall temperature is observed with a rise in Reynolds number and reduction in non-dimensional nozzle-tip to test object distance.
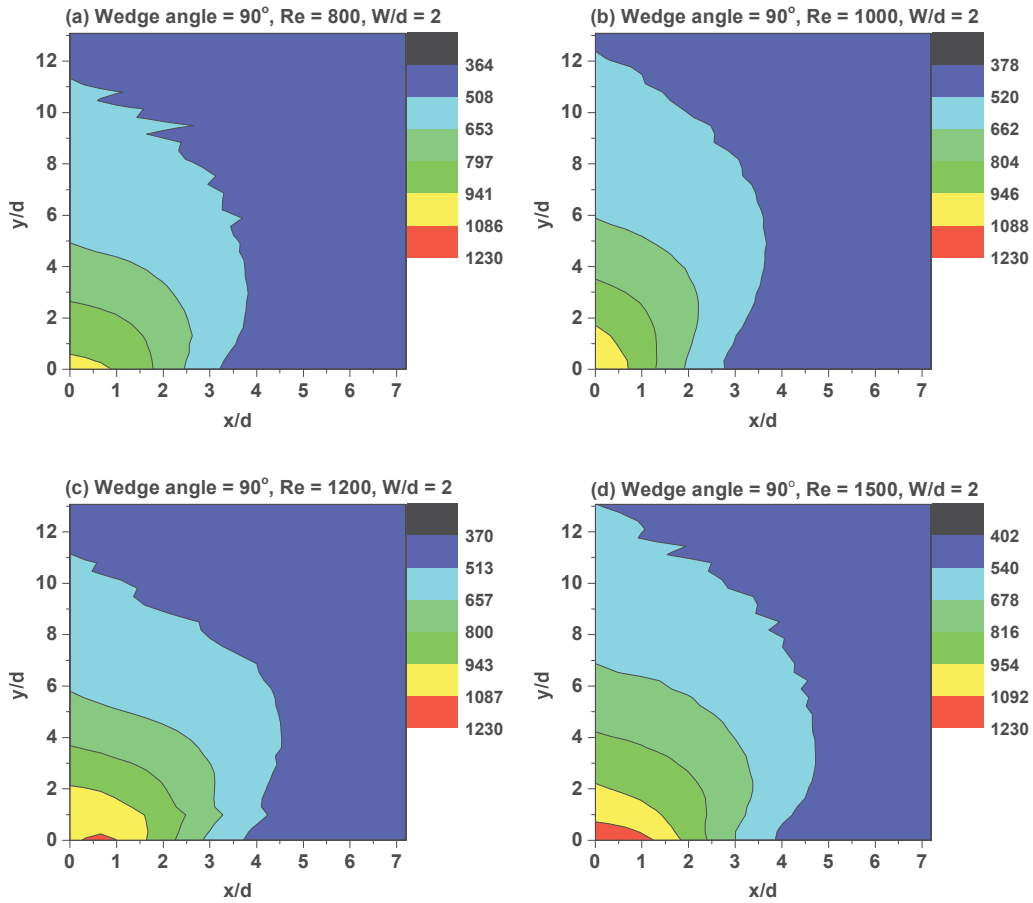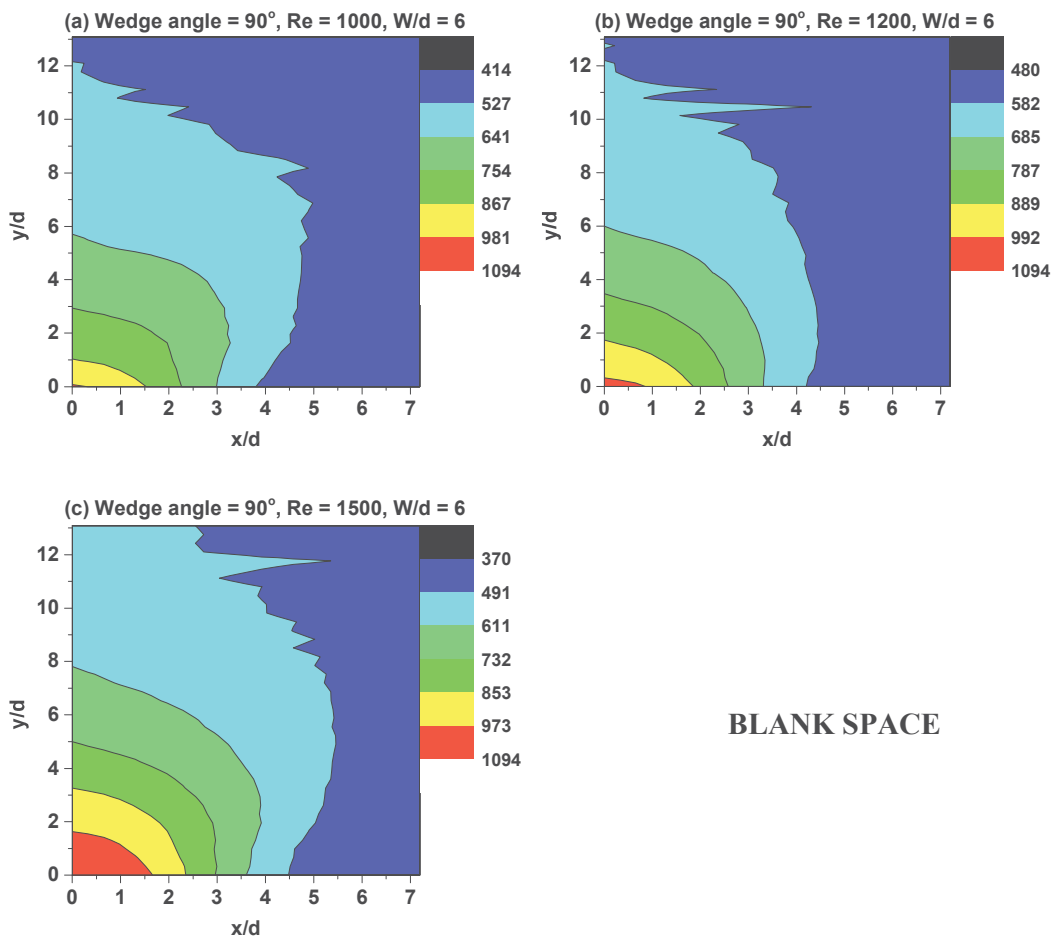

Figure 5.6   Effect of Reynolds number on adiabatic wall temperature (K) of methane-air flame jet impinging on the wedge-shaped test object (wedge-angle = 90º) with W/d = 6.

With reference to the wedge-shaped impinging test object shown in figure 4.12, the heat transfer coefficient and adiabatic wall temperature at both 'x' and 'y' axial lines are represented in succeeding paragraphs of this section. Figures 5.7 and 5.8 show the variation of heat transfer coefficient and adiabatic wall temperature along the x-direction. Heat transfer coefficient and adiabatic wall temperature at the point of

impingement (otherwise called stagnation point) improve with a rise in Reynolds number and reduction in nozzle tip to test object distance. The same effect was observed prior and discussed.
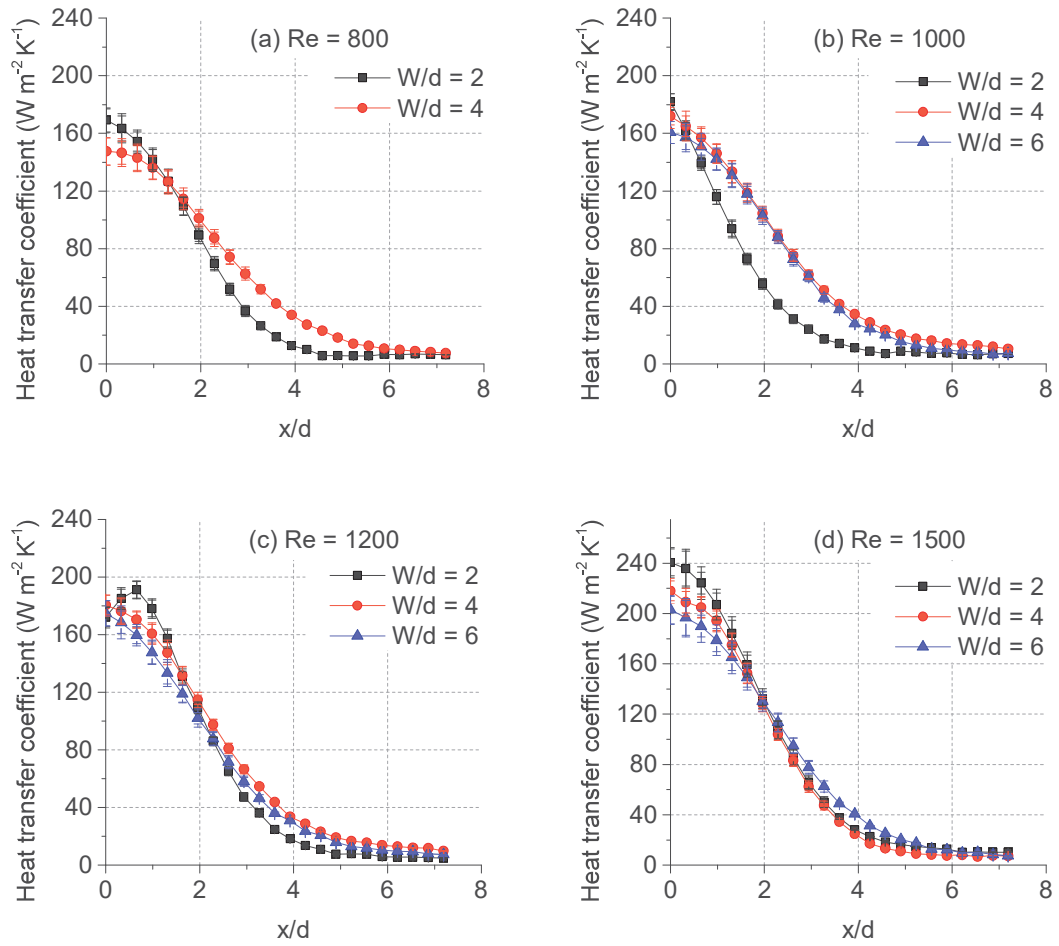
Figure 5.7   Variation of heat transfer coefficient at impinging face along the x-direction (wedge-angle = 90º).
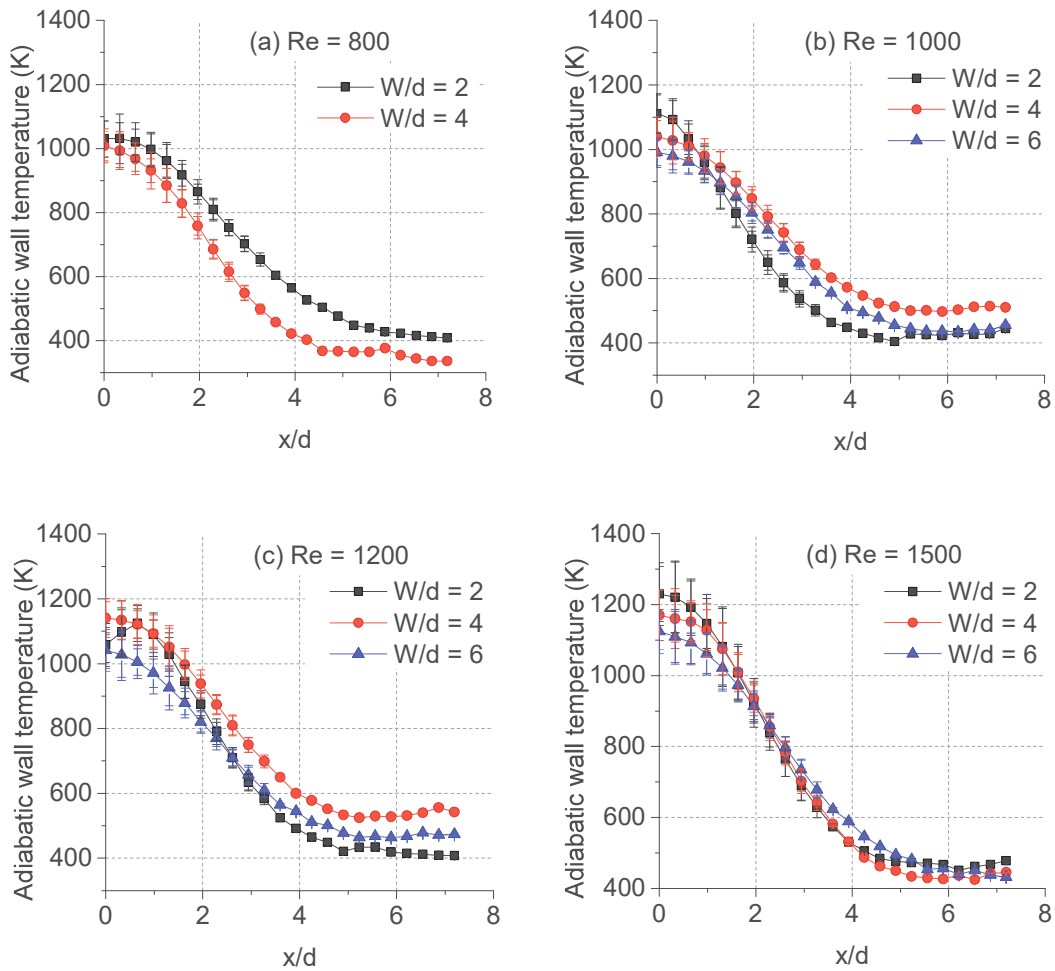
Figure 5.8 **Variation of adiabatic wall temperature at impinging face along the x-direction (wedge-angle = 90º).**

The observed trend of both the parameters along the x-direction remains same as those of flame jet impingement over a flat plate (refer figures 4.19-4.21). For cases with lesser nozzle tip to test object distance (i.e., W/d =2), the heating effect at the impinging zone is higher than the cases with W/d= 4 or 6. However, at locations away from the stagnation zone, the heating effect due to W/d =2 remains lesser as compared to W/d = 4 and 6. This kind of effect is mainly due to lesser lateral conduction and lowers forced convection effect at locations away from the point of impingement. The rate of lateral conduction remains low for Re = 800, because of a comparatively lower rate of combustion of methane (fuel) and hence low flame temperature as well as temperature

gradient within the test object material. Similarly, lower convection heat transfer in case of lesser Reynolds number is simply due to lesser jet velocity at the nozzle exit and lesser adiabatic wall temperature than the cases with higher Reynolds numbers. Referring to figures 5.7 and 5.8, it may be noted that heating effect due to flame impingement is significant up to x/d = 4.
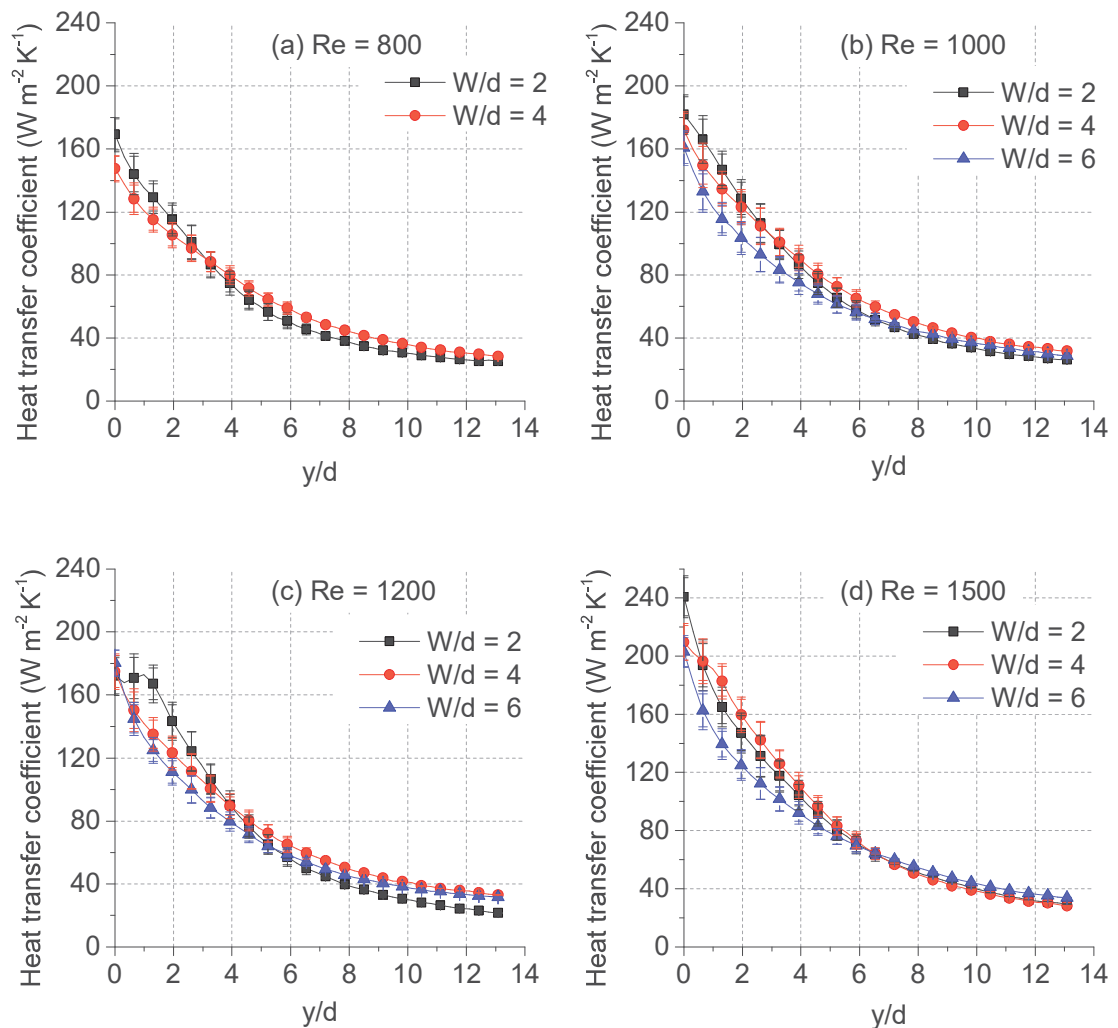
Figure 5.9 **Variation of heat transfer coefficient at impinging face along the y-direction (wedge-angle = 90º).**

In the present study on a wedge-shaped object, it is critical to view the trend and its variation along the test object's wings (y-direction). Accordingly, both heat transfer

coefficient and adiabatic wall temperature along y-direction are shown at figures 5.9 and 5.10, respectively. First of all, the trend of variation of these estimated parameters along the y-direction, which is an inclined surface, is different from that along the x-direction.
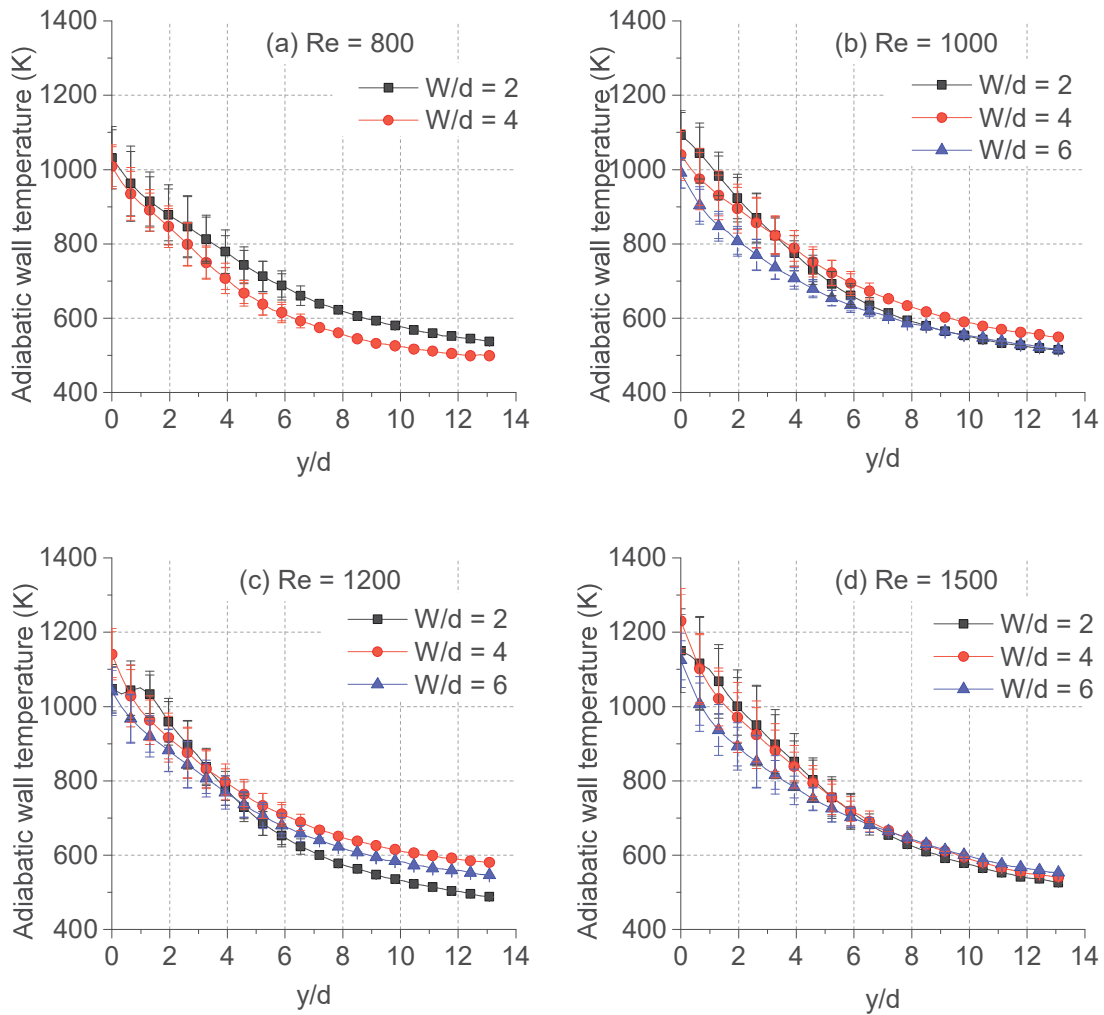
Figure 5.10   Variation of adiabatic wall temperature at impinging face along the y-direction (wedge-angle = 90º).

The maximum heating effect exists in the impinging zone, especially at y/d =0. Further, with an increase in 'y/d' value, both the parameters fall sharply. It may be noted that the

heat transfer coefficient drops by 50% of the stagnation point heating effect within y/d = 4. The drop-in-adiabatic-wall-temperature-by-50% varies from y/d = 4 (for Re = 800) to y/d = 10 (for Re = 1500). At higher Reynolds number, additional lateral conduction is observed. This typical trend of variation of both the parameters is dissimilar to that in case of flame jet impingement over a flat plate. These observations are justified with an argument that natural convection could be existing along the y-direction, in addition to the forced convection.

A notable difference in these parameters with respect to change in 'W/d' near the impinging zone (up to y = 4d) is observed to be existing, and for the zone beyond y = 4d, the negligible difference in heat transfer characteristics with respect to change in 'W/d' is observed. This means that the effect of flame jet impingement remains nearly up to y = 4d, and beyond y = 4d, merely the natural convection remains effective. The uncertainty of estimation of the unknown parameters reduces as we progress away from stagnation point. Higher temperatures near the stagnation point and faster change in temperature at the stagnation zone compared with the farther locations lead to higher uncertainties in measuring transient temperature and estimating both the parameters.

5.1.2 Wedge-angle 120º

Figure 5.11 Effect of Reynolds number on heat transfer coefficient (Wm^{-2}K^{-1}) of methane-air flame jet impinging on a wedge-shaped test object (wedge angle = 120º) with W/d = 2.

A second test object having a wedge angle equals 120°, keeping all other geometric and physical parameters of the object same is considered in the study. This extended study aims to look into the effect of impinging flame jet heat transfer when the wedge-angle is increased. Reynolds number and non-dimensional nozzle tip to test object distance are varied from 800-1500 and 2-6, respectively, which are same as that of the previous case. The experimental procedure and environmental conditions are maintained at par with those of the previous case. For W/d = 2, experiments were conducted for Reynolds number 800 and 1000. Contour plots in respect of heat transfer coefficient and adiabatic wall temperature are shown at figures 5.11 and 5.12, respectively. When we compare with similar cases of wedge-angle 90°, an approximately 10% increase in heat transfer coefficient and adiabatic wall temperature for Re = 1000 is observed, whereas a minor increase in heating effect for Re = 800 is observed.
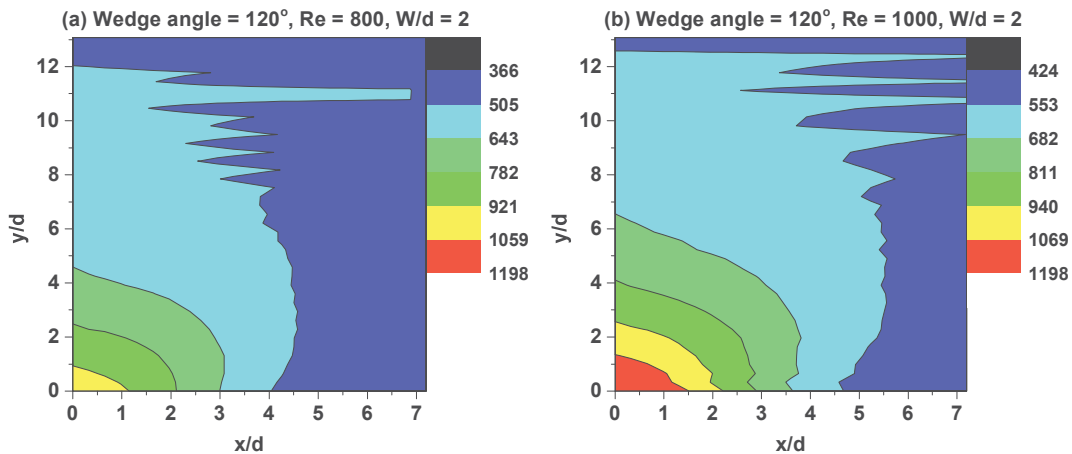
Figure 5.12   Effect of Reynolds number on adiabatic wall temperature (K) of methane-air flame jet impinging on the wedge-shaped test object (wedge angle = 120°) with W/d = 2.

Figure 5.13 shows the effect of Reynolds number on the heat transfer coefficient of methane-air flame jet impinging on the wedge-shaped test object (wedge-angle 120°) with W/d = 4. When compared with the corresponding plots in respect of wedge-angle 90° in figure 5.3, it is observed that the rise in heat transfer coefficient at the impinging zone is approximately 10% for Re = 1200 and 1500, whereas the same in case of Re = 800 and 1000 is approximately 5%. Effect of the flame jet on heat transfer coefficient

near impinging zone but along x-direction compared with y-direction is more; however, the spread of the same at locations away from the impinging zone along y-direction is more. This explains the lone effect of impinging flame jet and the existence of corresponding forced convention only at the impinging zone. Which further is more effective over a perpendicular edge as compared to an inclined surface. Similarly, for the location away from the impinging zone, natural convection along the inclined surface (y-direction) dominates the convection due to flame jet along the x-direction. It can be concluded that the additional heating effect observed along the inclined surface may be mainly due to natural convection.
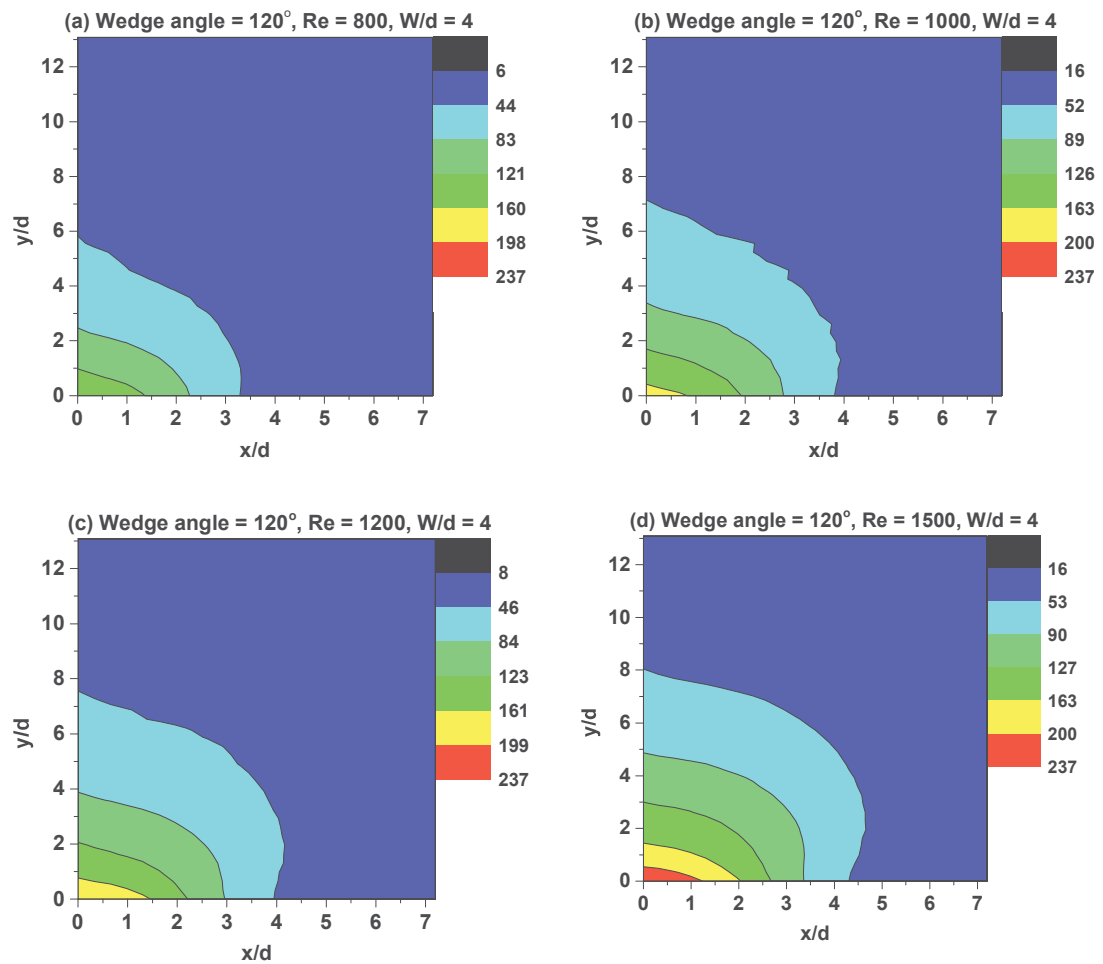
Figure 5.13 **Effect of Reynolds number on heat transfer coefficient (Wm^{-2}K^{-1}) of methane-air flame jet impinging on the wedge-shaped test object (wedge-angle = 120º) with W/d = 4.**

Adiabatic wall temperature over the impinging side is plotted in figure 5.14. Approximately 10% rise in adiabatic wall temperature as against the case of wedge-angle 90° for Re = 1200 and 1500 is observed. Improvement in heating effect for higher Reynolds number when the wedge-angle is increased from 90° to 120° is due to lowered effect of natural convection in case of later and increased effect of forced convection due to flame jet at higher Reynolds number. Additionally, as an example (refer figures 5.4 and 5.14), adiabatic wall temperature in case of wedge-angle 90° at around y/d = 5 remains approximately 750K, whereas the same in case of wedge-angle 120° at around y/d = 6 remain approximately 750K. This confirms improvement in the heating effect of the flame jet when the wedge-angle is increased from 90° to 120°.
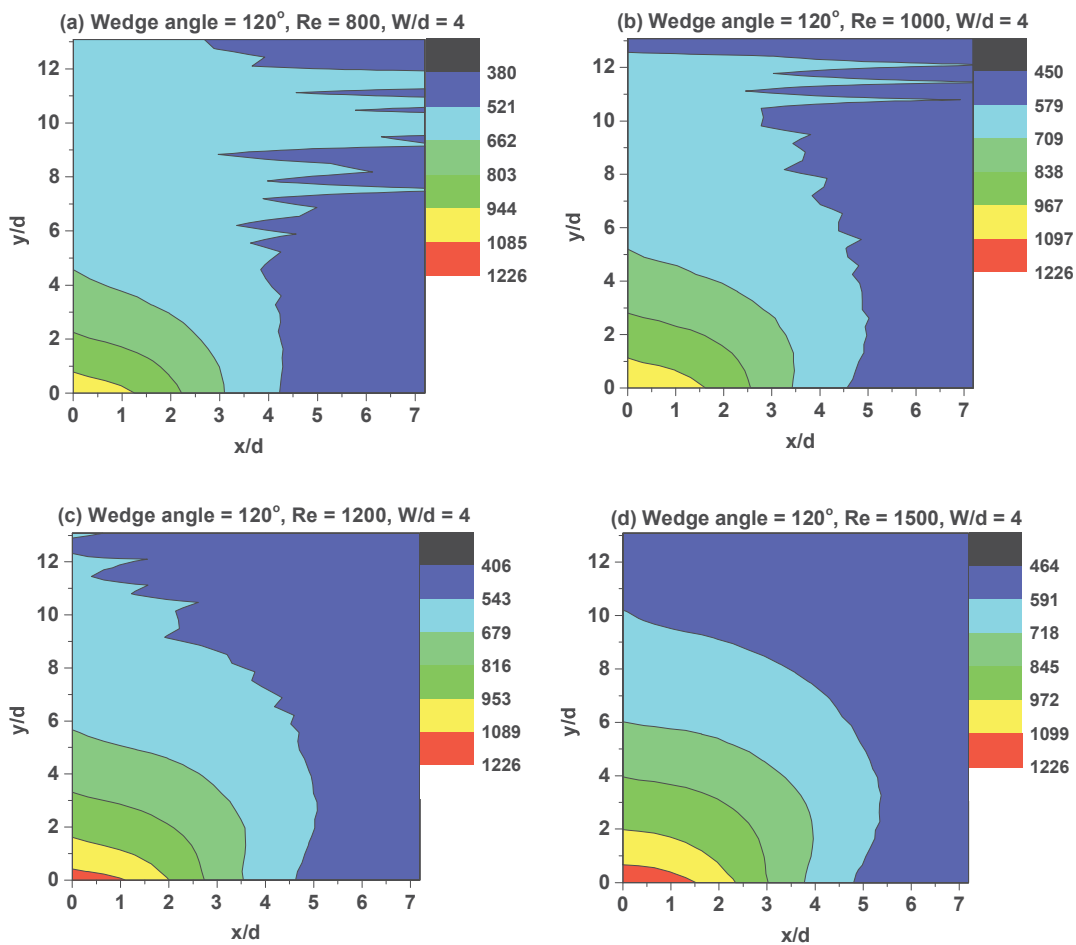
Figure 5.14   Effect of Reynolds number on adiabatic wall temperature (K) of methane-air flame jet impinging on the wedge-shaped test object (wedge-angle = 120°) with W/d = 4.

(a) Wedge angle = 120°, Re = 1000, W/d = 6

(b) Wedge angle = 120°, Re = 1200, W/d = 6

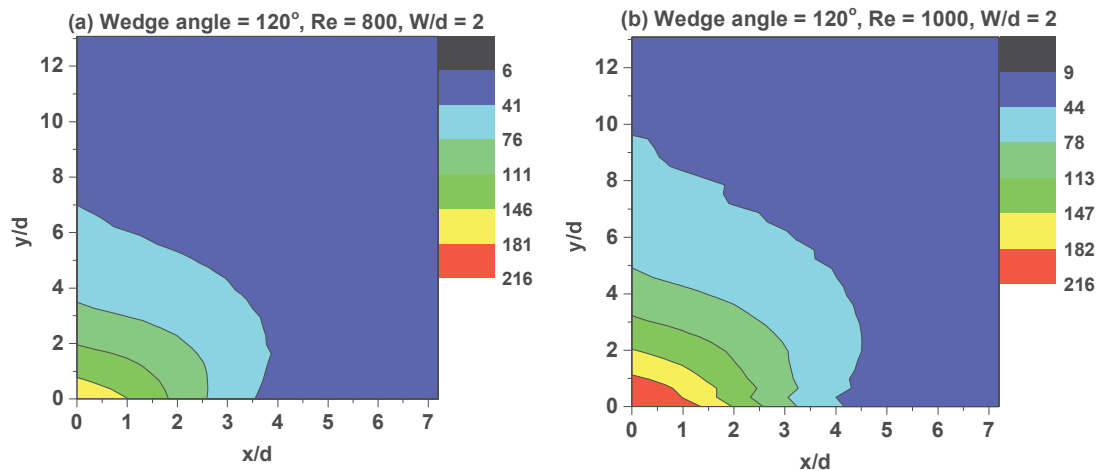**(c) Wedge angle = 120°, Re = 1500, W/d = 6**

BLANK SPACE
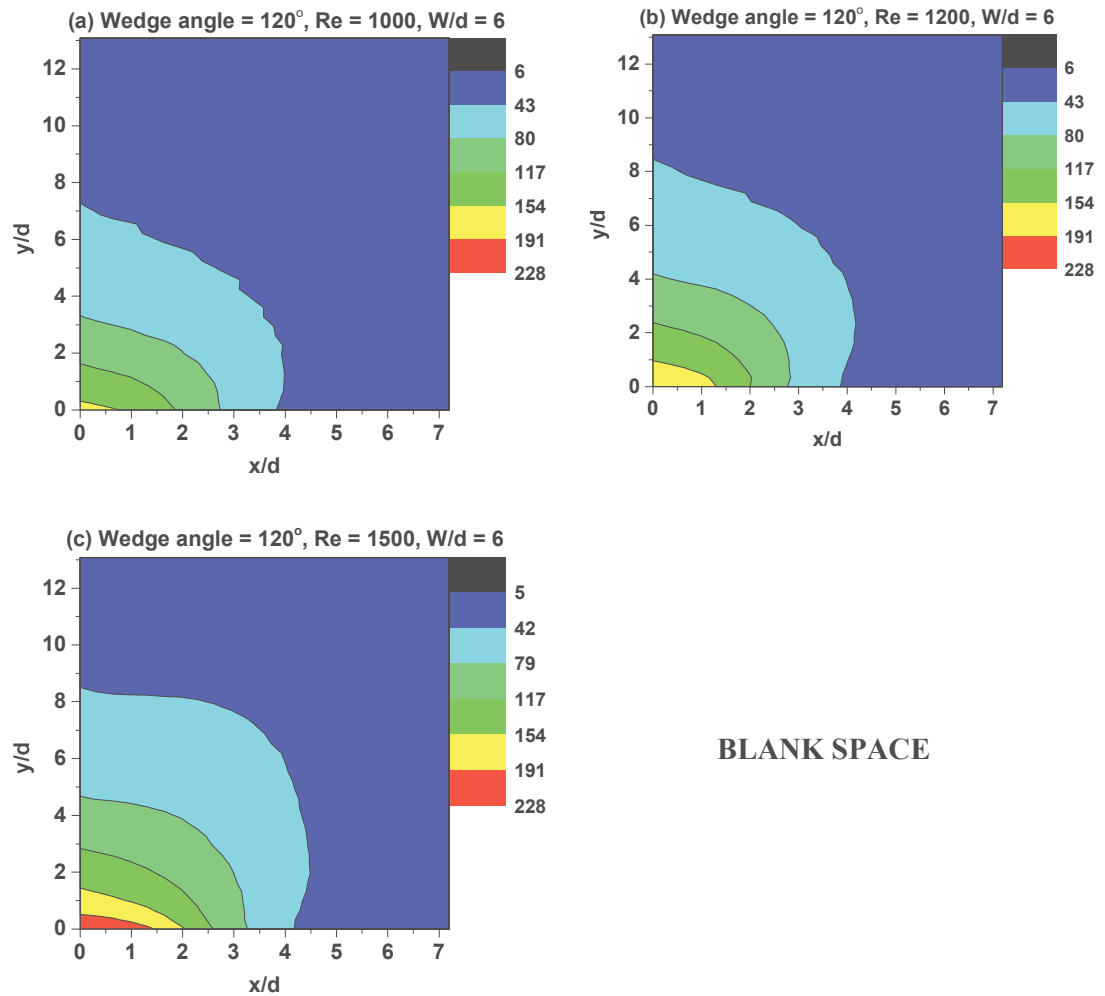
Figure 5.15   Effect of Reynolds number on heat transfer coefficient ($Wm^{-2}K^{-1}$) of methane-air flame jet impinging on the wedge-shaped test object (wedge-angle = 120°) with W/d = 6.

Figures 5.15 and 5.16 are the last set of contour plots of this study, which show the effect of Reynolds number on heat transfer characteristics of methane-air flame jet impinging on wedge-shaped test object with W/d = 6. 5-10% rise in both heat transfer coefficient and adiabatic wall temperature is observed in case of Reynolds number 1200 and 1500. Least increment is observed for Reynolds number 1000. This again validates that higher Reynolds number (for higher wedge-angle) can improve the heating transfer rate. This is due to the existence of turbulence near the impinging zone where the flame and exhaust gases have to change the flow direction.

91

(a) Wedge angle = 120°, Re = 1000, W/d = 6

(b) Wedge angle = 120°, Re = 1200, W/d = 6

(c) Wedge angle = 120°, Re = 1500, W/d = 6

BLANK SPACE
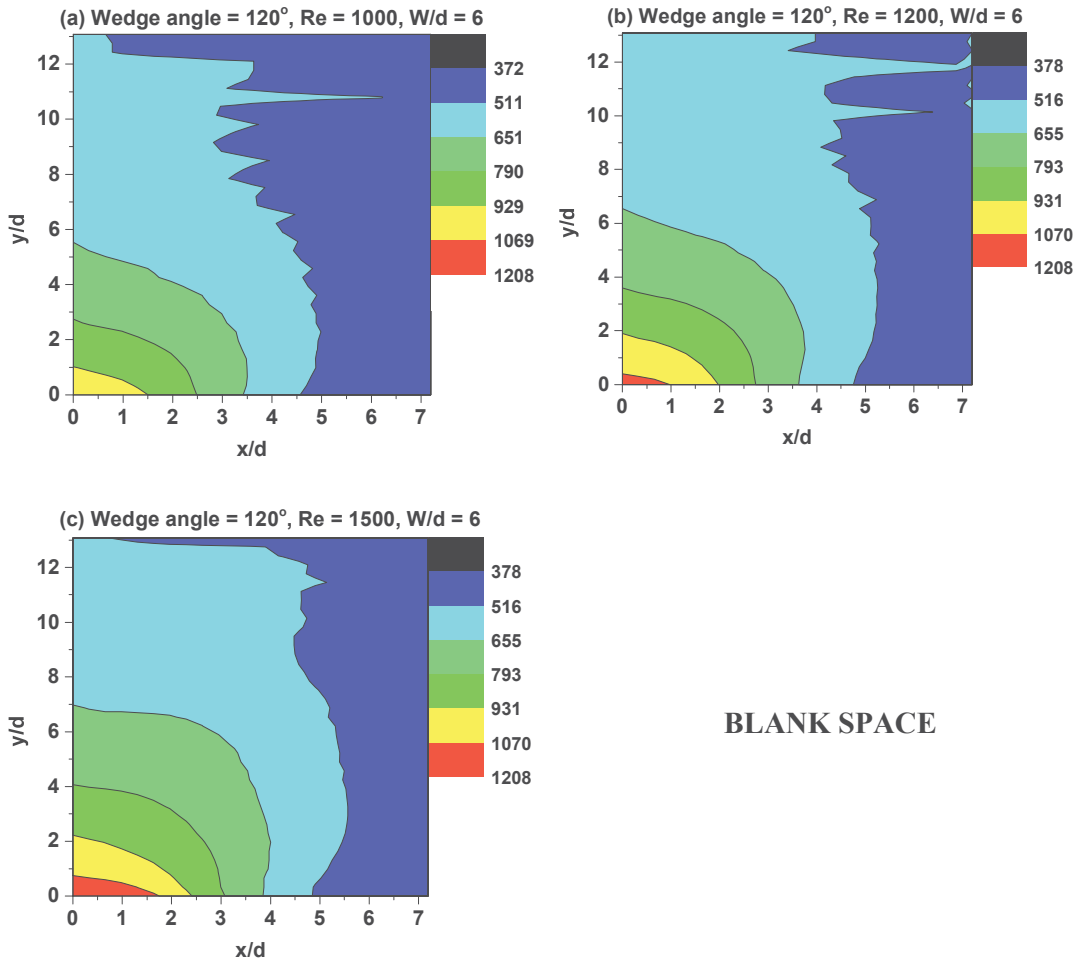
Figure 5.16   Effect of Reynolds number on adiabatic wall temperature (K) of methane-air flame jet impinging on the wedge-shaped test object (wedge-angle = 120º) with W/d = 6.

With reference to figure 5.16(c), temperature contour passing at x/d = 3 (along x-direction) approaches at y/d = 4 (along y-direction). Similarly with reference to figure 5.6(c), temperature contour passing at x/d = 3 (along x-direction) approaches at y/d = 5 (along y-direction). A similar trend is observed in all cases. This shows a reduction in heating effect along y-direction or reduction in the spread of heating effect along y-direction compared with x-direction, which is due to the reduced effect of natural convection when the wedge-angle is increased.
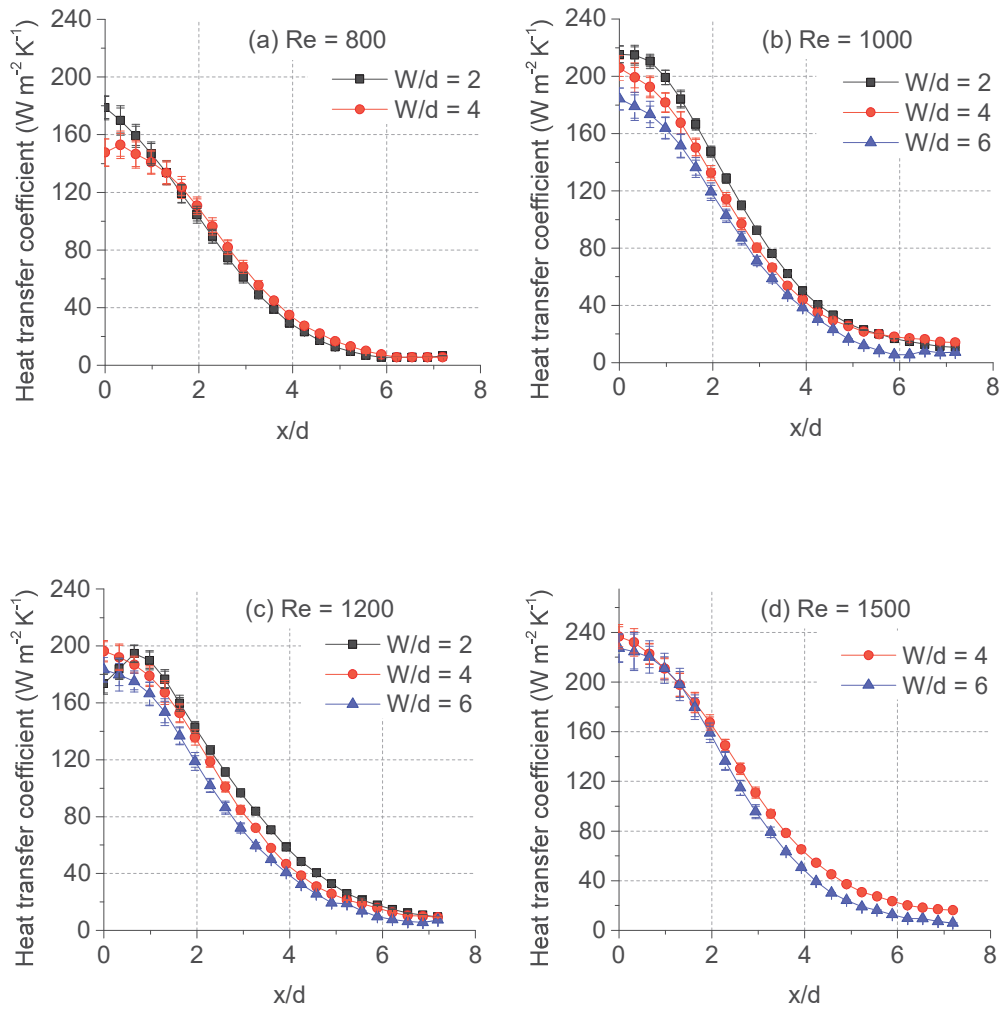
Figure 5.17   Variation of heat transfer coefficient at impinging face along the x-direction (wedge angle = 120º).

Heat transfer coefficient along x-direction with varying 'W/d' and Reynolds number are plotted in figure 5.17. As discussed earlier, the heating effect is observed to have improved by 5-10% as compared to previous test object having wedge-angle = 90º. Along x-direction, both the parameters follow a similar trend as that of a case of flame jet impingement over a flat plate. The trend is because of increased heat transfer at the impinging zone due to the noticeable effect of the flame jet to reduce the boundary layer.
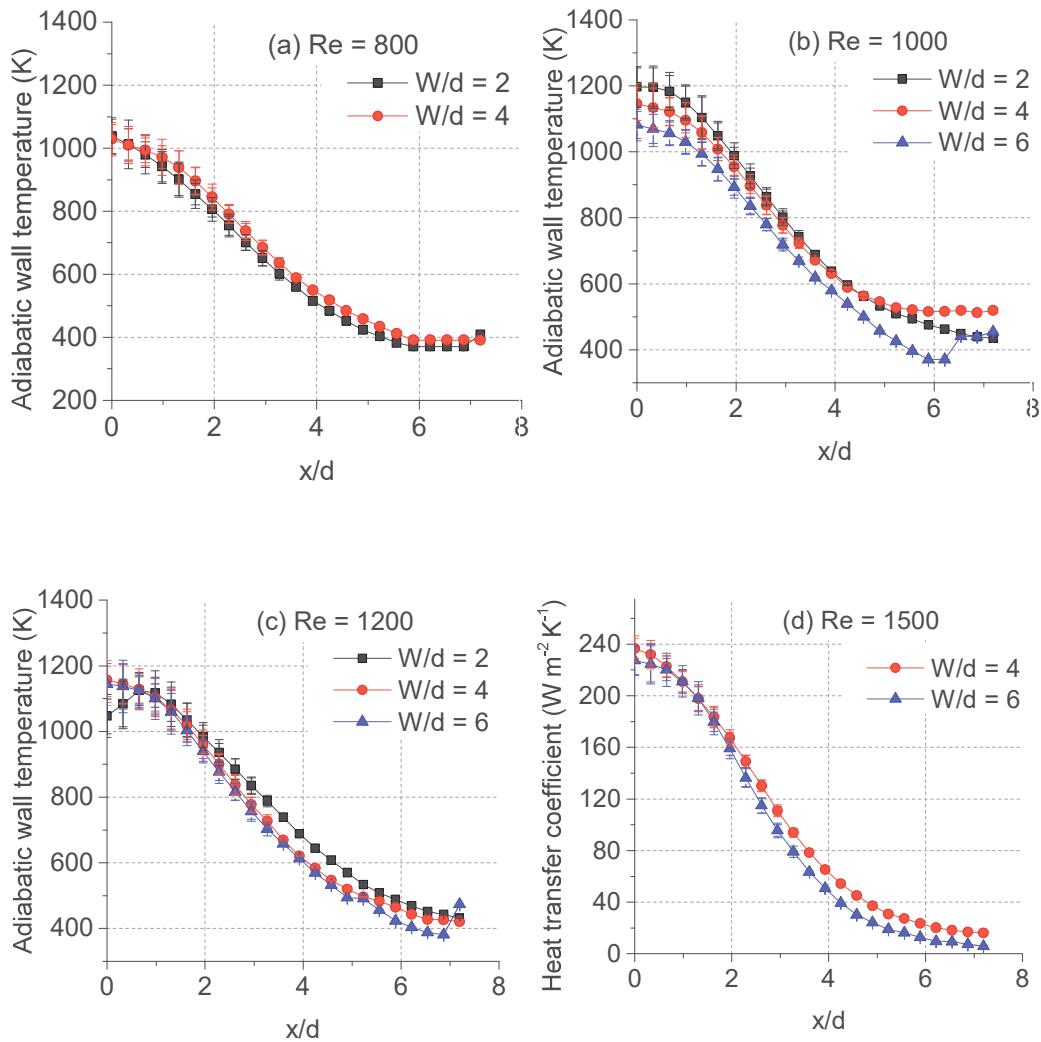
Figure 5.18 **Variation of adiabatic wall temperature at impinging face along the x-direction (wedge angle = 120º).**

The variation of adiabatic wall temperature at the impinging face of the test object having wedge-angle = 120º along x-direction is presented at figure 5.18. A similar effect on adiabatic wall temperature with regard to Reynolds number and W/d is observed. A comparative analysis between the results of both the test objects (wedge-angle 90º and 120º) is undertaken and presented in next section.
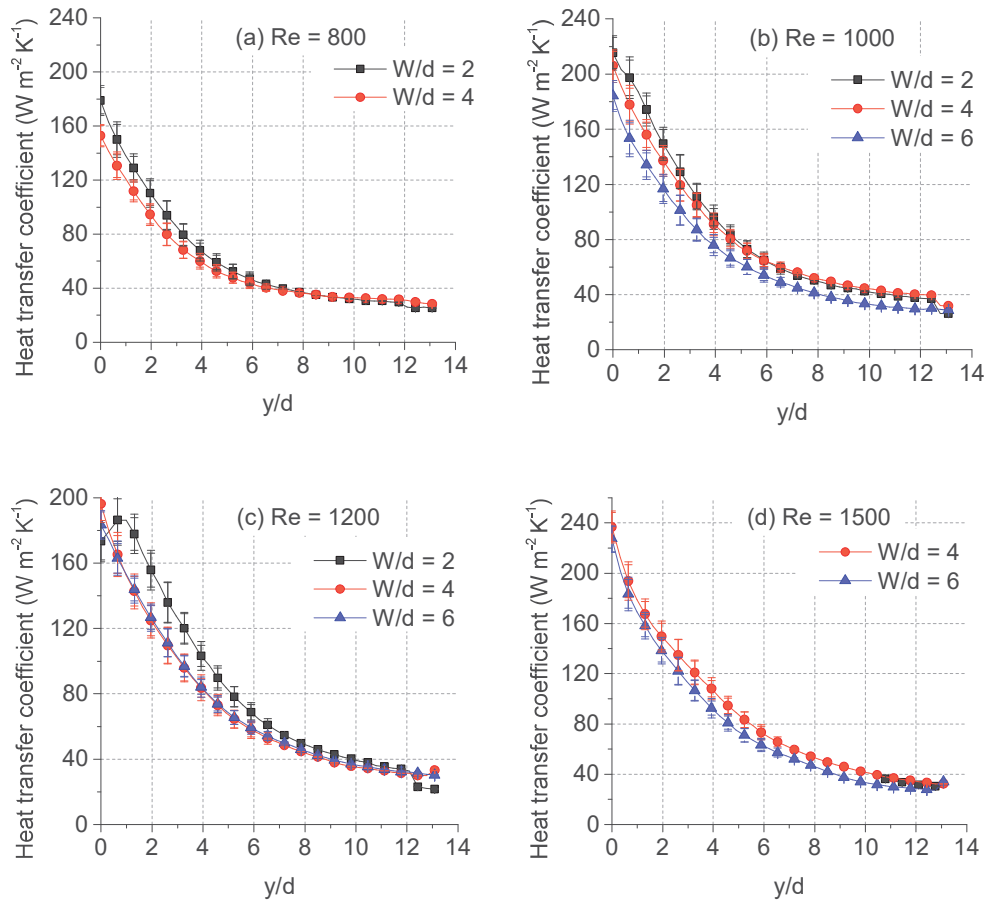
Figure 5.19   Variation of heat transfer coefficient at impinging face along the y-direction (wedge angle = 120º).

Figures 5.19 and 5.20 represent the effect of both Reynolds number and W/d on heat transfer coefficient and adiabatic wall temperature respectively. The observed variation of both the parameters is similar to those in case on wedge-angle = 90º. This kind of variation is unique to wedge-shaped object. The thermal effect along the wedge (y-direction) is found to be much farther compared to x-direction.
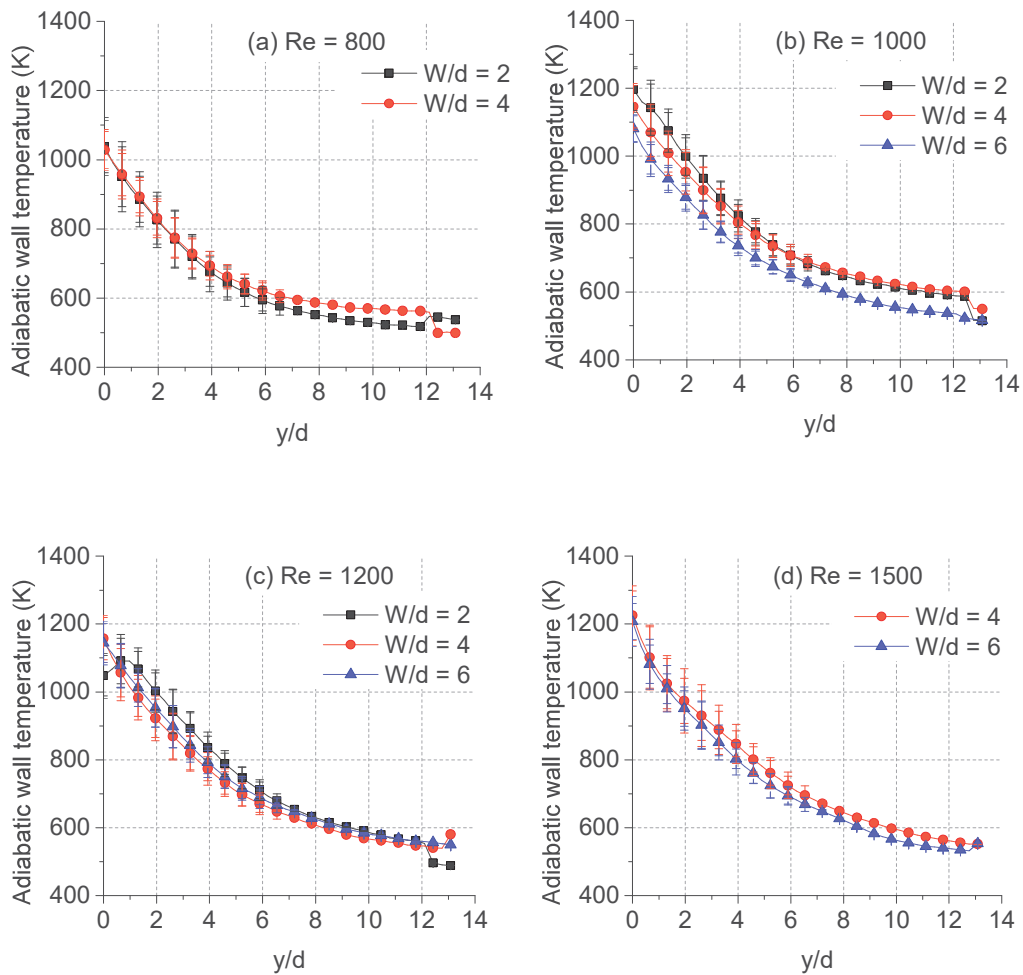
Figure 5.20   Variation of adiabatic wall temperature at impinging face along the y-direction (wedge angle = 120º).

5.2   Comparison of results in respect of Wedge-angle 90º and 120º

A comparative analysis of heat transfer characteristics in respect of both the test objects is undertaken in this section of the study. Analysis in this section shows the effect of wedge-angle on heat transfer characteristics of flame jet. As discussed earlier, experiments are undertaken on two different test object. The difference is based on wedge-angle (90º and 120º). Figure 5.21 shows comparative plots for W/d = 4, for Re = 800, 1000, 1200, 1500 along x-direction. The heat transfer coefficient along x-direction for wedge-angle = 120º is higher by approximately 10% when compared with

the same for wedge-angle = 90°. Maximum variation of heating effect near stagnation zone is observed. Lesser difference in estimated values of heat transfer coefficient over entire impinging zone is observed for Re = 800.
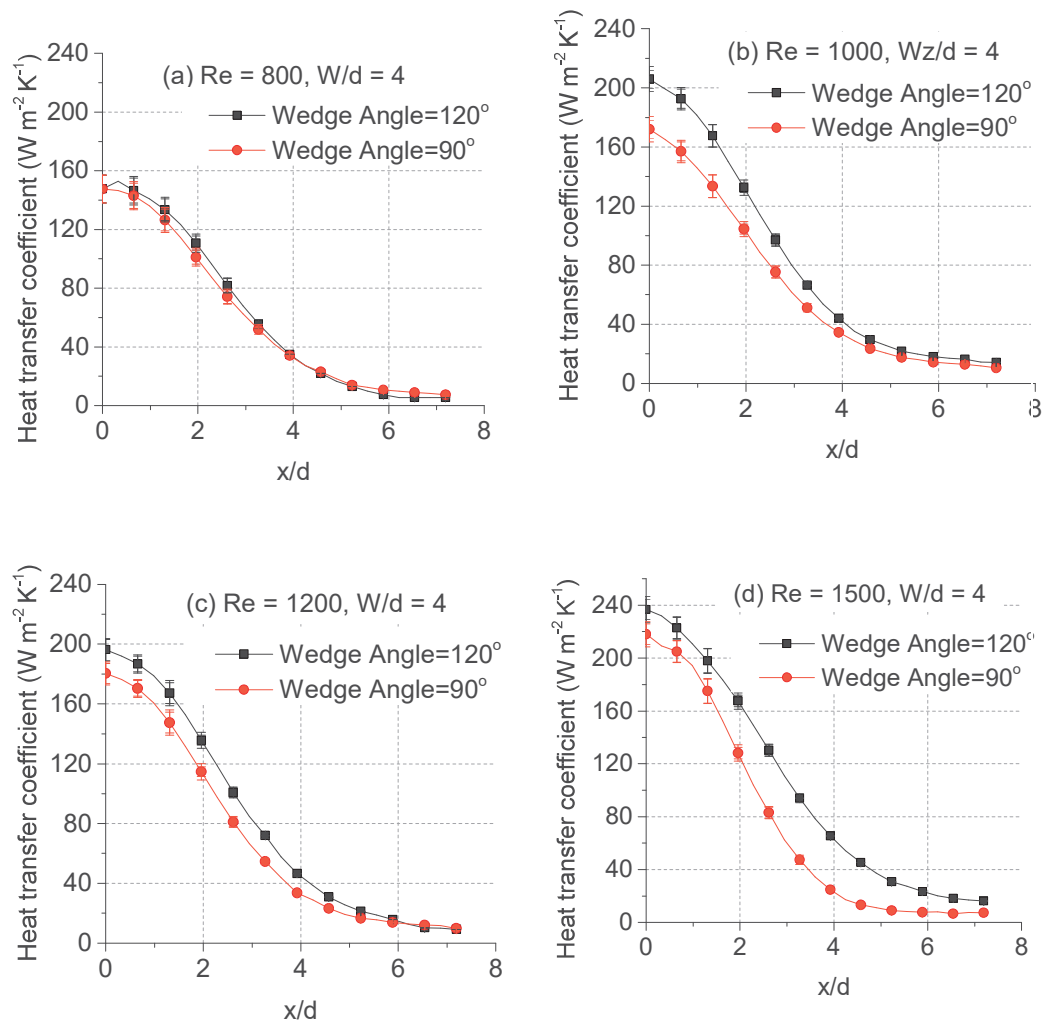
Figure 5.21   Comparison of heat transfer coefficient at impinging face along the x-direction (for W/d = 4).

Similarly, a comparative study on variation of adiabatic wall temperature over both the test objects at W/d = 4 is presented in figure 5.22. The adiabatic wall temperature over the impinging face of the test object having wedge angle = 120° is found to be higher

in comparison with the other test object. The deviation in this case is approximately 5%.
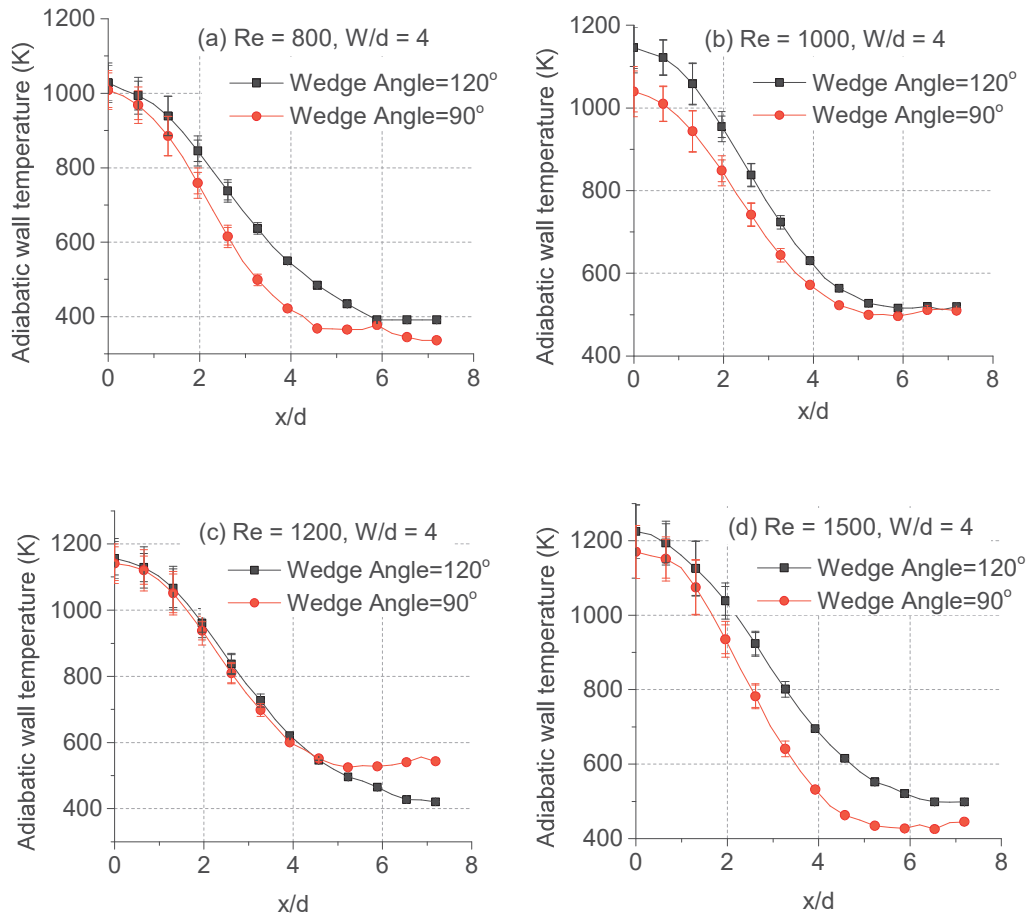
Figure 5.22   Comparison of adiabatic wall temperature at impinging face along the x-direction (for W/d = 4).

With increase in wedge-angle, the test object projected (top view) area increases. That means, the flame exhaust encounters additional drag effect (in case of wedge-angle = 120°) while flowing out under the test object at the wall jet region, which reduces the exit velocity of the exhaust. Additionally, the flame exhaust post impingement gets comparatively lesser effect of natural convection to flow the exhaust away in case of higher wedge-angle. Therefore, effective time of thermal interaction between the hot fluid and the test object at the wall jet region increases, leading to comparatively thicker

thermal boundary layer. Hence temperature gradient across the boundary layer increases and the heat transfer rate with higher wedge-angle increases.
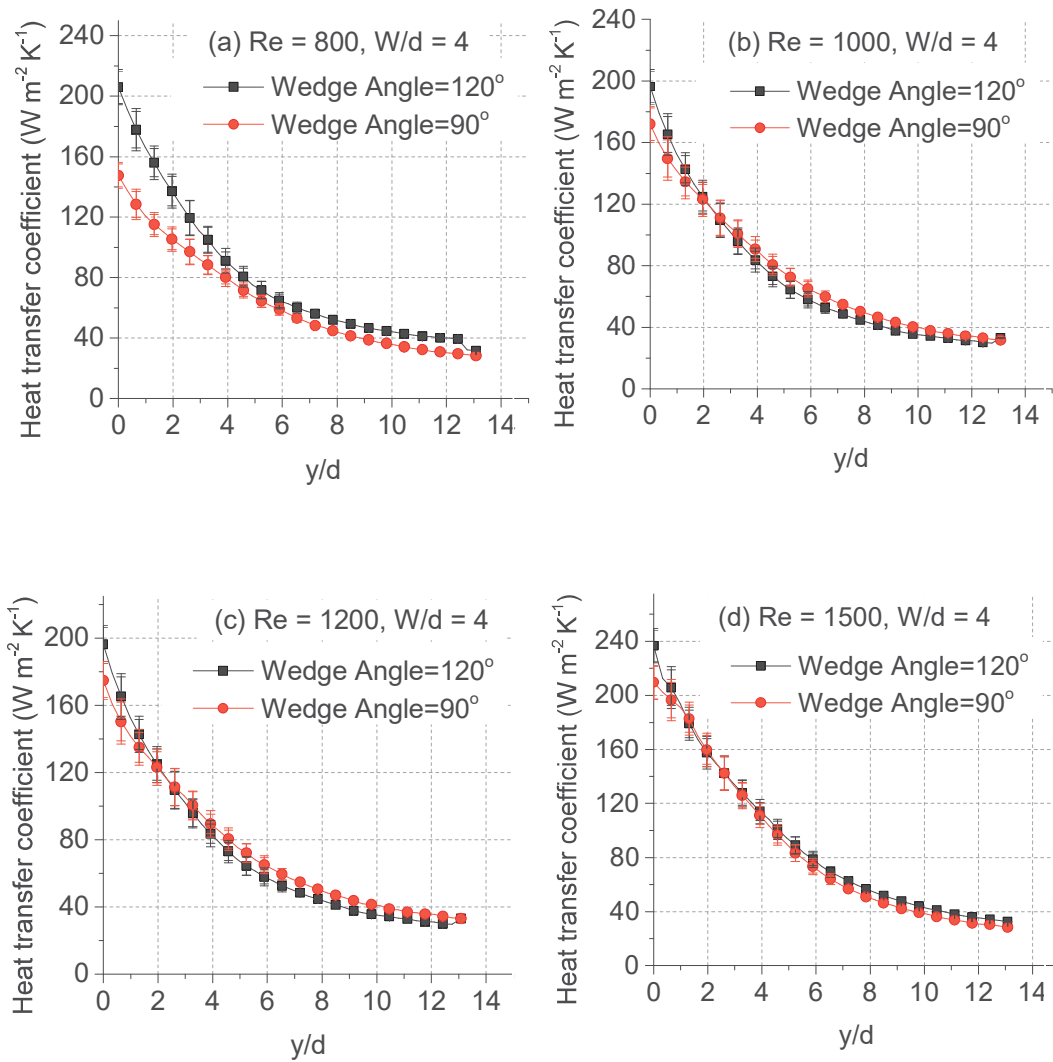
Figure 5.23   Comparison of heat transfer coefficient at impinging face along the y-direction (for W/d = 4).

Further, the comparisons of both heat transfer coefficient and adiabatic wall temperature along y-direction are carried out. The comparative plots for W/d =4 are shown in figures 5.23 and 5.24. Primary observation is that no significant effect of

wedge-angle when varied from 90° to 120° on the heat transfer characteristics along y-direction exists in most cases.
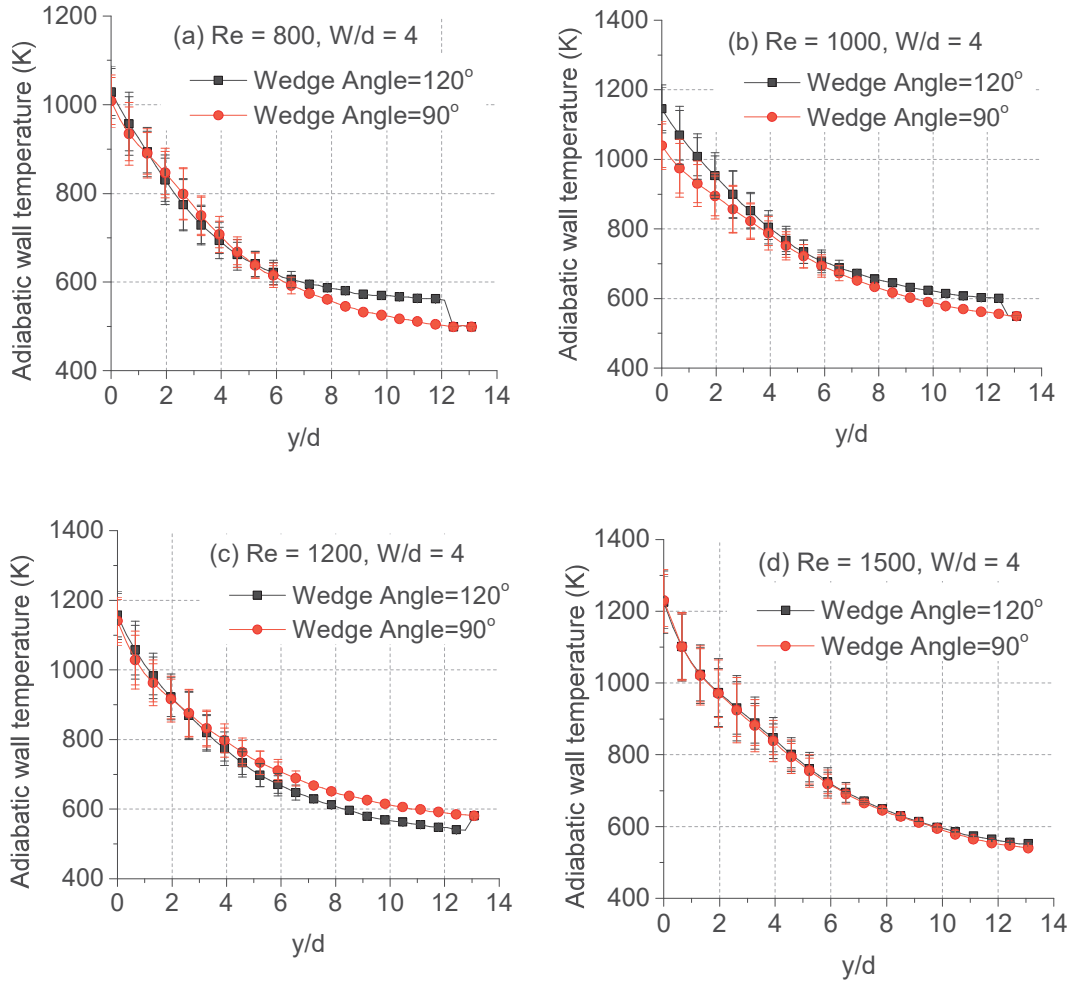
Figure 5.24 **Comparison of adiabatic wall temperature at impinging face along the y-direction (for W/d = 4).**

Chapter 6

CONCLUSIONS

In the present study, an analytical methodology for simultaneous estimation of both heat transfer coefficient, and adiabatic wall temperature using transient IHCP, is validated. A flat plate being impinged experimentally by methane-air flame jets of Reynolds number equals to 1000 and 1200, equivalence ratio equals to one and non-dimensional burner tip to impinging plate distance equals to four and six respectively were considered for demonstration of the proposed transient methodology. The only input for analysis is the transient temperature at the non-impinging face. Both radiation and convection mode of heat transfer at the exposed surfaces (boundaries) are accounted for in the proposed methodology. The analytical technique is applied to estimate the heat transfer characteristics over a wedge-shaped object when impinged by a methane-air flame. The salient features of this work are:-

(a)   The proposed analytical methodology undertakes transient conduction heat transfer analysis within the target material (impinging plate). Transient temperature history at the accessible face of the target body for as low as two to three seconds duration is sufficient input for analysis, thus being independent of external fluid flow conditions at the impinging face. It predicts the convective heat transfer characteristics at the boundary, which is inaccessible or unsuitable for any kind of measurement.

(b)   The effect of radiation heat transfer is incorporated in the solution procedure by using Green's Function Approach. It enables the technique to be used even at higher temperature applications such as analysis of heat transfer characteristics at the receiving end of a deflector plate of the missile launcher, etc.

(c)   Wedge-shaped test objects with wedge angles 90º and 120º are studied when impinged by flame jets with varied Reynolds number and nozzle tip to test object distance. Data analysis is undertaken using the proposed IHCP technique.

The findings of this study are:-

(i)   Near the impinging zone, the heating effect along the horizontal edge (x-direction) is higher as compared to the inclined wing (y-direction). However, the same is opposite for locations away from the impinging zone. Heating effect along y-direction in comparison with that along the x-direction is notable. Possible occurrence of natural convection due to inclined surface along y-direction as additional convection force leads to a higher heating effect.

(ii)   Effect of increasing the non-dimensional nozzle tip to test object distance from 2 to 4 on adiabatic wall temperature at the impinging zone is observed to be 5 - 10 % for Reynolds numbers 800 – 1500, respectively.

(iii)   The trend of variation of the estimated parameters along the y-direction, which is an inclined surface, is different than that along x-direction. The maximum heating effect exists in the impinging zone. It may be noted that the heating effect drops by 50% of the stagnation point heating effect within a radial distance of '4d'.

(iv)   Results in respect of wedge angle 90º and 120º shows that the rise in heat transfer coefficient and adiabatic wall temperature at the impinging zone in case of later is approximately 10% for Re = 1200 and 1500. In contrast, the same in the case of Re = 800 and 1000 is around 5%. Such effect is due to lesser natural convection effect and increased influence of forced convection due to flame jet at higher Reynolds number.

(v)   Adiabatic wall temperature in the case of wedge angle 90º at around y/d = 5 remains approximately 750K. In contrast, the same in wedge angle 120º at around y/d = 6 remains about 750K. The same is valid for all other cases. This confirms improvement in the heating effect of the flame jet when the wedge angle is increased from 90º to 120º.

6.1   Key Contributions

Aligned with the objectives of the research work, the contributions of the present study are mainly of two categories, which discussed briefly in next paragraph.

(a)   Proposed an analytical transient inverse heat conduction solution procedure using Green's function having following features:-

(i)   Experimentally obtained raw transient temperature at non-impinging face for a duration of two – three seconds is sufficient input for the analysis.

(ii)   Significant radiation effects due to high surface temperature is incorporated into the analytical procedure. The surface factors for calculating the radiation loss can also be included, without changing the algorithm.

(iii)   The proposed methodology can estimate the heat transfer coefficient and adiabatic wall temperature at the impinging face simultaneously.

(iv)   Uncertainty of the estimated parameters have been evaluated using Monte Carlo technique.

(b)   Undertakes experimental study of flame jet impingement heat transfer characteristics over wedge-shaped object with following parametric variations:-

(i)   Reynolds number if the flame jet = 800, 1000, 1200 and 1500.

(ii)   Dimensionless nozzle tip to impinging surface distance = 2, 4 and 6.

(iii)   Wedge-angle = 90º and 120º

6.2   **Future scope of work**

(a)   To undertake experiments on high speed inverted jets impinging over a wedge-shaped object to mimic true impinging effects of missile exhaust.

(b)   To implement the analytical technique for various other materials.

(c)   To propose an analytical technique by replacing LMA with Conjugate Gradient technique towards achieving higher robustness and efficiency of the algorithm.

APPENDIX A

Derivation of Green's Function

In this section, the Green's function of the problem under consideration is derived using classic Separation of Variable (SoV) technique. The advantage of Green's function is that solution of a differential equation (say, a transient heat conduction problem) can be represented in terms of Green's function. The solution procedure to derive the Green's function for an one dimensional transient heat conduction problem with transient convective boundary condition at one face and transient heat flux at another boundary is discussed in following five steps.

Step 1.   Consider the homogenous version of the PDEs at equations (3.5, 3.5.1, 3.5.2 and 3.5.3) suitable for SoV technique and redefine as below.

$$\frac{\partial^2 \psi}{\partial z^2} = \frac{1}{\alpha} \frac{\partial \psi}{\partial t} \quad \text{in } 0 < z < a, \quad t > 0 \text{ (Not modified and homogenous)} \qquad \text{A-1}$$

$$-\frac{\partial \psi}{\partial z} + H\psi = 0 \quad \text{at } z = 0, \quad t > 0 \text{ (Modified and homogenous)}$$

$$\frac{\partial \psi}{\partial z} = 0 \quad \text{at } z = a, \quad t > 0 \text{ (Modified and homogenous)}$$

$$\psi(z,0) = g(z) - T_{amb} \quad \text{in } 0 < z < L$$

 Step 2.   The solution of the formulations at *step 1* can be readily referred in literature (Ozısık, 1993) (Section 2-4,2-5) and the same is given by

$$\psi(z,t) = \sum_{n=1}^{\infty} \frac{2\left(\lambda_n^2 + H^2\right)}{a\left(\lambda_n^2 + H^2\right) + H} * \cos\left(\lambda_n \left(a - z\right)\right) * e^{-\lambda_n^2 \alpha(t)} \int_{x'=0}^{L} \left(g(z') - T_{amb}\right) \cos\left(\lambda_n \left(a - z'\right)\right) dz'$$

where, $\lambda_n \tan(\lambda_n a) = H$, $n = 1,2,3, ...$ \qquad A-2

The eigen values ' λ_n ' are the roots of the transcendental equation above.

Step 3.   The equation at step 2 can be rewritten as,

$$\psi(z,t) = \int\limits_{x'=0}^{a} \left[\sum_{n=1}^{\infty} \frac{2\left(\lambda_n^2 + H^2\right)}{a\left(\lambda_n^2 + H^2\right) + H} * \cos\left(\lambda_n\left(a-z\right)\right) * \cos\left(\lambda_n\left(a-z'\right)\right) * e^{-\lambda_n^2\alpha(t)} \right]$$

$$* \left(g(z') - T_{amb}\right) dz' \qquad\qquad \text{A-3}$$

Step 4.   From the fundamentals of Green's function (Ozısık, 1993) (Chapter 6), the standard expression for the solution to problem at *step 1,* having homogenous differential equation and boundary conditions with a non-homogenous initial condition is generalised as,

$$\psi(z,t) = \int\limits_{x'=0}^{a} G\left(z,t\big|z',\tau\right)_{\tau=0} F(z')dz' \qquad\qquad \text{A-4}$$

Where, 'G' is the Green's function and 'F' is the initial condition.

Step 5.   Comparing equation at step 4 and equation at step 3, appropriate Green's function is given by,

$$G\left(z,t\big|z',\tau\right) = \sum_{n=1}^{\infty} \frac{2\left(\lambda_n^2 + H^2\right)}{a\left(\lambda_n^2 + H^2\right) + H} * \cos\left(\lambda_n\left(a-z\right)\right) * \cos\left(\lambda_n\left(a-z'\right)\right) * e^{-\lambda_n^2\alpha(t-\tau)} \qquad \text{A-5}$$

In this step, as a standard procedure, t is to be replaced by $t - \tau$.

APPENDIX B

Calculation of Methane and Air flow rate for a given Reynolds number

Balanced chemical equation for combustion of methane and air is given below,

$$CH_4 + a\left(O_2 + 3.76\ N_2\right) \rightarrow xCO_2 + yH_2O + zCO + wO_2 + 3.76aN_2 \qquad \text{B-1}$$
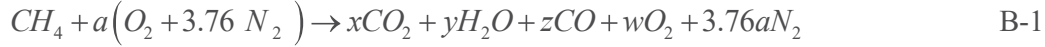
For $\phi = 1$, $a = 2$ and when ϕ is not equal to 1, $a = 2 / \phi$. Here, ϕ is the equivalence ratio.

The air/fuel (A/F) ratio and equivalence ratio (ϕ) are given by equation (B-2) and equation (B-3) respectively.

$$\frac{A}{F} = \frac{\dot{m}_{air}}{\dot{m}_{fuel}} \qquad \text{B-2}$$

$$\phi = \frac{\left(A/F\right)_{stoic}}{\left(A/F\right)_{act}} \qquad \text{B-3}$$

Mixture density and Mixture viscosity is calculated as per equation (B-4) and equation (B-5) respectively.

$$\rho_{mix} = \sum Y_I \rho_I = Y_{air}\frac{p_{air}}{R_{air}T_{air}} + Y_{CH_4}\frac{p_{CH_4}}{R_{CH_4}T_{CH_4}} \qquad \text{B-4}$$

At $\phi = 1$, $Y_{CH_4} = 0.054$, $Y_{air} = 0.946$

$$\mu_m = \frac{\sum \mu_i X_i \sqrt{M_i}}{\sum X_i \sqrt{M_i}} \qquad \text{B-5}$$

Mixture Reynolds number at the exit of burner is calculated as per equation (B-6)

$$\mathrm{Re} = \frac{\rho_{mix}\overline{u}d}{\mu} \qquad \text{B-6}$$

Methane-air mixture mass flow rate at the exit of the burner is calculated as per equation (B-7)

$$\dot{m}_{mix} = \pi \frac{d}{4} \text{Re} \, \mu_{mix} \qquad\qquad\qquad\qquad\qquad \text{B-7}$$

Equation (B-7) is derived from equation (B-6). Fuel and air mass flow rates are further calculated from the knowledge of individual mass fraction values. Corresponding volumetric flow rate of fuel and air are calculated (in ml per min) from the knowledge of density.

APPENDIX C

Calibration of Rotameters

Theoretical correction factors. The calibration of variable area flow meters for gases is prone to changes in density, temperature and pressure of medium. Thus, to know actual flow rate from indicated flow rate, a correction factor is needed. For gases of low density as compared to the density of the float, the volume flow rate is given by equation (C-1).

$$\dot{Q} \sim \frac{1}{\sqrt{\rho}} \qquad \text{C-1}$$

The interrelationship between two flow-rates correspond to certain position of the float at different working conditions can be written as equation (C-2 and C-3).

$$\dot{Q}_1 = \dot{Q}_2 \sqrt{\frac{\rho_2}{\rho_1}} \qquad \text{C-2}$$

$$\dot{Q}_1 = \dot{Q}_2\, K \qquad \text{where, K (Correction factor)} = \sqrt{\frac{\rho_2}{\rho_1}} \qquad \text{C-3}$$

Correction factors for same gas. The density of the medium at working conditions is frequently not known directly. It is linked to the variables pressure and temperature by way of the ideal gas equation (equation C-4).

$$\rho \sim \frac{p}{T} \qquad \text{C-4}$$

Thus, correction factor for one and same gas at constant temperature gets modified as equation C-5.

$$K_p = \sqrt{\frac{p_2}{p_1}} \qquad \text{C-5}$$

And when pressure remains constant, correction factor becomes as given in equation C-6.

$$K_T = \sqrt{\frac{T_1}{T_2}} \qquad \text{C-6}$$

When pressure as well as temperature varies, correction factor can be derived as equation C-7.

$$K_{p,T} = \sqrt{\frac{T_1}{T_2}} \times \sqrt{\frac{p_2}{p_1}}$$

C-7

Correction factors for different gas. If gas to be operated through rotameter is different than the gas used during calibration then correction factor given in equation C-2 can be used to know actual flow rate from indicated flow rate in rotameter. The correcting factors with reference to pressure and temperature are the same as mentioned in equation (C-5 to C-7).

APPENDIX D

Reynolds number wise rotameter reading

Mixture Reynolds Number	Rotameter Pressure	Volume flow rate (ml per min)		Corresponding rotameter reading	
		Methane	**Air**	**Methane**	**Air**
500		363	3445	137	1870
600		436	4134	163	2256
700		508	4823	188	2641
800		581	5511	213	3027
900	2 bar	653	6200	238	3412
1000		726	6889	264	3798
1100		799	7578	289	4183
1200		871	8267	314	4569
1300		944	8956	339	4954
1400		1016	9645	285	4242
1500	3 bar	1089	10334	305	4550
1600		1162	11023	325	4858
1700		1234	11712	284	4317
1800	4 bar	1307	12401	301	4577
1900		1379	13090	318	4836
2000		1452	13779	334	5095

APPENDIX E

MATLAB code

```matlab
clear all
clc

x = 0.004;      %plate thickness
k=14;        %plate thermal conductivity
rho=7700;    %plate material density
Cp=490;       %plate specific heat
alpha=k/(rho*Cp);   %plate thermal diffusivity
epsi = 0.95;
sigma = 5.67e-08; %W/m2 K^-4
L = x;
h_guess = 230; % Initial guess
T_ref_guess = 1210; % Initial guess
T_ref = T_ref_guess;
h = h_guess;% at the flame side
T_ref_old = T_ref_guess;
h_old = h_guess;
Damp_coeff = 100;
itermax = 20000;
T_i = 273+31.8;


%% EXPERIMENTAL TEMPERATURE INPUT
for row= 243:-5:40

    if row == 243
    rw=4;
    else
    h = htc(1);
    T_ref = Ref_temp(1);

    htc=[];
    Ref_temp=[];
    end
     km = 6;
    temp= sprintf('%d.csv',km);
    data= csvread(temp);
    data_final=data(243:-5:40,194:5:(194+110));
    mm = 1;
    T_m1 = data_final+273;
    xlswrite('T_m1.xlsx',T_m1);
     km = 30+km;
    temp= sprintf('%d.csv',km);
    data= csvread(temp);
```

```matlab
    data_final=data(243:-5:40,194:5:(194+110));
    mm = 2;
    T_m2 = data_final+273;  xlswrite('T_m2.xlsx',T_m2);
     km = 30+km;
    temp= sprintf('%d.csv',km);
    data= csvread(temp);
    data_final=data(243:-5:40,194:5:(194+110));
    mm = 2;
    T_m3 = data_final+273;   xlswrite('T_m3.xlsx',T_m3);
     km = 30+km;
    temp= sprintf('%d.csv',km);
    data= csvread(temp);
    data_final=data(243:-5:40,194:5:(194+110));
    mm = 2;
    T_m4 = data_final+273;    xlswrite('T_m4.xlsx',T_m4);
     km = 30+km;
    temp= sprintf('%d.csv',km);
    data= csvread(temp);
    data_final=data(243:-5:40,194:5:(194+110));
    mm = 2;
    T_m5 = data_final+273;  xlswrite('T_m5.xlsx',T_m5);
     km = 30+km;
    temp= sprintf('%d.csv',km);
    data= csvread(temp);
    data_final=data(243:-5:40,194:5:(194+110));
    mm = 2;
    T_m6 = data_final+273;  xlswrite('T_m6.xlsx',T_m6);

for km=6:30:160 % 235
    km = 6;
    temp= sprintf('%d.csv',km);
    data= csvread(temp);
    data_final=data(row,194:5:(194+110));
    mm = 1;
    mm= (km-30)/15;
    T_m(mm,:) = data_final+273;   % Measured/
experimental Temperature
end
siz = size(T_m);
r_d = 0:5*(0.6541):(siz(2)-1)*5*0.6541; % 0.6541 mm = 1
pixels, and x , y in mm
% pixelsize=1.3628/1000 * distance from object = 1.3628 *
0.001 * 480mm

r_d = r_d/10; % dimensionless

time = 0:(3/15):(siz(1)-1)*(3/15); % Frame rate = 15, two
frames are skipped, one is considered for analaysis
```

```matlab
min_r_square(length(r_d)) = zeros;
h_f(length(r_d)) = zeros;
for j=1:1:length(r_d)
    tic

    r_square = 100;
    for iter=1:1:itermax  %Iteration Loop Starts for
Algorithm

        r_square_old=r_square;
        r_square=0;
        h_f(j) = 2;
        H = h/k;
                        input = [H, L];
                        eigen = EGN(input);
                        lamda = eigen;
                        %% NUMERICAL INTEGRATION
                        for i = 2:1:length(time)
        rad = -epsi * sigma/k * (T_m(1:i,j).^4 - T_i.^4);
        conv = h_f(j)/k * (T_m(1:i,j) - T_i);
                            flux = rad + conv;
%
                            a = time(1);
                                b = time(i);
                            hh = time(2);
%
                                x = a:hh:b; % time array
                        for egn = 1:1:length(lamda)
lmn = exp(-alpha * lamda(egn) * lamda(egn) * (b - x));
y = prod([lmn;flux']); % function array
if i == 10
    x;
end
I(i,egn) = trapz(x,y);
                            end

                            end
                            s = size(I);
                            I = I(2:s(1),:);
        for i=2:1:length(time)
        T_w(i)= T_m(i,j);
                            for ss = 1:1:5
                                if ss == 2
                                    T_ref = T_ref + 5;
                                end
                                if ss == 3, T_ref = T_ref -
10;end
        if ss == 4, T_ref = T_ref + 5; H = (h + 1)/k;end
```

```matlab
                 if ss == 5, H = (h - 2)/k;end

        commonterm = alpha * 2 * (prod([lamda;lamda]) +
H*H) ./ ((L * (prod([lamda;lamda]) + H*H)) + H);

   commonterm = prod([commonterm;cos(lamda * 0.01 * L)]);
G_Fn_1 = H * (T_ref - T_i) * prod([cos(lamda * L);(1-
exp(-alpha * prod([lamda;lamda]) * time(i)))]) ./ (alpha
* prod([lamda;lamda]));

GF = prod([commonterm;(G_Fn_1 + I(i-1,:))]);

                         if ss == 1
                             temp = sum(GF) + T_i;
                             T_e(i,j) = temp;
                             r(i-1,1) = T_w(i) - temp;
%Residual Vector[rj=Pi(x,t)-Yj)]
                             r_square = r_square + (r(i-
1,1))^2;
                         end
                         if ss == 2
                          temp2 = sum(GF) + T_i;
                         end
                         if ss == 3
                          temp3 = sum(GF) + T_i;
                          J_Tref(i-1,1) = 0.1 * (temp2 -
temp3); %Jacobian of Tref
                         end
                         if ss == 4
                          temp4 = sum(GF) + T_i;
                         end
                         if ss == 5
                          temp5 = sum(GF) + T_i;
                          H = (h + 1)/k;
                          J_h(i-1,1) = 0.5 * (temp4 -
temp5);    %Jacobian of h
                         end
                         end
end

        J=[J_Tref J_h]; %Jacobian Matrix
        D=J'*J;
        ck = isnan(D);
        if (sum(sum(ck)) > 0)
            break
        end

        diagonal=diag(D);
```

```matlab
        G=[diagonal(1),0;0,diagonal(2)];

        p=inv(D+Damp_coeff*G)*(J'*r); %Direction Vector
        p_save_Taw(iter,j)=p(1,1);
        p_save_h(iter,j)=p(2,1);
        r_square_save(iter,j)=r_square; % Residual
Convergence for each iteration
if iter>1

            if (abs(h_old - h) < 0.39)&& (abs(T_ref_old -
T_ref) < 0.99)

            if abs(r_square_save(iter,1)-
r_square_save(iter-1,1)) < 0.5 %Convergence Criteria to
stop the iteration

            min_r_square(j) = r_square;

            break;
            end
            end
                if
(r_square_save(iter,1)>r_square_save(iter-1,1))
                    min_r_square(j) = r_square;
                    break;
                end
end
    h_old = h;
    T_ref_old = T_ref;
    T_ref = T_ref + p(1,1); % Update the 'Tref' for the
Next Iteration
    h=h+p(2,1); % Update the 'h' for the Next Iteration

    end
    res(:,j) = r;
    Jac_h(:,j) = J_h;
    Jac_Tref(:,j) = J_Tref;
    Ref_temp(j)=T_ref;
    htc(j)=h;
    toc
    if (sum(sum(ck)) > 0)
            break
    end
end
if (rw==4)
result(1,1)=h_guess; % for htc
result(2,1)=T_ref_guess;
result(3,1)=Damp_coeff;
```

```matlab
result(4,1:length(htc))=r_d(1:length(htc));
result1(1,1)=h_guess; % for temperature
result1(2,1)=T_ref_guess;
result1(3,1)=Damp_coeff;
result1(4,1:length(htc))=r_d(1:length(htc));
end
rw=rw+1;
diff=length(result(4,:))-length(htc);
if diff>0
htc(end+1:end+diff)=htc(end);
result(rw,:)=htc;
Ref_temp(end+1:end+diff)=Ref_temp(end);
result1(rw,:)=Ref_temp;
else
    if diff<0
        result(rw,:)=htc(1:length(result(4,:)));
        result1(rw,:)=Ref_temp(1:length(result(4,:)));
    else
        result(rw,:)=htc;
        result1(rw,:)=Ref_temp;
    end
end
end

xlswrite('result_h.xlsx',result);
xlswrite('result_Tref.xlsx',result1);
xlswrite('min_r_square.xlsx',min_r_square);
xlswrite('Jaco_h.xlsx',Jac_h);
xlswrite('Jaco_Tref.xlsx',Jac_Tref);
xlswrite('T_m.xlsx',T_m);
xlswrite('T_e.xlsx',T_e);
xlswrite('times.xlsx',time);
xlswrite('r_d.xlsx',r_d);
```

CONTINUED - CODE FOR CALCULATING UNCERTANTIES USING MONTE-CARLO TECHNIQUE

```matlab
%% START Monte Carlo Unceratinity Estimation

    Ref_temp_MCMC =[];
    h_MCMC = [];
    T_e(1,:) = T_m(1,:);
for j=1:1:length(r_d)

for sm=1:1:500
        sm
    T_measured = T_m(:,j)';
    T_estimated = T_e(:,j)';
```

```matlab
    T_ref = result(3,j);   %Initial Guess for Reference
Temperature
    h = result(2,j);       %Initial Guess for Heat Transfer
Coefficient

LSE = [T_estimated - T_measured]*[T_estimated -
T_measured]'; % Least Square Error

sigmaa = sqrt(LSE/(length(time)-1));
T_MonteCarlo = T_estimated' +
norminv(rand(length(time),1),0,sigmaa);

    r_square = 100;

    T_w = T_MonteCarlo;

for iter=1:1:itermax   %Iteration Loop Starts for
Algorithm

        r_square=0; %Initialize R^2
        r_square_old=r_square;
        h_f(j) = 2;
        H = h/k;
                        input = [H, L];
                        eigen = EGN(input);
                        lamda = eigen;
                        %% NUMERICAL INTEGRATION
                        for i = 2:1:length(time)
                    rad = -epsi * sigma/k *
(T_w(1:i).^4 - T_i.^4);
                            conv = h_f(j)/k * (T_w(1:i)
- T_i);

                            flux = rad + conv;
                            a = time(1);
                                b = time(i);
                            hh = time(2);
                                x = a:hh:b; % time array
                        for egn = 1:1:length(lamda)
lmn = exp(-alpha * lamda(egn) * lamda(egn) * (b - x));
y = prod([lmn;flux']); % function array
if i == 10
    x;
end
I(i,egn) = trapz(x,y);
                            end
                            end
                            s = size(I);
                            I = I(2:s(1),:);
```

```matlab
    for i=2:1:length(time)
    T_w(i)= T_m(i,j);

                        for ss = 1:1:5
                            if ss == 2
                                T_ref = T_ref + 5;
                            end
                            if ss == 3, T_ref = T_ref -
10;end
                            if ss == 4, T_ref = T_ref +
5; H = (h + 1)/k;end
                            if ss == 5, H = (h -
2)/k;end

commonterm = alpha * 2 * (prod([lamda;lamda]) + H*H) ./
((L * (prod([lamda;lamda]) + H*H)) + H);

commonterm = prod([commonterm;cos(lamda * 0.01 * L)]);

G_Fn_1 = H * (T_ref - T_i) * prod([cos(lamda * L);(1-
exp(-alpha * prod([lamda;lamda]) * time(i)))]) ./ (alpha
* prod([lamda;lamda]));
                        GF = prod([commonterm;(G_Fn_1 +
I(i-1,:))]);

                        if ss == 1
                            temp = sum(GF) + T_i;
                            T_e(i,j) = temp;
                            r(i-1,1) = T_w(i) - temp;
                            r_square = r_square + (r(i-
1,1))^2;
                        end
                        if ss == 2
                         temp2 = sum(GF) + T_i;
                        end
                        if ss == 3
                         temp3 = sum(GF) + T_i;
                J_Tref(i-1,1) = 0.1 * (temp2 - temp3);
%Jacobian of Tref
                        end
                        if ss == 4
                         temp4 = sum(GF) + T_i;
                        end
                        if ss == 5
                         temp5 = sum(GF) + T_i;
                         H = (h + 1)/k;
                J_h(i-1,1) = 0.5 * (temp4 - temp5);
%Jacobian of h
```

```matlab
                        end
                    end
end

        J=[J_Tref J_h]; %Jacobian Matrix
        D=J'*J;
        diagonal=diag(D);
        G=[diagonal(1),0;0,diagonal(2)];

        p=inv(D+Damp_coeff*G)*(J'*r); %Direction Vector
        p_save_Taw(iter,j)=p(1,1);
        p_save_h(iter,j)=p(2,1);
r_square_save(iter,j)=r_square; % Residual Convergence
for each iteration
if iter>5

            if (abs(h_old - h) < 0.2)&& (abs(T_ref_old -
T_ref) < 0.99)

            if abs(r_square_save(iter,1)-
r_square_save(iter-1,1)) < 1  %Convergence Criteria to
stop the iteration

%               min_r_square(j) = r_square;

            break

            end
            end
end
        r_square

    h_old = h;
    T_ref_old = T_ref;
   T_ref = T_ref + p(1,1); % Update the 'Tref' for the
Next Iteration
    h=h+p(2,1); % Update the 'h' for the Next Iteration


end

    Ref_temp(sm)=T_ref;
    htc(sm)=h;

    end
    Ref_temp_MCMC = [Ref_temp_MCMC;Ref_temp];
    h_MCMC = [h_MCMC;htc];
```

```
end
xlswrite('Ref_temp_MCMC.xlsx',Ref_temp_MCMC);
xlswrite('h_MCMC.xlsx',h_MCMC);
%% FREQUENCY DISTRIBUTION

%% SORTING each POPULATION AND CONSIDER 95% CONFIDENCE
LEVEL
A = sort(h_MCMC');
B = sort(Ref_temp_MCMC');
A = [A(13,:);A(250,:);A(486,:)];
B = [B(13,:);B(250,:);B(486,:)];

xlswrite('Ref_temp_Errorrange_MC.xlsx',B);
xlswrite('h_Errorrange_MC.xlsx',A);
```

FUNCTION FOR CALCULATING EIGEN VALUES (GREEN'S FUNCTION)

```
function eigen = EGN(x)
% TO find the eigen values - one dimension, both side
convection BC
H = x(1);
L = x(2);


lamda = 0:10:100000;

f = prod([lamda;tan(L * lamda)]) - H;

 ii=1;
     for nn = 1:length(f)-1
         if (f(nn)<=0 && f(nn+1)>0)
         sol_point(ii) = lamda(nn);
             ii=ii+1;
         end
     end
 %FINDING EIGEN VALUES " (lamda*lamda-H1*H2)*TAN(LAMDA*L)
- LAMDA*(H1+H2)"
        lamda = [];
        for nn=1:ii-1
           xy=sol_point(nn);
              for r=1:10000
                 xold=xy;
                 f = xy * tan(xy * L) - H;
  df= L * xy * sec(L * xy) * sec(L * xy) + tan(L * xy);
                 xy = xy - f/df;
                 if ( abs(xy-xold) < 0.01)
                     lamda(nn)=xy;
                     break;
```

```
                end
              end
           end
        eigen = lamda;
  end
```

APPENDIX F

Actual values of heat transfer coefficient and adiabatic wall temperature along with their deviations with respect to the present study (Re = 1000, W/d = 4) over a flat plate are presented below. The deviations are represented by 'Δh' and 'ΔT_{aw}'.

r/d	Present Study		3D Modal analysis (Kadam et al. 2018)				Hindasageri et al. 2014				Kuntikana and Prabhu, 2016	
	h	T_{aw}	H	T_{aw}	Δh (%)	ΔT_{aw} (%)	h	T_{aw}	Δh (%)	ΔT_{aw} (%)	h	Δh (%)
0	168	906	157	914	11 (7)	8 (1)	176	901	8 (5)	5 (1)	170	2 (1)
1	144	862	149	882	5 (3)	20 (2)	150	866	6 (4)	4 (1)	147	3 (2)
2	79	685	107	785	28 (17)	100 (11)	103	798	24 (14)	113 (12)	78	1 (1)
3	43	558	72	652	29 (17)	94 (10)	52	688	9 (5)	130 (14)	30	13 (8)
4	25	481	58	530	33 (20)	49 (5)	23	590	2 (1)	109 (12)	16	9 (5)
5	19	455	-	-	-	-	23	590	4 (2)	135 (15)	9	10 (6)

REFERENCES

Agrawal, G. K., Chakraborty, S. and Som, S. K. (2010). "Heat transfer characteristics of premixed flame impinging upwards to plane surfaces inclined with the flame jet axis." International journal of heat and mass transfer, 53(9-10), 1899-1907.

Anderson, C. A. (1961). "Blast deflectors." US Patent No. 3,014,410, Washington, DC.

Baughn, J.W. and Shimizu, S. (1989). "Heat transfer measurements from a surface with uniform heat flux and an impinging jet." Journal of Heat Transfer (Transactions of the ASME (American Society of Mechanical Engineers), Series C; (United States), 111(4), 22-25.

Baukal Jr, C. E. (2000). "Heat transfer in industrial combustion." *CRC press., N.W. Corporate Blvd., Boca Raton*. ISBN 0-8493-1699-5.

Baukal, C.E. and Gebhart, B. (1995). "A Review of Flame Impingement Heat Transfer Studies Part 2: Measurements." Combustion science and technology, 104(4-6), 359-385.

Baukal, C. E. and Gebhart, B. (1996-a). "A review of semi-analytical solutions for flame impingement heat transfer." International journal of heat and mass transfer, 39(14), 2989-3002.

Baukal Jr, C. E. and Gebhart, B. (1996-b). "A review of empirical flame impingement heat transfer correlations." International journal of heat and fluid flow, 17(4), 386-396.

Beck, J.V., Blackwell, B. and St Clair Jr, CR (1985). "Inverse Heat Conduction: Ill-Posed Problems." A Wiley-Interscience, New York.

Bee, J. M. and Chigier, N. A. (1968). "Impinging jet flames." Combustion and flame, 12(6), 575-586.

Beitelmal, A. H., Saad, M. A. and Patel, C. D. (2000). "Effects of surface roughness on the average heat transfer of an impinging air jet." International communications in heat and mass transfer, 27(1), 1-12.

Bejan, A. (2013). "Convection heat transfer." John wiley and sons, 4th edition.

Brandt, R., Bird, C., & Neuer, G. (2008). "Emissivity reference paints for high temperature applications." Measurement, 41(7), 731-736.

Briggs, D.C., Ciappi, J.I. and Kraft III, WR, Lockheed M. C. (2003). "Self-contained canister missile launcher with tubular exhaust uptake ducts." US Patent 6,584,882.

Buchlin, J.M. (2011). "Convective heat transfer in impinging-gas-jet arrangements." Journal of Appl. Fluid Mechanics, 4(2), 137-149.

Calle, L., Hintze, P., Parlier, C., Sampson, J., Curran, J., Kolody, M. and Perusich, S. (2010). "Refractory materials for flame deflector protection." In AIAA SPACE 2010 Conference and exposition, 8749-52.

Carlomagno, G.M. and Cardone, G. (2010). "Infrared thermography for convective heat transfer measurements." Experiments in fluids, 49(6), 1187-1218.

Carlomagno, G.M. and Ianiro, A. (2014). "Thermo-fluid-dynamics of submerged jets impinging at short nozzle-to-plate distance: A review." Experimental thermal and fluid science, 58, 15-35.

Carslaw, H.S. and Jaeger, J.C. (1959). "Conduction of heat in solids." Oxford: Clarendon press, 2nd edition.

Chan, T. L., C. W. Leung, K. Jambunathan, S. Ashforth-Frost, Y. Zhou and M. H. Liu. (2002). "Heat transfer characteristics of a slot jet impinging on a semi-circular convex surface." International journal of heat and mass transfer 45(5), 993-1006.

Chander, S. and Ray, A. (2005). "Flame impingement heat transfer: a review." Energy conversion and management, 46(18-19), 2803-2837.

Chander, S. and Ray, A. (2006). "Influence of burner geometry on heat transfer characteristics of methane/air flame impinging on flat surface." Experimental heat transfer, 19(1),15-38.

Chander, S. and Ray, A. (2007). "Heat transfer characteristics of three interacting methane/air flame jets impinging on a flat surface." International journal of heat and mass transfer, 50(3-4), 640-653.

Chander, S. and Ray, A. (2008). "An experimental and numerical study of stagnation point heat transfer for methane/air laminar flame impinging on a flat surface." International journal of heat and mass transfer, 51(13-14), 3595-3607.

Chander, S. and Ray, A. (2011). "Experimental and numerical study on the occurrence of off-stagnation peak in heat flux for laminar methane/air flame impinging on a flat surface." International journal of heat and mass transfer, 54(5-6), 1179-1186.

Colaço, M.J., Orlande, H.R., and Dulikravich, G.S. (2006). "Inverse and optimization problems in heat transfer." Journal of the brazilian society of mechanical sciences and engineering, 28, 1-24.

Conolly, R. and Davies, R. M. (1972). "A study of convective heat transfer from flames." International journal of heat and mass transfer, 15(11), 2155-2172.

Cooper, D. Jackson, D.C., Launder, B.E. and Liao, G.X. (1993). "Impinging jet studies for turbulence model assessment—I. Flow-field experiments." International journal of heat and mass transfer, 36(10), 2675-2684.

Cox, M. G., and Siebert, B. R. (2006). "The use of a Monte Carlo method for evaluating uncertainty and expanded uncertainty." Metrologia, 43(4), 178-188.

Craft, T.J. Graham, L.J.W. and Launder, B.E. (1993). "Impinging jet studies for turbulence model assessment—II. An examination of the performance of four turbulence models." International journal of heat and mass transfer, 36(10), 2685-2697.

Cremers, M.F.G., Remie, M.J., Schreel, KRAM and de Goey, LPH (2010). "Thermochemical heat release of laminar stagnation flames of fuel and oxygen." International journal of heat and mass transfer, 53(5-6), 952-961.

Davies, D.R. (1979). "Heat transfer from working flame burners." Doctoral dissertation, University of Salford, UK.

Dewan, A., Dutta, R. and Srinivasan, B. (2012). "Recent trends in computation of turbulent jet impingement heat transfer." Heat transfer engineering, 33(4-5), 447-460.

Diller, T.E. (1993). "Advances in heat flux measurements." Advances in heat transfer, Elsevier, 23, 279-368.

Dong, L. L., Leung, C. W. and Cheung, C. S. (2002). "Heat transfer characteristics of premixed butane/air flame jet impinging on an inclined flat surface." Heat and mass transfer, 39(1), 19-26.

Evans, R.L. and Sparks, OL (1963). "Launch deflector design criteria and their application to the Saturn C-1 deflector," Technical note d-1275, NASA.

Fay, J. A. and Riddell, F. R. (1958). "Theory of stagnation point heat transfer in dissociated air." Journal of the aerospace sciences, 25(2), 73-85.

Feng, Z.C., Chen, J.K., Zhang, Y. and Griggs Jr, JL (2011). "Estimation of front surface temperature and heat flux of a locally heated plate from distributed sensor data on the back surface." International journal of heat and mass transfer, 54(15-16), 3431-3439.

Fenot, M., Dorignac, E. and Vullierme, J.J. (2008). "An experimental study on hot round jets impinging a concave surface." International journal of heat and fluid flow, 29(4), 945-956.

Fénot, M., Vullierme, J.J. and Dorignac, E. (2005). "A heat transfer measurement of jet impingement with high injection temperature." Comptes rendus mécanique, 333(10), 778-782.

Fernandes, A. P., Dos Santos, M. B., and Guimarães, G. (2015). "An analytical transfer function method to solve inverse heat conduction problems." Applied mathematical modelling, 39(22), 6897-6914.

Frankel, J.I., Keyhani, M., Arimilli, R.V. and Wu, J. (2008). "A new multidimensional integral relationship between heat flux and temperature for direct internal assessment of heat flux." Zeitschrift für angewandte mathematik und physik, 59(5), 869-888.

Frankel, J.I., Keyhani, M. and Arimilli, R.V. (2010). "New Orthotropic, Two-Dimensional, Transient Heat-Flux/Temperature Integral Relationship for Half-Space Diffusion." Journal of thermophysics and heat transfer, 24(1), 215-218.

Fu, D. and Hao, H. (2015). "Investigations for missile launching in an improved concentric canister launcher." Journal of spacecraft and rockets, 52(5), 1510-1515.

Gan, T., Ming, T., Fang, W., Liu, Y., Miao, L., Ren, K., and Ahmadi, M. H. (2019). "Heat transfer enhancement of a microchannel heat sink with the combination of impinging jets, dimples, and side outlets." Journal of thermal analysis and calorimetry, 1-12. *https://doi.org/10.1007/s10973-019-08754-z*

Gardon, R. and Akfirat, J.C. (1965). "The role of turbulence in determining the heat-transfer characteristics of impinging jets." International journal of heat and mass transfer, 8(10), 1261-1272.

Gardon, R. (1962). "Heat transfer between a flat plate and jets of air impinging on it." International developments in heat transfer (ASME), 454-460.

Ghasemian, M., Ramiar, A., and Ranjbar, A. A. (2019). "Numerical investigation of boiling heat transfer in a quenching process of jet impingement considering solid temperature distribution." Journal of thermal analysis and calorimetry, 136(6), 2409-2420.

Goldstein, R. J. and Franchett, M. E. (1988). "Heat transfer from a flat surface to an oblique impinging jet." Journal of heat transfer, 110, 84–90.

Grenson, P., Léon, O., Reulet, P. and Aupoix, B. (2016). "Investigation of an impinging heated jet for a small nozzle-to-plate distance and high Reynolds number: An extensive experimental approach." International journal of heat and mass transfer, 102, 801-815.

Hadipour, A., Zargarabadi, M. R. and Dehghan, M. (2020). "Effect of micro-pin characteristics on flow and heat transfer by a circular jet impinging to the flat surface." Journal of thermal analysis and calorimetry, 140, 943–951.

Hargrave, G. K. and Kilham, J. K. (1984). "The effect of turbulence intensity on convective heat transfer from premixed methane-air flames." Industrial chemical engineering symposium, 2(86), 1025-1034.

Hahn, D.W. and Özişik, M.N. (2012). "Heat Conduction Fundamentals." Wiley Online Library, Third edition, 300-349.

Hindasageri, V., Vedula, R. P., and Prabhu, S. V. (2012). "Blowoff Stability of Methane-Air Premixed Flame on Tube Burners." International journal of emerging multidisciplinary fluid sciences, 3(4), 209-226.

Hindasageri, V., Vedula, R.P. and Prabhu, S.V. (2014-a). "A novel concept to estimate the steady state heat flux from impinging premixed flame jets in an enclosure by numerical IHCP technique." International journal of heat and mass transfer, 79, 342-352.

Hindasageri, V., Vedula, R.P. and Prabhu, S.V. (2014-b). "A novel method of estimation of adiabatic wall temperature for impinging premixed flame jets." International journal of heat and mass transfer, (77), 185-193.

Hindasageri, V., Vedula, R. P. and Prabhu, S. V. (2014-c). "Heat transfer distribution for impinging methane–air premixed flame jets." Applied thermal engineering, 73(1), 461-473.

Hofmann, H.M., Kind, M. and Martin, H. (2007). "Measurements on steady state heat transfer and flow structure and new correlations for heat and mass transfer in submerged impinging jets." International journal of heat and mass transfer, 50(19-20), 3957-3965.

Hoogendoorn, C.J. (1977). The effect of turbulence on heat transfer at a stagnation point. International journal of heat and mass transfer, 20(12), 1333-1338.

Hrycak P. (1983). "Heat transfer from round impinging jets to a flat plate." International journal of heat and mass transfer, 26(12), 1857–1865.

Hu, W., Xie, J., Chau, H. W. and Si, B. C. (2015). "Evaluation of parameter uncertainties in nonlinear regression using the Microsoft Excel Spreadsheet." Environmental systems research, 4(1), 1-12. *https://doi.org/10.1186/s40068-015-0031-4*

Huang, X. Q., Leung, C. W., Chan, C. K., and Probert, S. D. (2006). "Thermal characteristics of a premixed impinging circular laminar-flame jet with induced swirl." Applied energy, 83(4), 401-411.

Jackson, E. G. and Kilham, J. K. (1956). "Heat transfer from combustion products by forced convection." Industrial and engineering chemistry, 48(11), 2077-2079.

Jambunathan, K., Lai, E., Moss, M.A. and Button, BL (1992). A review of heat transfer data for single circular jet impingement. International journal of heat and fluid flow, 13(2), 106-115.

Kadam AR, Tajik AR, and Hindasageri V. (2016). "Heat transfer distribution of impinging flame and air jets–a comparative study." Applied thermal engineering. 92, 42-49.

Kadam, A. R., Prabhu, S. V., and Hindasageri, V. (2018). "Simultaneous estimation of heat transfer coefficient and reference temperature from impinging flame jets." International journal of thermal sciences, 131, 48-57.

Kadam, A. R., Parida, R. K., Hindasageri, V. and Kumar, G. N. (2019). "Heat transfer distribution of premixed methane-air laminar flame jets impinging on ribbed surfaces." Applied thermal engineering, 163, 1143-52.

Karwa, N., Gambaryan-Roisman, T., Stephan, P., and Tropea, C. (2011). "Experimental investigation of circular free-surface jet impingement quenching: transient hydrodynamics and heat transfer." Experimental thermal and fluid science, 35(7), 1435-1443.

Katti, V. and Prabhu, S.V. (2008). "Experimental study and theoretical analysis of local heat transfer distribution between smooth flat surface and impinging air jet from a circular straight pipe nozzle." International journal of heat and mass transfer, 51(17-18), 4480-4495.

Kennedy, R.E., Olmsted, G.S., Ryan, R.E. and Tavares, J., Northrop Grumman Corp, (1998). "Missile launcher apparatus." U.S. patent 5,847,307.

Kowsary, F., Razzaghi, H. and Ashjaee, M. (2020). "Experimental design for estimation of the distribution of the convective heat transfer coefficient for a bubbly impinging jet." Journal of thermal analysis and calorimetry, 140(1), 439-456.

Kuczera, G. and Parent, E. (1998). "Monte Carlo assessment of parameter uncertainty in conceptual catchment models: the Metropolis algorithm." Journal of hydrology, 211(1-4), 69-85.

Kulish, V.V. and Novozhilov, V.B. (2003). "The relationship between the local temperature and the local heat flux within a one-dimensional semi-infinite domain of heat wave propagation." Mathematical problems in engineering, (4), 173-179.

Kuntikana, P. and Prabhu, S. V. (2016-a). "Isothermal air jet and premixed flame jet impingement: heat transfer characterisation and comparison." International journal of thermal sciences, 100, 401-415.

Kuntikana, P. and Prabhu, S. V. (2016-b). "Heat transfer characteristics of premixed methane–air flame jet impinging obliquely onto a flat surface." International journal of heat and mass transfer, 101, 133-146.

Lee, JLSJ (1999). "Stagnation region heat transfer of a turbulent axisymmetric jet impingement." Experimental heat transfer, 12(2), 137-156.

Lewis, B., and Von Elbe, G. (1943). Stability and structure of burner flames. The journal of chemical physics, 11(2), 75-97.

Loubat, R., Reulet, P., Estebe, B. and Millan, P. (2004). "Heat flux characterisation in hot jet and flame/ wall interaction by IHCP resolution coupled with infrared measurements." Quantitative infrared thermography journal, 1(2), 205-228.

Lytle, D. and Webb, B.W. (1994). "Air jet impingement heat transfer at low nozzle-plate spacing." International journal of heat and mass transfer, 37(12), 1687-1697.

Ma, C. F., Zheng, Q., Sun, H., Wu, K., Gomi, T. and Webb, B. W. (1997). "Local characteristics of impingement heat transfer with oblique round free-surface jets of large Prandtl number liquid." International journal of heat and mass transfer, 40(10), 2249-2259.

Mansfield, J. M., and Winefordner, J. D. (1968). "Measurement of flow rate and pressure of gases in flame spectrometry." Analytica chimica acta, 40, 357-359.

Marquardt, D. W. (1963). "An algorithm for least-squares estimation of nonlinear parameters." Journal of the society for industrial and applied mathematics, 11(2), 431-441.

Martin, R.W. and Rice, PS, Raytheon Co, (2012). "Translating adjacent-blast shield and method for protecting external slots of missiles in launcher tubes." US Patent 8,186,260.

Milson, A. and Chigier, N. A. (1973). "Studies of methane and methane-air flames impinging on a cold plate." Combustion and flame, 21(3), 295-305.

Moffat, R. J. (1985). "Using uncertainty analysis in the planning of an experiment." Journal of fluid engineering, 107(2), 173-178.

Mohaghegh, M. R. and Rahimi, A. B. (2019). "Single-and two-phase water jet impingement heat transfer on a hot moving surface." Journal of thermal analysis and calorimetry, 137(4), 1401-1411.

Morse, P. M., and Feshbach, H. (1953). "Methods of Theoretical Physics." London: Vol. 1-2. McGraw-Hill.

Mozumder, A. K., Monde, M., Woodfield, P. L., and Islam, M. A. (2006). "Maximum heat flux in relation to quenching of a high temperature surface with liquid jet impingement." International journal of heat and mass transfer, 49(17-18), 2877-2888.

Naphon, P., Wiriyasart, S., Arisariyawong, T., and Nakharintr, L. (2019). "ANN, numerical and experimental analysis on the jet impingement nanofluids flow and heat transfer characteristics in the micro-channel heat sink." International journal of heat and mass transfer, 131, 329-340.

Orlande, H. R. (2012). "Inverse problems in heat transfer: new trends on solution methodologies and applications." Journal of heat transfer, 134(3), 25-47.

Ozisik, M. N. (2002). "Boundary value problems of heat conduction." New York, Courier Corporation.

Ozısık, M. N. (1993). "Heat conduction." New York: John Wiley and Sons.

Parida, R.K., Madav, V. and Hindasageri, V. (2020). "Analytical solution to transient inverse heat conduction problem using Green's function." Journal of thermal analysis and calorimetry. *https://doi.org/10.1007/s10973-020-09803-8*

Piesik, E. T. (1990). "Rocket exhaust deflector." US Patent 4,934, Washington, DC.

Qiu, D., Wang, C., Luo, L., Wang, S., Zhao, Z., and Wang, Z. (2019). "On heat transfer and flow characteristics of jets impinging onto a concave surface with varying jet

arrangements." Journal of thermal analysis and calorimetry, 1-12. *https://doi.org/10.1007/s10973-019-08901-6*

Remie, M.J., Särner, G., Cremers, M.F.G., Omrane, A., Schreel, KRAM, Aldén, L.E.M. and De Goey, LPH (2008). "Heat-transfer distribution for an impinging laminar flame jet to a flat plate." International journal of heat and mass transfer, 51(11-12), 3144-3152.

Remie, M.J., Cremers, M.F.G., Schreel, KRAM and De Goey, LPH (2007). "Analysis of the heat transfer of an impinging laminar flame jet." International journal of heat and mass transfer, 50(13-14), pp.2816-2827.

Santora, H.R., Lunday, G.P. and Benson, J.A., Boeing north American inc., (1960). "Rocket engine assembly testing and launching apparatus." U.S. patent 2,925,013.

Sibulkin, M. (1952). "Heat transfer near the forward stagnation point of a body revolution." Journal of the aeronautical sciences, 9, 570-571.

Sparrow, E. M. and Lovell, B. J. (1980). "Heat transfer characteristics of an obliquely impinging circular jet." Journal of heat transfer, 102(2), 202–209.

Sparrow, E.M., Haji-Sheikh, A. and Lundgren, T.S. (1964). "The inverse problem in transient heat conduction." Journal of applied mechanics, 31(3), 369-375.

Stevens, J. and Webb, B. W. (1991). "The effect of inclination on local heat transfer under an axisymmetric, free liquid jet." International journal of heat and mass transfer, 34(4-5), 1227-1236.

Sutton, G. P. (2003). "History of liquid propellant rocket engines in the United States." Journal of propulsion and power, 19(6), 978-1007.

Urone, P., and Ross, R. C. (1979). 'Pressure change effects on Rotameter air flow rates." Environmental science and technology, 13(6), 732-734.

Van der Meer, T.H. (1987). "Heat transfer from impinging flame jets, PhD Theses." Delft University of Technology

Van der Meer, T. H. (1991). "Stagnation point heat transfer from turbulent low Reynolds number jets and flame jets." Experimental thermal and fluid science, 4(1), 115-126.

Veillon, C., and Park, J. Y. (1970). "Correct procedures for calibration and use of Rotameter-type gas flow measuring devices." Analytical chemistry, 42(6), 684-685.

Vinze, R., Limeye, M.D. and Prabhu, S.V. (2017). "Influence of the elliptical and circular orifices on the local heat transfer distribution of a flat plate impinged by under-expanded jets." Heat and mass transfer, 53(4), 1439-1455.

Vipat, O., Feng, S. S., Kim, T., Pradeep, A. M. and Lu, T. J. (2009). "Asymmetric entrainment effect on the local surface temperature of a flat plate heated by an obliquely impinging two-dimensional jet." International journal of heat and mass transfer, 52(21-22), 5250-5257.

Viskanta, R. (1993). "Heat transfer to impinging isothermal gas and flame jets." Experimental thermal and fluid science, 6(2), 111-134.

Webster, H. L. (1977). "Gas flow modeling of variable area flowmeters/ rotameters." In 23rd International instrumentation symposium, 23, 417-424.

Yagala,J.J. and Anderson, JR, L. (1982). "Internal ballistics and missile launch environment for the vertical launching system." In 3rd joint thermophysics, fluids, plasma and heat transfer conference, 855.

Yagla, J. J. (1997). "Concentric canister launcher." Naval engineers journal, 109(3), 313-327.

Yan, X. and Saniei, N. (1997). "Heat transfer from an obliquely impinging circular, air jet to a flat plate." International journal of heat and fluid flow, 18(6), 591-599.

Zhen, H. S., Leung, C. W., and Cheung, C. S. (2012). "Heat transfer characteristics of an impinging premixed annular flame jet." Applied thermal engineering, 36, 386-392.

Zuckerman, N. and Lior, N. (2006). "Jet impingement heat transfer: physics, correlations, and numerical modeling." Advances in heat transfer, 39, 565-631.

BIO-DATA

1.   **Name.**   Commander Ritesh Kumar Parida (Indian Navy)

2.   **Email and contact number**. ritesh.parida@gmail.com, (Mob) 9497233901

3.   **Academic Qualification**.

Ser	Degree	Year	institute	Subject	Percentage
(a)	B Tech	2002-06	NIT Kurukshetra	Mechanical Engineering	77%
(b)	M Tech	2010-12	IIT Delhi	Thermal Engineering	8.7 CGPA

4.   **Journal publications based on PhD work**.

(a)   Parida, R.K., Madav, V. & Hindasageri, V. (2020). Analytical solution to transient inverse heat conduction problem using Green's function. J Therm Anal Calorim. https://doi.org/10.1007/s 10973-020-09803-8.

(b)   Parida, R. K., Kadam, A. R., Hindasageri, V., & Vasudeva, M. (2019). Application of green's function to establish a technique in predicting jet impingement convective heat transfer rate from transient temperature measurements. In Numerical Heat Transfer and Fluid Flow (385-391). Springer, Singapore.

(c)   Parida, R. K., Kadam, A. R., Kumar, C., Vasudeva, M., Kumar, G. N., & Hindasageri, V. (2018). Experimental study on effect of pressure on volumetric gas flow rate through a variable area flow meter (rotameter). International Journal of Mechanical and Production Engineering Research and Development, 8, 1299-1308.

(d)   Under review post 1st revision.   Parida, R.K., Madav, V. and Hindasageri, V. "Heat transfer characterisation of impinging flame jet over a wedge." Applied Thermal Engineering. Elsevier.

5.   **Conferences based on PhD work**.

(a)   Parida, R.K., Madav, V. and Hindasageri, V. "Analytical Transient IHCP using Green's Function", International Mechanical Engineering Congress (IMEC-2019), NIT Tiruchirappalli, India, 29 Nov - 01 Dec 2019.

(b)   Parida R.K., Kadam A.R., Hindasageri V., and Vasudeva M. "Application of Green's Function to Establish a Technique in Predicting Jet Impingement Convective Heat Transfer Rate from Transient Temperature Measurements", International Conference on Numerical Heat Transfer and Fluid Flow, NIT Warangal, India - 19-21 Jan 2018.

(c)   Parida, R.K., Kadam, A. R., Kumar, C., Vasudeva M., Kumar G. N., & Hindasageri, V. "Experimental study on effect of pressure on volumetric gas flow rate through a variable area flow meter (rotameter)." International Conference on Mechanical and Industrial System Engineering (ICMISE-2018), 2018, Graphic Era University Dehradun, 01-02 Jun 2018.

***